



XXII International Seminar on Physics and Chemistry of Solids

Book of Abstracts



**June 17-19, 2020
Lviv, Ukraine**



Lviv City Council
Lviv Convention Bureau
Ivan Franko National University of Lviv
Jan Dlugosz University in Czestochowa

XXII International Seminar on Physics and Chemistry of Solids

Book of Abstracts

June 17-19, 2020
Lviv, Ukraine

SCIENTIFIC COMMITTEE

Zygmunt Bąk
Wojciech Ciesielski
Grygoriy Dmytriv
Jozef Drabowicz
Jacek Filipecki
Roman Gladyshevskii (chairman)
Janusz Kapuśniak (co-chairman)
Volodymyr Kapustianyk
Małgorzata Makowska-Janusik
Stepan Mudry
Vasyl Stadnyk
Volodymyr Tkachuk
Anatolii Voloshinovskii
Petro Yakibchuk

ORGANIZING COMMITTEE

Oleg Bovgyra
Yaroslav Chornodolskyy
Andryj Korolyshyn
Stepan Mudry (chairman)
Volodymyr Pavlyuk
Yuriy Plevachuk
Viktor Prysyzhnyuk
Ihor Shtablavyi
Vasyl Sklyarchuk
Anatolii Voloshinovskii (co-chairman)
Ivan Shcherba

SEMINAR SECRETARY

Ihor Shtablavyi

Faculty of Physics

Ivan Franko National University of Lviv

Kyryla and Mefodia Str., 8a, Lviv, 79005, Ukraine.

Phone: + 38-032-239-45-94

Phone: + 38-067-451-59-52

e-mail: ispcs2020@gmail.com

LECTURES

HYDROGENERATION PROPERTIES OF $Gd_{1-x}Ti_xNi$ ($0 < x < 1$)

K.Kluziak¹, V.Pavlyuk^{1,2}

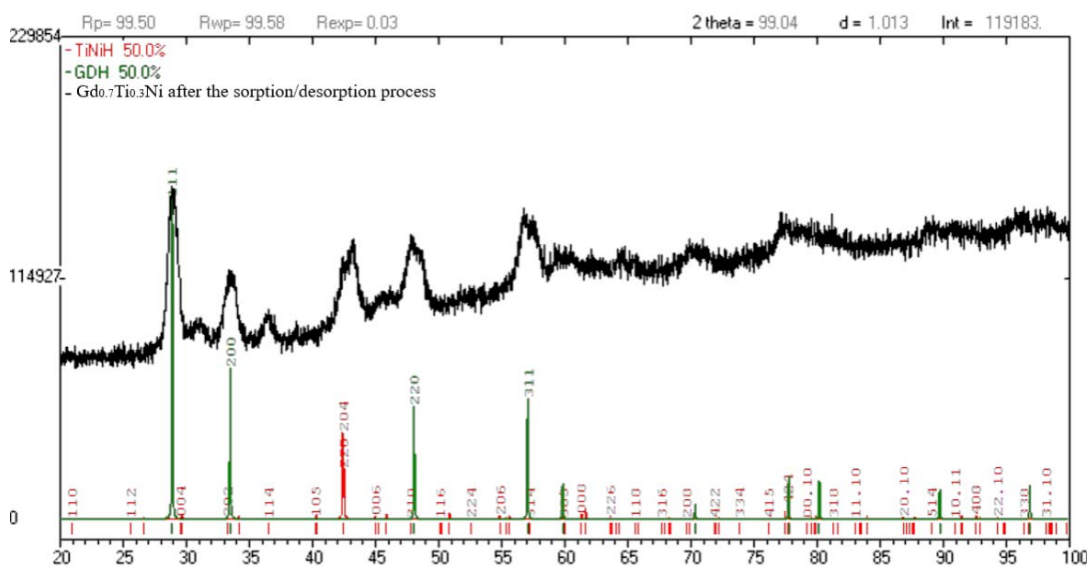
¹*Institute of Chemistry, Jan Dlugosz University in Czestochowa, al. Armii Krajowej 13/15, 42-200 Czestochowa, Poland, e-mail: karolina_kluziak@o2.pl*

²*Department of Inorganic Chemistry, Ivan Franko National University of Lviv, Kyryla and Mefodiya str. 6, 79005 Lviv, Ukraine*

Rare-earth based alloys are the most popular combinations for creating electrode materials for nickel-hydride cells. Good hydrogen storage properties of rare-earth metals are known, thanks to the introduction of the third component in the form of titanium the kinetics of hydrogen sorption/desorption have been improved and corrosion resistance has been increased.

The synthesized $Gd_{1-x}Ti_xNi$ ($0 < x < 1$) alloys were studied by various experimental techniques, such as XDR, SEM, EPMA, gas and electrochemical hydrogenations.

Our research showed that partial replacement of gadolinium atoms by titanium improves the sorption properties of this system. Moreover, a solid solution based on GdNi and TiNi is formed, which was confirmed by tests carried out using a powder diffractometry method. X-ray data carried out after the hydrogenation process show that the hydride phase $Gd_{1-x}Ti_xNiH_{1.6}$ crystallizes in a orthorhombic structure (*Cmcm* space group, $a=3.951 \text{ \AA}$, $b=11.055 \text{ \AA}$, $c=4.562 \text{ \AA}$) Diffraction data for dehydrogenated samples (after desorption test) show that the $Gd_{1-x}Ti_xNiH_{1.6}$ hydride phase decomposes on a two GdH_2 (cubic) and $TiNiH_x$ (tetragonal) hydride phases (Fig.1).



Financial support from the National Science Centre, Poland NCN (No 2017/25/B/ST8/02179)

CsPbBr₃ PARTICLES CREATION IN KBr MATRIX

M. Dendebera¹, Ya. Chornodolsky¹, O. Antonyak¹, A. Zhyshkovych¹,
T. Demkiv¹, V. Mikhailik², V. Vistovsky¹, A. Voloshinovskii¹

¹ Ivan Franko National University of Lviv, 8 Kyryla and Mefodiya str., 79005, Lviv, Ukraine.

² Diamond Light Source, Harwell Campus, Didcot, OX11 0DE, UK.

Single crystals and nanoparticles of the perovskite family attract general attention of scientists as new class of materials with remarkable optical and electronic properties enabling creation of advanced optoelectronic devices, photoconverters, detectors of ionizing radiation, etc. The luminescent mechanism in the crystals and nanoparticles of perovskites remains a topic of continuous interest. The study of the luminescent parameters of perovskite microcrystals and nanoparticles embedded in dielectric crystals or polymers allows to elucidate the relaxation processes due to reduced impact of surface.

Micro- and nanosized CsPbBr₃ particles embedded in the KBr matrix were obtained by growing KBr crystals doped with 1 mol.% CsPbBr₃. The spectral kinetic parameters of the luminescence of CsPbBr₃ particles embedded in KBr under excitation by laser diode with $\lambda = 405$ nm were studied in the temperature range of 14-300 K. The luminescence of CsPbBr₃ microcrystals at 77 K reveals narrow near-edge bands peaked at 530.6 and 535.7 nm, exhibiting the luminescence decay time constants in the nanosecond range. The bands can be tentatively assigned to direct exciton at the R point of Brillouin zone and indirect transitions from Rashba valleys. The fast (~ 1.8 ns) and slow (~ 80 ns) components of the luminescence decay kinetics at $T = 50$ K is attributed to the radiative transitions from singlet and triplet states of the exciton split by exchange interaction. The doublet structure of the near-edge luminescence is characteristic for bulk CsPbBr₃ samples [1], on the other hand, the samples reveal activation barrier for the luminescence quenching equal to 180 meV, that is characteristic for the luminescence of nanoparticles. This suggests the formation during the synthesis of embedded CsPbBr₃ particles in the form of plates or nanowires with at least one of the sizes in the nano- or microscale. The shift of the near-edge luminescence band at 77 K from 529 nm in a single crystal to 530.6 nm in embedded microcrystals can be attributed to the hydrostatic pressure of the matrix leading to the shift of CsPbBr₃ microcrystal energy levels. Besides above free exciton luminescence the wide luminescence band with the long decay time constant at 560 nm supposedly is assigned to the emission of self-trapped excitons and the recombination of electronic excitations on defects.

[1] M. Dendebera et al. *J. Luminescence*. 225 (2020) 117346.

FAST COMPOSITE POLYSTYRENE SCINTILLATORS WITH EMBEDDED NANOPARTICLES

T. Demkiv, V. Vistovsky, M. Dendebera, L. Demkiv,
A. Zhyshkovych, A. Voloshinovskii

Ivan Franko National University of Lviv, Lviv 79000,
8 Kyryla i Mefodiya str., Ukraine

The growing needs for radiation control for the radioactive materials movement, monitoring of the radiation background over large areas, etc., require the creation of new materials for detecting ionizing radiation, which would be technological, cheap to manufacture and would demonstrate high light output and fast operation. One of the directions of such materials creation is development of polystyrene composite scintillators with embedded nanoparticles of inorganic compounds. The composites exhibit the high yields and short luminescence decay times proper for polystyrene scintillators and the high absorption capacity of inorganic scintillators [1]. One of the main ways of scintillations in such composites is associated with the transfer of absorbed energy by nanoparticles to polystyrene matrix via the external photoeffect mechanism – the escape of an electron from the nanoparticle into the environment of the polystyrene matrix. To provide additional convincing evidence of the electronic mechanism excitation of luminescent polystyrene, a study of the luminescence of polystyrene composites with embedded LaF₃ nanoparticles which do not demonstrate effective luminescence in the absorption of polystyrene and its activators under the X-rays action is performed.

Thin-film polymer scintillators based on scintillation polystyrene with n-terphenyl and POPOR activators and embedded LaF₃ nanoparticles of different sizes are obtained and the spectral-kinetic properties of their luminescence are studied. It was found, that the luminescence spectra of polystyrene composites with embedded LaF₃ nanoparticles consist of two emission bands with maxima of peaked at 350 and 420 nm, which correspond to the luminescence of polystyrene activators n-terphenyl and POPOP, respectively. The registration efficiency of ionizing radiation of polystyrene composite with embedded non-luminescent nanoparticles LaF₃ (40 wt.%) increases by an order of magnitude compared with the efficiency of polystyrene scintillator without nanoparticles.

The luminescence decay kinetics of composites is characterized by decay time constant of ~3 ns that is characteristic for a polystyrene scintillator without nanoparticles. The presence of luminescent response of nanocomposite scintillators with embedded non-luminescent LaF₃ nanoparticles gives reason to state that the main mechanism of scintillation in the nanocomposite is the electronic mechanism.

[1] T. M. Demkiv et al., Nucl. Instruments Methods Phys. Res. 810 (2016) 1–5.

ORAL PRESENTATIONS

NANOSTRUCTURED DIAMOND-METAL COMPOSITES AS POTENTIAL ADVANCED MATERIAL

Artemenko A.¹, Babčenko O.¹, Remeš Z.¹, Aubrechtová Dragounová K.¹,
Wågberg T.², Lundberg P.², Jia X.², Kromka A.¹

¹ Institute of Physics of the Czech Academy of Sciences, Cukrovarnická 10, 16200 Prague 6, Czech Republic

² Department of Physics, Umeå University, Linnaeus väg 24, Umeå 90187, Sweden

Nanocrystalline diamond (NCD) films are known due to their controllable electrical and excellent optical properties. Recently, NCD films are studied as a promising platform for the development of opto-electronic devices (solar cells, photodiodes, LED lights, etc).

In this work we present the investigation of potential opto-electrical properties of the flat (RMS roughness ~ 20 nm) and nanoporous (nanostructured) NCD films grown on Si or optically transparent (JGS1) substrates with different amount of embedded Ag nanoparticles (AgNPs). The AgNPs with the size from 5 to 100 nm were deposited on the top of diamond films. After AgNPs deposition, the samples were re-grown with NCD film (150-200 nm) for embedding AgNPs into the diamond film. The cross-section SEM images showed that for nanoporous diamond AgNPs are distributed in the volume of diamond pores when for flat NCD films particles reminded close to the surface. The UV-ViS measurements of the flat and nanoporous NCD films with/without embedded AgNPs showed the difference between the samples. The correlation of UV-ViS results with Raman, SEM and XPS data will be discussed.

The work is supported by Operational Programme Research, Development and Education financed by European Structural and Investment Funds and the Czech Ministry of Education, Youth and Sports (Project No. CZ.02.2.69/0.0/0.0/18_053/0016627).

CONDUCTIVITY OF CsPbBr₃ AT AMBIENT CONDITIONS

L.-I. Bulyk^{1,2}, T. Demkiv¹, O. Antonyak¹, T. Malyi¹, R. Gamernyk¹,
V. Vistovskyi¹, A. Voloshinovskii¹, A. Suchocki²

¹ Ivan Franko National University of Lviv, 8a Kyryla i Mefodiya St., 79005, Lviv, Ukraine

² Institute of Physics, Polish Academy of Sciences, Warsaw 02-668, Poland

All-inorganic metal halide perovskite materials have drawn huge interest of research society in recent years. Due to their unique properties, these perovskites are perspective to be used for LEDs, photodetectors, laser mediums, solar cells, scintillators, etc. In this study the CsPbBr₃ crystals are grown by the Stockbacher method from the melt. Resistance of samples prepared for electrical measurements by different methods are measured. Two samples are cleaved from bigger piece, and one sample is polished in order to reach regular shape.

Studied material is known to be very soft, and in addition, due to interaction with water, it may change its structural phase. In order to check the phase, Raman measurements are performed for as-synthesized sample, polished and cleaved samples. Obtained Raman spectra are very similar for all samples. The only difference is in relative intensity of vibration modes in the vicinity of 127 - 175 cm⁻¹. That difference may be caused by appearance of additional Cs₄PbBr₆ phase in polished sample.

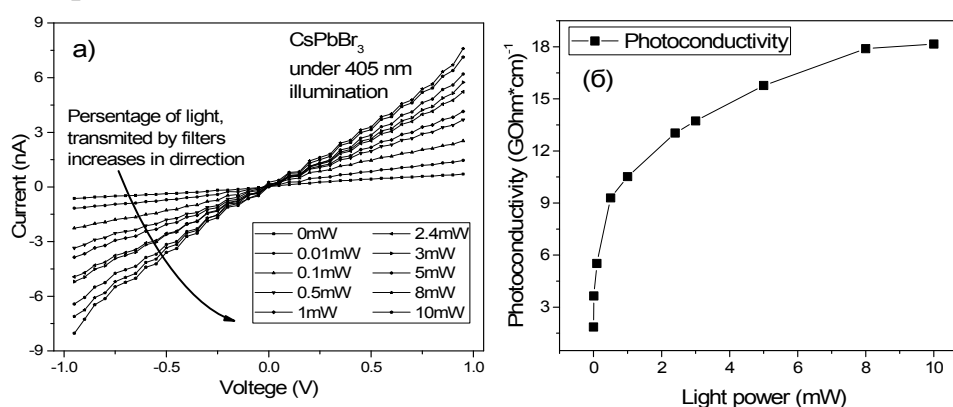


Figure 1. Photoconductivity of CsPbBr₃ under 405 nm laser illumination.

Contacts on cleaved samples are prepared parallel and perpendicular to axis perpendicular to cleaving surface. Resistance along that axis are revealed to be almost two times smaller, then resistance parallel to the axis. The dependence of the current value on current direction is analyzed.

The parameters (the applied voltage, the illuminance of the sample), which provides the linearity of the volt-ampere characteristic at illumination by a laser 405 nm (Fig. 1a) are determined. A nonlinear increase of current with saturation output with increasing of illuminance are revealed (Fig. 1b).

[1] J. van der Geer, J.A.J. Hanraads, R.A. Lupton, J. Sci. Commun. 163 (2000) 51-59.

[2] W. Strunk Jr., E.B. White, The Elements of Style, third ed., Macmillan, New York, 1979.

METAL CORROSION TESTING IN THE ENVIRONMENT

R. Dzhala¹, B. Verbenets², V. Dzhala³, B. Horon⁴, V. Lozovan⁵

G.V. Karpenko Physico-Mechanical Institute of National Academy of Sciences of Ukraine,
Department of electrophysical methods of non-destructive testing. 5 Naukova st., 79060 Lviv
¹ dzhala.rm@gmail.com, ² bohdan_v@meta.ua, ³ vjoe@ipm.lviv.ua

The main criterion for corrosion protection of metal structures in an electrically conductive medium is considered polarization potential U_{PP} .

The potential difference U_{MG} between the metal surface and the reference electrode (RE) measure to determine the U_{PP} . But this U_{MG} consists of a polarization component and an ohmic voltage drop IR due to the passage of current I through the effective resistance R between the RE and the test metal.

Compensatory and relaxation methods are known for removing the ohmic component of U_{IR} , which have disadvantages. These shortcomings are deprived of a new method for determining the PP by measuring constant and alternating electrical voltages between the metal and the RE (U_{MG} and V_{MG}) and between the electrodes in the environment (U_{GG} and V_{GG}) [1]. PP is determined by formulas

$$U_{PP} = U_{MG} - U_{IR}, \quad \text{where the ohmic component } U_{IR} = V_{MG} U_{GG} / V_{GG}.$$

Alternating voltages V_{MG} and V_{GG} can be measured at the frequency of the alternating component (harmonics) of the cathodic protection installation or a special generator. The V_{GG} / U_{GG} ratio is the measured harmonic coefficient.

Electric currents have valuable information about corrosion processes of metal in conductive medium. Current distribution is most sensitive to composition of environment and insulation state.

For increasing of efficiency and informativeness of corrosion state testing in underground pipelines was researches and development of electromagnetic method and devices for non-contact measurements of currents [2, 3].

- [1] R.M. Dzhala, B.Ya. Verbenets', M.I. Mel'nyk, A.B. Mytskyk, R.S. Savula, O.M. Semenyuk. New methods for the corrosion monitoring of underground pipelines according to the measurement of currents and potentials. Materials Science. Vol. 52, № 5. March 2017. P. 732-741.
- [2] Technical diagnostics of materials and structures: Reference manual / Ed.-in-chief Z.T. Nazarchuk. Vol.4: Electrophysical methods for nondestructive testing of defects in structural elements / Dzhala R.M., Dzhala V.R., Ivasiv I.B., Rybachuk V.G., Uchanin V.M. Lviv: Prostir-M. 2018. 356 p. (In Ukr.)
- [3] R. Dzhala, V. Dzhala, B. Horon, O. Senyuk, B. Verbenets. Information Technology of Surveys and Diagnostics of Underground Pipelines. XIth International Scientific and Practical Conference on Electronics and Information Technologies (ELIT). Lviv, September 16-18, 2019. Proceedings. P. 214-217.

QUANTUM-TOPOLOGICAL ANALYSIS OF STOCK MARKET DATA

Solomiia Leno

¹leno@ucu.edu.ua

Stock market prices prove themselves as strong indicators of wellness not only of a single company but of the whole country and even the whole world. These days, after COVID-19 pandemic started, the stock market lives in a period called the stock market crash. Many people are interested in predicting such an event and thus being able to overcome them as it brings a lot of damage to everyone.

This paper addresses the problem of efficient implementation of algorithms for detecting stock market crashes. The proposed solution is based on implementing the persistent homology approach [1] by tools of quantum computing [2][3]. Main idea is that the nature of quantum computations allows one to perform highly-dimensional analysis in a more efficient way as well as process more data than classical computers' implementations.

This algorithm was tested on data on The S&P 500 Industrial Index during eight historical market crashes [4] including the current one, caused by COVID-19. Due to flaws of quantum nature, the results on real-life data show around 71% of accuracy while the results of classical implementations show accuracy of 92%.

[1] Fugacci, Ulderico & Scaramuccia, Sara & Iuricich, Federico & De Floriani, Leila. Persistent homology: a step-by-step introduction for newcomers. (2016).

[2] Lloyd, Seth & Garnerone, Silvano & Zanardi, Paolo. Quantum algorithms for topological and geometric analysis of big data. Nature Communications. (2014)

[3] Vakarchuk I. Quantum mechanics. Lviv State University of Ivan Franko (1998). 614.

[4] Yahoo! Finance. S&P 500 (^GSPC). Historical data. (2020)

FORMATION OF NANOPHASE IN THE AMORPHOUS MATRIX OF THE $\text{Co}_{77}\text{Si}_{11}\text{B}_{12}$ ALLOY DURING NON-ISOTHERMAL HEATING

Lopachak M.M.¹, Boichyshyn L.M.¹, Nosenko V.K.²,
Hertsyk O.M.¹, Kovbuz M.O.¹

¹ Ivan Franko National University of Lviv, Kyryla i Mefodia 6, 79005 Lviv, Ukraine

² G.V. Kurdyumov Institute for Metal Physics of the National Academy of Academy of Science of Ukraine, Academician Vernadsky Boulevard 36, UA-03142 Kyiv, Ukraine

Amorphous metal alloys (AMA) based on cobalt have unique physicochemical properties, in particular special magnetic properties, which is why they are used for recording and storage of information [1]. Controlled synthesis of nanocomposites “amorphous metal matrix/nanocrystal Co” is a significant factor because the hcp-Co structure has a high anisotropic magnetic coercivity, which makes the alloy better for magnetic recordings, while fcc-Co is useful as soft magnetic material [2]. Based on the curve of heat release on heating (Fig.1), obtained by the differential scanning calorimetry (DSC), it is seen that in AMA $\text{Co}_{77}\text{Si}_{11}\text{B}_{12}$ in the range of 700 - 900 K there are 3 structural transformations associated with the formation of clusters and crystalline phases. The Matusita model was used to determine the kinetic parameters of the process of nanocrystals formation in the amorphous matrix of the investigated alloy. According to the average value of the growth parameter m , it was determined that the AMA's crystallization process of the Co-Si-B system depends on the heating rate and the nature of the alloying application. The growth of Co nanocrystals in AMA $\text{Co}_{77}\text{Si}_{11}\text{B}_{12}$ at heating rates of 10 and 20 K / min occurs at a 3-dimensional mechanism, and the value of $p = 0.5$ indicates diffusion-controlled crystallization.

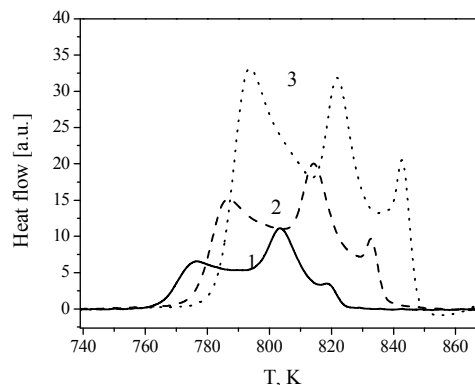


Figure 1: DSC curves of $\text{Co}_{77}\text{Si}_{11}\text{B}_{12}$ at three different heating rates: 1 – 5 K/min; 2 – 10 K/min; 3 – 20 K/min.

- [1] S. Atalay, N. Bayri G., J. Magn. Mater. 272–276 (2004) 1365-1367.
[2] V.A.P.O. Shea, I.P.R. Moreira, A. Roldán, F. Illas, J. Chem. Phys. 133 (2010) 8.

PHOTOELASTIC PROPERTIES OF K_2SO_4 DOPED WITH COPPER

V. Y. Stadnyk¹, R. B. Matviiv¹, R.S. Brezvin¹, P.A. Shchepanskyi^{1,2}

¹ Ivan Franko National University of Lviv, Dragomanova St., 19, 79005 Lviv, Ukraine
e-mail: vasylstadnyk@ukr.net

² Jan Dlugosz University in Częstochowa, Al. Armii Krajowej 13/15, 42-200 Częstochowa, Poland

Potassium sulfate (PS) crystals K_2SO_4 have specific physical properties allowing them to be used in electromagnetic radiation control devices. In order to control the physical properties of the crystals and expand the limits of their applications the introduction of substitutional impurities was proposed. Therefore, the purpose of this work is to investigate the effect of Cu^{2+} transition metal impurity on the photoelastic properties of PS crystals.

Crystals for investigation were obtained by slow-evaporation method at room temperature from an aqueous solution of salts of pure K_2SO_4 and copper sulfate pentahydrate $CuSO_4 \cdot 5H_2O$, the mass of which was 1.7% and 3% of the total mass of dissolved salts. Based on the experimental results of the refractive properties of the crystals, the combined π_{im}^0 and absolute π_{im} piezo-optic coefficients were calculated. A slight decrease of the obtained coefficients in comparison with that of pure PS crystal were detected, indicating an increase in the mechanical stiffness of the doped crystals. A significant dispersion dependence of the piezo-optic coefficients ($d\pi_{im}^0/d\lambda \approx 8...11$ Br/nm) was revealed. The matrices of the elastic-optical coefficients p_{in} for crystals with 1.7% and 3% of copper impurity are constructed. It is shown that the elastic-optical effect, as well as the piezo-optical one, is quite noticeable – the largest values of p_{in} are in the range from 0.20 to 0.30.

The acousto-optical (AO) efficiency M_2 of doped PS crystals is evaluated on the basis of the elastic-optic coefficients, velocity of acoustic waves, crystal density and their refractive indices. It is established that the maximum values of the coefficients of acousto-optic interaction of doped PS crystals are almost an order of magnitude higher than that of quartz and strontium borate, suitable for AO modulation of light in the ultraviolet spectral range. This indicates that doped potassium sulfate crystals, due to their short-wavelength limit of the transparency region ~ 170 nm, can be used for AO modulation of ultraviolet radiation.

REFRACTIVE AND SPECTRAL-BARIC PROPERTIES OF K₂SO₄ CRYSTALS DOPED WITH COPPER

V. Y. Stadnyk¹, R. B. Matviiv¹, P. A. Shchepanskyi^{1,2}, M. Ya. Rudysh^{1,2}

¹ Ivan Franko National University of Lviv, Dragomanova St., 19, 79005 Lviv, Ukraine
e-mail: vasylstadnyk@ukr.net

² Jan Długosz University in Częstochowa, Al. Armii Krajowej 13/15, 42-200 Częstochowa,
Poland

Crystals of potassium sulfate (PS) K₂SO₄ are typical representatives of a dielectric crystals and are characterized by a phase transition (PT) at $T = 860$ K from the center-symmetric paraelectric phase (space group symmetry $D_{6h}^6 - P6_3 / mmc$) to the orthorhombic ferroelastic phase (space group symmetry $D_{2h}^{16} - Pmcn$). PS crystals are widely used in optoelectronics, crystal-optics sensing (sensors of temperature, pressure and electromagnetic radiation) and for acousto-optical modulation of ultraviolet radiation. Their application field is constantly expanding and one of the effective mechanisms for changing the physical parameters of crystals is the introduction of impurities. The purpose of this work is to investigate the effect of Cu²⁺ impurity on PS crystals.

Crystals for the investigation were obtained by slow-evaporation method at room temperature from an aqueous solution of salts of pure K₂SO₄ and copper sulfate pentahydrate CuSO₄·5H₂O, the mass of which was 1.7% and 3% of the total mass of dissolved salts. Investigation of the spectral dependences of the refractive indices n_i of PS crystals with copper impurity showed that introduction of the impurity leads to a decrease in n_i by about $1-3 \times 10^{-3}$, and the relationships between their values $n_z > n_x > n_y$ and the dispersion variations $dn_z/d\lambda > dn_x/d\lambda > dn_y/d\lambda$ remain unchanged. It is shown that the introduction of the dopant causes the shift in the position of UV oscillators centers λ_{01} to the long-wavelength region of the spectrum and the decrease of strain of the respective oscillators.

It is found that the introduction of the impurity slightly changes the absolute value of birefringence Δn_i , without changing the nature of its dispersion $|\partial \Delta n_x / \partial \lambda| > |\partial \Delta n_y / \partial \lambda| > |\partial \Delta n_z / \partial \lambda|$. The introduction of impurity increases the absolute values of birefringence by 5.2×10^{-4} and 6.8×10^{-4} in the X - and Y -directions and decreases it by 1.4×10^{-4} and 2.1×10^{-4} in the Z -direction for impurity contents 1.7% and 3.0%, respectively. It is established that the action of uniaxial pressure along the X -axis leads to an increase in Δn_z and a decrease in Δn_y ; along the Y axis, the birefringence Δn_z decreases, and Δn_x increases, and at uniaxial pressure along the Z -axis, Δn_x increases, and Δn_y decreases.

INVESTIGATION OF OPTICALLY ANISOTROPIC MgZnO/6H-SiC AND MgZnO/Al₂O₃ STRUCTURES BY INFRARED SPECTROSCOPY METHOD

O.V. Melnichuk¹, Ye.F. Venger², I.V. Venger², L.Yu. Melnichuk¹,
N.O. Korsunskaya², L.Yu. Khomenkova^{2,3}

¹Mykola Gogol State University of Nizhyn,

2 Hrafska Str., Nizhyn 16600, Ukraine, e-mail: mov310310@gmail.com

²V. Lashkaryov Institute of Semiconductor Physics of NAS of Ukraine,
41 Pr. Nauky, 03650 Kyiv, Ukraine

³National University "Kyiv-Mohyla Academy", 2 Skovorody str., Kyiv 04070, Ukraine

During the last years, the interest to MgZnO films grown on dielectric and semiconductor optically-isotropic and optically-anisotropic substrates had been increased significantly due to their application in different types of chemical and radiation detectors as well as in optoelectronic devices operating on the use of the bulk and surface waves. In present work, the Mg_xZn_{1-x}O films situated on optically-anisotropic 6H-SiC and Al₂O₃ substrates were studied by means of infrared reflection (IRR) spectroscopy. The specular infrared reflectivity of these structures in the range of "residual rays" of the film and substrate was studied versus film thickness and Mg content.

To simulate the IRR spectra of Mg_xZn_{1-x}O/Al₂O₃ and Mg_xZn_{1-x}O/6H-SiC structures for the orientation of electrical field $E \perp C$, we have applied the model of additive contribution of oscillators to dielectric permittivity of Mg_xZn_{1-x}O, 6H-SiC and Al₂O₃ materials using self-consistent parameters for ZnO, MgO, SiC and Al₂O₃. Optical and electro-physical parameters were estimated using the simulation. The validity of this approach was proved by the methods of polariton spectroscopy and Hall effect as well as by the agreement of obtained results with those published by other research groups.

For Mg_xZn_{1-x}O/6H-SiC structures, the spectral ranges of the sensitivity of IRR coefficient toward the variation of film thickness, doping level of the film and the substrate was shown using Kramers-Kronig relation. It was shown that the parameters of phonon and plasmon subsystems of Mg_xZn_{1-x}O of different composition can be obtained by means of dispersion analysis of IRR spectra. The application of this approach was discussed for the films with $x=0.2$.

Theoretical model allowed the determination of the spectral ranges of the existence of surface polaritons in Mg_xZn_{1-x}O/6H-SiC structures was developed. A 3D surface of attenuated total reflection was obtained that permitted the demonstration of interaction of phonon and plasmon subsystems of Mg_xZn_{1-x}O film and 6H-SiC.

SIMULATION OF COVID-19 CONTAINMENT APPROACHES BY SEIR MODEL

Y. Ilnytskiy¹, Y. Pasichnyk², A. Botsula³, M. Morhunenko⁴, O. Farenjuk⁵

¹ iln@icmp.lviv.ua

² pasichnyk.y@ucu.edu.ua

³ botsula@ucu.edu.ua

⁴ morgunenko@ucu.edu.ua

⁵ indrekis@icmp.lviv.ua

The world faced the COVID-19 needs understanding how virus spreading can be controlled or terminated. While vaccines are actively developed, probably, the vaccine would not be available until next year [1]. So, quarantine and social distancing are the main methods available to authorities. Modeling is the main method to evaluate possible interventions before reliable data are available. We used the SEIR model [2] (Susceptible – Exposed – Infectious – Removed) extended with the new state “Isolated”, that can be described with the following parameters: death rate, incubation period and rate of asymptomatic disease [3]. Also, the SEIR model was tested in Kenya [4] and Wuhan [5] on COVID-19. Parameters of the pandemic were taken from [6]. The simulation allowed us to estimate the optimal number of isolation places in hospitals for the different death rates.

[1] Tung Thanh Le, et al., "The COVID-19 vaccine development landscape", *Nature Reviews Drug Discovery*, vol. 19, 305-306, 09 April 2020.

[2] W. O. Kermack, A. G. McKendrick, "A Contribution to the Mathematical Theory of Epidemics", *Proceedings of the Royal Society of London. Series A, Containing Papers of a Mathematical and Physical Character*, 115(772), 700–721, 1927; *Bulletin of Mathematical Biology*. 53 (1–2): 33–55, 1991.

[3] Г.І. Ільницький, Я.М. Ільницький, “Моделювання поширення захворювань із мультирезистентними збудниками”, “Наукоємні технології”, vol. 28, No 4, 2015.

[4] Duncan K. Gathungu, et al., “Modeling the Effects of Non-Pharmaceutical Interventions on COVID-19 Spread in Kenya”, *medRxiv* 2020.05.14.20102087.

[5] Qianying Lin et al., “A conceptual model for the coronavirus disease 2019 (COVID-19) outbreak in Wuhan, China with individual reaction and governmental action”, *International Journal of Infectious Diseases*, vol. 93, 211-216, April 2020.

[6] Coronavirus disease 2019 (COVID-19) situation report, World Health Organization, 2 April 2020.

SYNTHESIS, CHARACTERIZATION AND BIOLOGICAL APPLICATIONS OF POLYMER GRAFTED BRUSHES AND THEIR METALIC NANOCOMPOSITES

Nastyshyn S.¹, Stetsyshyn Yu.², Lishchynskiy O.², Shymborska Y.², K. Awsiuk¹, Budkowski A¹. and Raczkowska J.¹

¹Smoluchowski Institute of Physics, Jagiellonian University, Łojasiewicza 11, 30-348 Krakow, Poland

² Lviv Polytechnic National University, St. George's Square 2, 79013 Lviv, Ukraine

Polymer grafted brushes are a class of polymers in which one of the molecule's ends is grafted to a solid substrate. To fabricate the polymer grafted brushes we employ the surface initiated atom transfer radical polymerization.

We fabricated and studied physicochemical properties of three types of polymer grafted brushes: poly(4-vinylpyridine) (PVP), poly(di(ethylene glycol)methyl ether methacrylate (POEGMA), and poly(4-vinylpyridine-*co*-oligo(ethylene glycol)ethyl ether methacrylate (P(VP-*co*-OEGMA))) as well as nanocomposite POEGMA brush with embedded silver nanoparticles. The temperatures of conformational transitions for mentioned polymer grafted brushes are established with temperature measurements of the water contact angle. Chemical compositions of fabricated materials are proved with the time of flight secondary ion spectrometry. The formation of silver nanoparticles is studied with the atomic force microscopy.

The PVP, POEGMA, and P(VP-*co*-OEGMA) brushes are used as substrates to study the proliferation of the granulosa cells and oocyte-cumulus complexes on them. Also, we have studied the antibacterial properties of silver nanoparticles embedded in POEGMA brush below and above the conformational transition temperature concerning the Gram-positive and Gram-negative bacteria as well as the cytotoxicity concerning human skin cells and cancer melanoma cells.

We have established that only the P(VP-*co*-OEGMA) copolymer coating provides the formation of dispersed and small but numerous cell conglomerates as well as high cumulus expansion in oocyte-cumulus complexes with highly homogeneous cumulus layers surrounding the oocytes. Also, we have shown that the nanocomposite POEGMA and silver nanoparticles of the appropriate amount shows the thermo-switchable antibacterial properties without cytotoxicity against human skin cells, and has slight, but detectable, anticancer properties.

CRYSTAL STRUCTURE OF Mg_{0.23}NiSn_{1.77}

Pavlyuk N.^{1,2}, Dmytriv G.¹, Ciesielski W.², Pavlyuk V.^{1,2}, Ehrenberg H.³

¹*Department of Inorganic Chemistry, Ivan Franko National University of Lviv, Kyryla and Mefodiya str. 6, 79005 Lviv, Ukraine*

²*Institute of Chemistry, Jan Dlugosz University in Czestochowa, al. Armii Krajowej 13/15, 42-200 Czestochowa, Poland,*

³*Karlsruhe Institute of Technology (KIT), Institute for Applied Materials (IAM), Hermann-von-Helmholtz-Platz 1, D-76344 Eggenstein-Leopoldshafen Germany*

All preparation steps were performed in a glove box under dried argon atmosphere. Melting of metals was carried out within sealed tantalum crucibles in an induction furnace at 1100 °C. The single crystal was investigated by means of Oxford Diffraction Xcalibur diffractometer with CCD detector. The crystal structure of Mg_{0.23}NiSn_{1.77} intermetallic phase was successfully solved by direct methods and refined in space group *Fddd*. The refined lattice parameters are: $a = 5.1196(3) \text{ \AA}$, $b = 9.0845(4) \text{ \AA}$, $c = 17.7358(9) \text{ \AA}$. Atomic coordinates and thermal displacement parameters are listed in Table 1. Finally, all parameters are refined to $R_1 = 0.014$ and $wR_2 = 0.049$ using 221 independent reflections with $I > 2\sigma(I)$. Significant differences in composition and unit cell dimensions of Mg_{0.2}NiSn_{1.8} comparing to previously known phase Mg_{1.6}NiSn_{0.4} ($a = 5.146 \text{ \AA}$, $b = 9.11 \text{ \AA}$, $c = 17.77 \text{ \AA}$) [1] are observed. These differences indicate that Mg_{0.23}NiSn_{1.77} and Mg_{1.6}NiSn_{0.4} are two different phases of the Mg-Ni-Sn system that are formed in different concentration regions.

Table 1. Fractional atomic coordinates, isotropic anisotropic displacement parameters (\AA^2)

Atoms	Sites	x/a	y/b	z/c	$U_{\text{iso}}^*/U_{\text{eq}}$	<i>S.O.F.</i>
Sn1	<i>16g</i>	1/8	5/8	0.21419	0.0113(3)	0.77(1)
Mg1	<i>16g</i>	1/8	5/8	0.21419	0.0113(3)	0.23(1)
Sn2	<i>16g</i>	5/8	5/8	0.25243	0.0120(2)	1.00
Ni3	<i>16f</i>	7/8	0.53390	3/8	0.0094(3)	1.00
Atoms	U_{11}	U_{22}	U_{33}	U_{12}	U_{13}	U_{23}
Sn1	0.00951	0.01026	0.01434	0.00090	0.00000	0.00000
Mg1	0.00951	0.01026	0.01434	0.00090	0.00000	0.00000
Sn2	0.01193	0.01110	0.01310	0.00086	0.00000	0.00000
Ni3	0.01005	0.00886	0.00942	0.00000	-0.00237	0.00000

[1]. Hlukhyy V., Rodewald U.C., Püttgen R. *Z. Anorg. Allg. Chemie.* (2005), 631, 2997-3001.

Funding for this research was provided by National Science Centre, Poland (No. 2017/25/B/ST8/02179)

FREQUENCY SPECTRUM OF SURFACE PLASMON-POLARITON WAVES: INFLUENCE OF COULOMB CORRELATIONS

Kostrobij Petro¹, Markovych Bogdan², Polovyi Vitalii³

^{1,2,3} 5 Metropolian Andrey str., Building 4, Room 213, 79013, Lviv, Ukraine.

The model that describes the influence of Coulomb correlations [1] on a frequency spectrum of plasmon-polariton waves [2] in electroneutral structures dielectric/metal/dielectric is investigated. It is shown that for atomically thin metal films (ATMF), such correlations affects both the quantum-dimensional behavior of the frequency spectrum as a function of the thickness of the metal film and significantly improves the correlation of theoretical calculations and experiment compared to the case of correct taking into account of the electroneutrality condition [3] (Fig. 1).

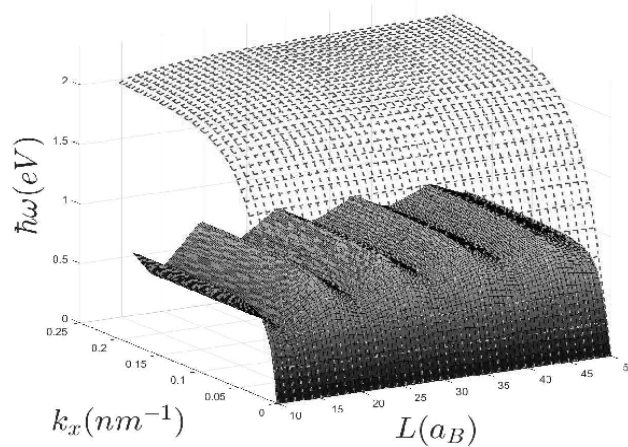


Figure 1: Comparison of the dependences of the frequency spectrum on the ATMF thickness for the structure SiO/Ag/Si dashed surface - the condition of electroneutrality; solid surface - Coulomb correlations.

- [1] P. Kostrobij, B. Markovych, Effect of Coulomb interaction on chemical potential of metal film. *Phil. Mag.* 98 (21), 1991–2002, 2018.
- [2] S. Maier, *Plasmonics: Fundamentals and Application*. Springer – Verlag, 2007.
- [3] P. Kostrobij, B. Markovych, V. Polovyi, Influence of the Thickness of a Metal Nanofilm on the Spectrum of Surface Plasmons, *Math. Model. Comput.* Vol. 6, No. 2, p. 297–303, 2019.

PASSIVATION OF SIGE SURFACES BY COLLAPSING BUBBLES AT THE SURFACE/REACTIVE ETCHANT INTERFACE

Shmid V¹, A. Podolian, A. Nadtochiy, O. Korotchenkov
¹shmdvi@gmail.com

Depositing a passivation film on Si/Ge surfaces is of great interest for electronics and photovoltaics. However, standard high-temperature passivation steps, based on oxidizing at ~ 1000 °C, degrade the carrier lifetime. To improve the lifetimes in Si/Ge, here we use sonochemical treatments in chloroform (CHCl₃) and dichloromethane (CH₂Cl₂). It is suggested that these carbon sources are decomposed into hydrocarbon chains due to extreme conditions in the solvents and at the etchant/solid interfaces, as temperatures of ~ 5000 °C, pressures of ~ 50 MPa and cooling rates greater than 10^9 K/s are achieved after the growth and following collapse of cavitation bubbles [1]. The carbon atoms can then form bonds with the Si atoms thus producing long-chain species on solid Si/Ge surfaces, as evidenced by the scanning electron microscopy (SEM) images and energy-dispersive X-ray (EDX) spectra shown in Fig. 1. It is seen that an appreciable amount of carbon appears in Fig. 1(b), which is taken in the area B in (a) containing one of the surface species. An increased surface photovoltage signal (up to an order of magnitude), which is accompanied by prolonged decay times (as much as $\sim 50\%$), is observed on Si and Si/Ge surfaces. The effect is not observable in distilled water, indicating that CH-containing radicals are likely to be responsible for the observed improvements. It is suggested that the reactive Si dangling bonds revealed on the surface of Si and Si/Ge alloys are saturated by the hydrocarbon species to passivate the surface. We believe that such bubbles collapsing at the surface/reactive etchant interface can bring a treatment step used for the surface passivation in Si/Ge-based electronic devices.

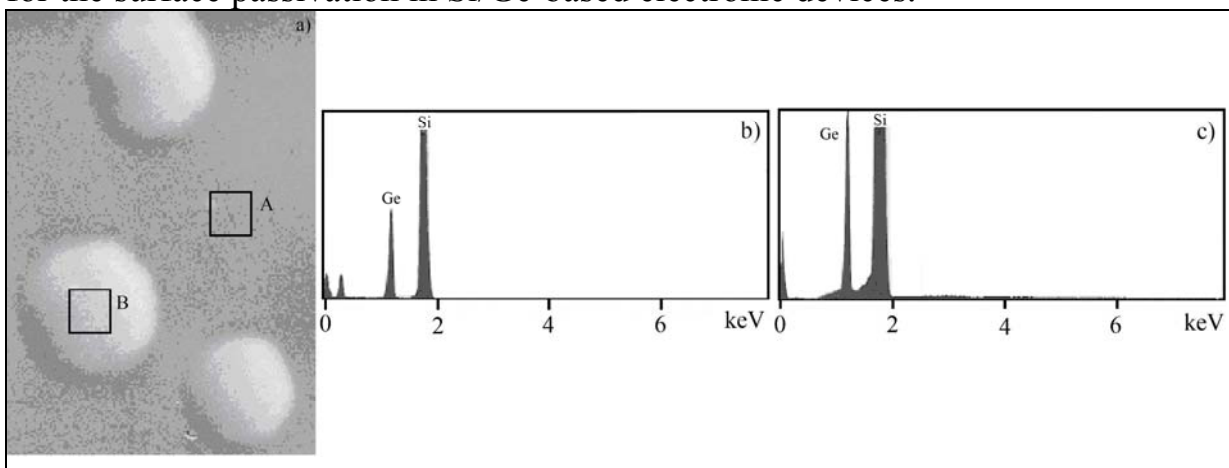


Fig. 1. (a) SEM image taken on the Si/Ge surface; (b) and (c) EDX spectra measured in the surface areas A and B marked in (a).

[1] K. S. Suslick, *Science*, 247, 1439-1445 (1990).

MOLECULAR DYNAMIC SIMULATIONS OF THE INTERLAYER STRUCTURE AT THE BOUNDARY OF METAL-SILICON SYSTEM

I. Shtablavyi, V. Plechystyy, S. Mudry

Ivan Franko National University of Lviv, Kyrylo i Mephodiy 8, 79005 L'viv, Ukraine

Silicon still is the basis of semiconductor electronics despite significant progress in the study of other types of materials. The reason for this is that silicon possesses a unique set of properties whose values are stable over time and over a wide range of temperatures. Different types of metals were used to create electrical contacts and transistors and continue to be used to form interconnects in the most advanced electronics devices. However, due to the miniaturization of electronic devices, the processes, taking place in a volume that is commensurate with the size of an atom, appear on the foreground. In particular, as a result of the intensive interaction of silicon and metals, the diffusion processes of mixing of these species in the nanoscale level can occur even at room temperature. Such interaction was studied in detail by experimental methods and attempts of such investigations by computer simulation methods have been undertaken. These studies have shown the possibility of forming eutectics and intermetallic phases on the boundary between metals and silicon as a result of heating.

To the best our knowledge, there are currently no comprehensive results of a detailed study of the annealing process of thin films of metals on the silicon surface by molecular dynamics. On the other hand, such studies will allow us to study not only the result of diffusion but also its process in time. For this reason, in this work the diffusion process of 2 – 10 gold and copper atomic monolayers on the silicon (111) surface in the temperature range 450-1150 °C was investigated.

LIGHT-MATTER INTERACTION IN GRAPHENE NANOHYBRIDS AND THEIR APPLICATION OF NANOSENSORS AND NANOSWITCHES

Mahi R. Singh

Department of Physics and Astronomy, The University of Western Ontario, London,
Canada

There is a considerable interest in developing nanoscale plasmonic devices by combining graphene with quantum emitters (QEs) and metallic nanoparticles into hybrid nanostructures. Graphene was invented theoretically by Wallace in 1947 [1] and he found that graphene is a gapless material. Later, Wallace and I found more gapless materials such as Cd_3AS_2 , HgTe which have direct band gaps [2]. On the other hand, graphene plasmons provide an attractive alternative to noble metal plasmons. It is because they exhibit much tighter confinement, small Ohmic losses and have relatively long propagation distances. The SPPs in graphene can also be tunable via electrostatic gating technique. Graphene has also emerged as a very promising candidate for THz to visible frequency applications since its plasmonic resonance frequency lies in this range. The aim of this paper is to study the light-matter interaction for these nanohybrids. We found that the coupling of surface plasmons in graphene and optical photons in the polar material produces phonon-plasmon polaritons (PPPs). On the other hand, the couplings of photons with surface plasmons of graphene produce surface-plasmon polaritons (SPPs). Using the second quantized formulation for SPPs and PPs interaction and density matrix method we have calculated photoluminescence of the quantum emitters. We show that when the exciton energy of the quantum emitter is in resonant with the SPP and PPP energies the absorption and photoluminescence in the quantum emitter are enhanced in the terahertz range. The enhancement is due to the transfer of SPP and PPP energies from the graphene flake to the quantum emitter. We have also compared our theory with photoluminescence experiments of ZnO-MGF hybrid system deposited on SiO_2 polar crystals and a good agreement between theory and experiments has been found [5]. The energy transfer from the graphene to the quantum emitter can be controlled by applying external pump lasers or stress and strain fields. This means that the energy transfer from the QDs to the graphene can be switched ON and OFF by external ultrafast laser. These are interesting findings and they can be used to fabricate switches and sensors.

*Part of this work was done with Boris Apter, Holon Institute of Technology, 58102 Holon, Israel

1. P. R. Wallace, *Phys. Rev.* 71, 622 (1947).
2. M. Singh, P. R. Wallace, *J. Phys. C* 20, 2169 (1987); *J. Phys. C* 16, 3877 (1983).
3. T. Low. and P. Avouris, *AC Nano* 8, 1086 (2014) and references therein.
4. J. Cox, M.R. Singh, G. Gumbs, M. Antón and F, Carreño, *Phys. Rev. B* 86, 125452 (2012)
5. Mahi R. Singh, M. Brzozowski² and B. Apter, *J. Appl. Phys.* 120, 124308 (2016).

NANOCRYSTALLIZATION IN RAPIDLY-QUENCHED $\text{Al}_{70}\text{Si}_{20}\text{Ni}_{10}$ ALLOY

Yulia Nykyruy, Stepan Mudry, Igor Shtablayvi, Yuriy Kulyk, Vitaliy Prunitsa
*Metal Physics Department, Ivan Franko National University of Lviv, Lviv,
Ukraine*

The physical properties of material especially at an amorphous or nanocrystalline state depend on its structure and phase composition. In turn, material structure, as well as phase composition, is depending on the production method and treatment. Using rapid quenching from a melt it is available to achieve an amorphous or nanocrystalline state of a material that is significantly preferred by its properties from a crystalline state. These states (amorphous and nanocrystalline) are metastable ones and processes of structure evolution of such materials are interesting to studying from fundamental view-point and necessary for practical application.

In this work we studied the heating-induced structure changes in the rapidly quenched $\text{Al}_{70}\text{Si}_{20}\text{Ni}_{10}$ alloy using the X-ray diffraction analysis (XRD), scanning electron microscopy (SEM) and differential thermal analysis (DTA) methods. The results of the investigation showed that the as-quenched alloy structure is amorphous-nanocrystalline. Heating-induced crystallization starts at 116.6 C. Hexagonal h-phase and Al of nanocrystalline grain size were observed at the initial crystallization process.

Previously we studied the heating-induced structure changes in the rapidly quenched $\text{Al}_{65}\text{Si}_{25}\text{Ni}_{10}$ alloy [1, 2] using the same methods. A comparison of obtained results allows supposing that Si content affects the structure formation at the quenching process and heat-induced structure evolution in Al-Si-Ni alloys.

1. Nykyruy, Y., Mudry, S., Kulyk, Y. et al. Structure and phase transformations of amorphous-nanocrystalline Al-based alloy. *Appl Nanosci* (2020). <https://doi.org/10.1007/s13204-020-01340-y>
2. Y. Nykyruy, S. Mudry, V. Prunitsa and B. Venhryn, "Structure Investigation of Rapidly Quenched $\text{Al}_{65}\text{Si}_{25}\text{Ni}_{10}$ Amorphous Alloy After Izothermal Annealing," *2020 IEEE 15th International Conference on Advanced Trends in Radioelectronics, Telecommunications and Computer Engineering (TCSET)*, Lviv-Slavske, Ukraine, 2020, pp. 993-996, doi: 10.1109/TCSET49122.2020.235587 .

POSTER SESSION

ALLOYS, INTERMETALLIC COMPOUNDS AND THEIR APPLICATIONS

THE INFLUENCE OF THERMODYNAMIC CONDITIONS OF CONDENSATION PROCESS ON PHYSICAL PROPERTIES OF SENSOR MATERIALS

Yatsyshyn B.P.¹, Domantsevich N.I.²

¹ bogdan.yatsyshyn7@gmail.com

² nina.domantzevich@gmail.com

The influence of the condensation and growth processes on the formation of the structure and electro physical properties of thin film materials based on ternary compounds with rare earth metal (La, Sc), transition metal (Fe, Co, Ni) and semiconductor Ge is considered. The condensates were obtained by the method of coordinated evaporation of the alloys in a vacuum of $2 \cdot 10^{-3}$ Pa with a condensation rate of 4 to 30 nm / s on siall substrates. Alloys with a transition metal content of 20 - 40 at. % with a tendency to amorphization as objects of research were taken.

The enthalpy of condensation formation was calculated based on the rate of growth and the magnitudes of the transition temperatures from amorphous to crystalline state. The differences of the calculated enthalpy values for the films obtained at small thermodynamic vapor saturation were calculated. These calculations were done according to the two considered models. The deviations of the enthalpy, which were calculated on the basis of formulas by crystallization temperatures ($\Delta H = T_{cr}/7,5$), deduced by Buschow K.H.J., are relate to the characteristics of materials described by anomalous temperature dependences.

The crystallization of films obtained under different thermodynamic conditions has certain kinetic features. The crystallization process occurred in an avalanche in materials obtained at high growth rates, and in the case of low growth rates– in stages, with transitions to different metastable states. At the same time, the crystallization temperature of the condensates obtained at low growth rates was shifted towards higher temperatures. The process of crystallization of films is characterized by a consistent decrease in the value of the resistivity up to the time of complete crystallization of the film material, and increasing the amount of 5d-metal in the film leads to an increase in the crystallization temperature, regardless of the conditions of condensation.

In general, the crystallization of condensates takes place in the temperature range from 500 K to 730 K. The dependence of changes in crystallization temperatures on the type and content of REM, as well as the conditions of condensation formation, are determined.

The study of the structure of the film surface confirmed the possibility of forming a defective structure under certain conditions of condensation and definite the correspondence of the obtained calculated data on the deviation of the enthalpy of formation. These thin film materials meet the anomalous electro-physical characteristics.

STRUCTURAL AND ELECTRIC CHARACTERISTICS OF $R_{1.9}Cu_{9.2}Sn_{2.8}$ COMPOUNDS ($R = Ce, Sm, Gd-Lu$)

M. Rudchenko¹, L. Romaka¹, B. Kuzhel¹, V.V. Romaka^{2,3},
M. Konyk¹, Yu. Stadnyk¹

¹Ivan Franko National University of Lviv, Kyryla and Mefodiya Str., 6, 79005, Lviv, Ukraine

²Lviv Polytechnic National University, Ustyianovycha Str. 5, 79013, Lviv, Ukraine

³Leibniz Institute for Solid State and Materials Research Dresden, Helmholtzstr. 20, 01069
Dresden, Germany

A series of isotypic $R_{1.9}Cu_{9.2}Sn_{2.8}$ compounds, where $R = Ce, Sm, Gd-Lu$, was synthesized by arc-melting, annealed at 1070 K and studied by X-ray powder diffraction and scanning electron microscopy. The $R_{1.9}Cu_{9.2}Sn_{2.8}$ stannides crystallize in a partly disordered substitution variant of the $CeNi_5Sn$ structure type (space group $P6_3/mmc$) [1, 2].

The electrical resistivity (ρ) of the $R_{1.9}Cu_{9.2}Sn_{2.8}$ compounds was measured in the temperature range 4.2-300 K employing a two-probe method. All investigated compounds exhibit a metallic-like type of conductivity. No anomaly on the $\rho(T)$ dependence for $Lu_{1.9}Cu_{9.2}Sn_{2.8}$ stannide was observed due to its Pauli paramagnetism [3]. For the compounds with magnetic rare-earths $R = Gd, Tb$, and Dy , some change of a slope on the $\rho(T)$ dependencies is observed at the transition temperature ($T_{tr} = 10.3, 9.6, 8.9$ K, respectively) which corresponds to the temperature of their magnetic ordering. The resistivity of the $Ce_{1.9}Cu_{9.2}Sn_{2.8}$ compound has a higher magnitude compared to the other $R_{1.9}Cu_{9.2}Sn_{2.8}$ stannides being about $145 \mu\Omega \cdot cm$ at 4.2 K, it reaches $172 \mu\Omega \cdot cm$ at 300 K. At low temperatures change of the slope on the $\rho(T)$ dependence is observed at 18 K which can indicate the magnetic ordering of the $Ce_{1.9}Cu_{9.2}Sn_{2.8}$ compound.

For the $R_{1.9}Cu_{9.2}Sn_{2.8}$ compounds with Ho, Er , and Tm , no anomaly on the $\rho(T)$ dependencies was observed down to 4.2 K.

- [1] V.V. Romaka, D. Fruchart, R. Gladyshevskii, N. Koblyuk, J. Alloys Compd. 460 (2008) 283-288.
- [2] V.V. Romaka, L.P. Romaka, V.Ya. Krajovskyj, Yu.V. Stadnyk, Stannides of rare earth and transition metals, Lviv Polytech. Univ. 2015., 224 p.
- [3] V. Romaka, Yu. Gorelenko, L. Romaka, Visnyk Lviv. Univ. Ser. Chem. 50 (2009) 10-17.

STRUCTURE AND PROPERTIES OF RCr₆Ge₆ GERMANIDES

L. Romaka¹, M. Konyk¹, V.V. Romaka^{2,3}, B. Kuzhel¹, Yu. Stadnyk¹

¹Ivan Franko National University of Lviv, Kyryla and Mefodiya Str., 6, 79005, Lviv, Ukraine

²Lviv Polytechnic National University, Ustyianovycha Str. 5, 79013, Lviv, Ukraine

³Leibniz Institute for Solid State and Materials Research Dresden, Helmholtzstr. 20, 01069 Dresden, Germany

A series of RCr₆Ge₆ compounds (R = Y, Gd, Tb, Dy, Ho, Er, Tm, Yb, and Lu) was synthesized by arc-melting, annealed at 1070 K and characterized by XRPD and EDX analyses. Several new representatives of this series: TmCr₆Ge₆, YbCr₆Ge₆, and LuCr₆Ge₆ were found and appeared to be isotype to the previously studied RCr₆Ge₆ germanides with Y, Gd-Er, which crystallize in the MgFe₆Ge₆ structure type (space group *P6/mmm*). In addition, for ErCr₆Ge₆ and YCr₆Ge₆ compounds, a differential thermal analysis (synchronous LINSEIS STA PT 1600 thermoanalyzer) was performed and showed that they exist up 1126 K and 1120 K, respectively.

The temperature dependencies of the electrical resistivity were measured in the temperature range 11-300 K using the helium cryostat with a closed cycle (Advanced Research Systems, USA). A character of the electrical resistivity indicates a metallic type of conductivity for all studied compounds in the whole temperature region. For GdCr₆Ge₆ and TbCr₆Ge₆ the anomalies on the resistivity curves are observed at temperatures that correspond to their magnetic ordering [1,2]. In the paramagnetic region, the resistivity data of the RCr₆Ge₆ germanides can be approximated by the Bloch–Gruneisen–Mott (BGM). For YCr₆Ge₆ and LuCr₆Ge₆ the DFT modeling was performed and is in agreement with transport data.

We thank the Ministry of Education and Science of Ukraine (Project No. 0118U003609), BMBF project No. 01DK18002 and Ulrike Nitzsche for technical assistance.

- [1] J.H. Brabers, K.H.J. Buschow, F.R. de Boer, *J. Alloys Compd.* 205, 77 (1994).
[2] P. Schobinger-Papamantellos, J. Rodriguez-Carvajal, K.H.J. Buschow, *J. Alloys Compd.* 255, 67 (1997).

CRYSTAL STRUCTURE OF THE NEW TERNARY COMPOUND $\text{La}_3\text{Fe}_{6.36}\text{Zn}_{29.64}$

N. Chorna¹, O. Zelinska¹, G. Dmytriv¹, V. Pavlyuk¹,
A. Zelinskiy¹, V. Kordan¹, A. Mar²

¹*Department of Inorganic Chemistry, Ivan Franko National University of Lviv,
Kyryla i Mefodiya St. 6, 79005 Lviv, Ukraine*

²*Department of Chemistry, University of Alberta, T6G 2G2 Edmonton, Canada
nata.chorna15@gmail.com*

Investigation of the La–Fe–Zn phase diagram in a region with high concentration of zinc has revealed a new compound with tetragonal symmetry and $\sim\text{LaFe}_2\text{Zn}_{10}$ composition which may be interesting in terms of magnetic and hydrogen sorption properties.

A sample for investigation was synthesized by direct reaction of metals in evacuated fused-silica ampoules heated to 900 °C and slowly cooled to 500 °C, than annealed at this temperature for 2 weeks and quenched in cold water. The crystal structure of the compound was investigated by single crystal X-ray diffraction (Bruker PLATFORM/SMART APEX II CCD diffractometer; Mo $K\alpha$ -radiation, ω -scan, $2.46 < \theta < 26.33^\circ$). A structure solution by direct methods and refinement using full-matrix least-squares refinements on F^2 were carried out using SHELXS-97 and SHELXL-97 [1, 2] program packages, respectively.

The title compound crystallizes in a derivate from the $\text{Ce}_3\text{Zn}_{22}$ -type structure (space group $I4_1/amd$, Pearson code $tI144$, $Z = 2$) with lattice parameters $a = 8.9777(2)$ Å, $c = 21.4820(8)$ Å, $V = 1731.43(8)$ Å³, ($R_1 = 0.0611$, $wR_2 = 0.124$). Two split positions Zn1/Fe1 and Zn2/Fe2 are distinguishing feature of this structure. It should be noted that this compound is disordered derivate of the hexagonal CaCu_5 -type (space group $P6/mmm$) as well as other Zn-rich ternary phases which often crystallize in different derivatives of this structure type such as $\text{Th}_2\text{Ni}_{17}$, $\text{Th}_2\text{Zn}_{17}$, $\text{Ce}_2\text{Ge}_3\text{Zn}_6$, $\text{Gd}_2\text{Co}_3\text{Zn}_{14}$ etc.

Table 1. Atomic coordinates and isotropic displacement parameters

Atom	Site	Occupation	x	y	z	U_{eq} , Å ²
La1	8e	1.0	1/2	3/4	0.06585(15)	0.010(1)
Zn1	8e	0.50(1)	1/2	3/4	0.3109(4)	0.0149(18)
Fe1	16h	0.50(1)	1/2	0.6044(14)	0.3046(6)	0.010(2)
Zn2	16h	0.44(1)	0.6522(16)	3/4	0.2023(6)	0.016(3)
Fe2	16h	0.56(1)	0	0.4722(16)	0.0635(6)	0.015(3)
Zn3	16g	1.0	0.2393(4)	0.5107(4)	1/8	0.013(1)
Zn4	16f	1.0	0.2713(7)	1/2	0	0.024(1)
Zn5	16h	1.0	1/2	0.3985(5)	0.0739(2)	0.010(1)
Zn6	16h	1.0	1/2	0.5158(6)	0.1899(2)	0.014(1)

[1] Sheldrick, G. M. (2008). *Acta Cryst.* A64, 112–122.

[2] Sheldrick, G. M. (2015). *Acta Cryst.* C71, 3–8.

STUDY OF SEMICONDUCTING THERMOELECTRIC MATERIAL $\text{Er}_{1-x}\text{Zr}_x\text{NiSb}$

Yu. Stadnyk¹, L. Romaka¹, V.A. Romaka², A. Horyn¹,
V. Krayovskii², P. Klyzub¹, M. Rokomanyuk²

¹Ivan Franko National University of Lviv, Kyryla and Mefodiya Str. 6,
Lviv 79005, Ukraine,

²National University "Lvivska Politechnika", S. Bandera Str. 12, Lviv 79013, Ukraine

RNiSb compounds (R-rare earth metal) and corresponding solid solutions with the MgAgAs structure type (space group $F\bar{4}3m$) are semiconductors and promising thermoelectric materials.

The structural, kinetic, energy state and magnetic characteristics of the $\text{Er}_{1-x}\text{Zr}_x\text{NiSb}$ ($x=0-0.10$) solid solution were investigated. Structural studies of $\text{Er}_{1-x}\text{Zr}_x\text{NiSb}$ showed that impurity Zr atoms can partially occupy different crystallographic positions in the ErNiSb structure and generate the structural defects of the different nature. Temperature dependencies of electric resistivity $\ln(\rho(1/T))$ and thermopower coefficient $\alpha(1/T)$ of $\text{Er}_{1-x}\text{Zr}_x\text{NiSb}$, $x=0-0.03$, are typical for compensated semiconductors with activation parts which indicates the location of the Fermi level ε_F in the band gap. Positive sign of the thermopower coefficient $\alpha(T,x)$ of the ErNiSb compound showed the hole-type of the conductivity and location of the Fermi level near the valence band at a distance $\varepsilon_1^p=45.2$ meV. Introduction in the ErNiSb compound the lowest concentration of the Zr atoms ($x=0.005$) does not change the thermopower coefficient sign, results in a decreasing of the resistivity values and depth of the the Fermi level up to $\varepsilon_1^p=39.8$ meV. For a p -type semiconductor, this is possible when the concentration of acceptors increases and the concentration of free holes become higher. Thus, at $x=0.005$ Zr atoms do not occupy $4a$ position of the Er atoms and the donors are not generated.

At $x=0.01$ the sign of the thermopower coefficient $\alpha(T,x)$ of $\text{Er}_{1-x}\text{Zr}_x\text{NiSb}$ is negative at all temperatures and electrons are the main charge carriers. At $x=0.01$ the Fermi level lies near the conduction band at a distance 6.7 meV. At higher Zr content ($0.01 < x$) the sign of the thermopower coefficient $\alpha(T,x)$ remains negative at all temperatures and activation parts on $\ln(\rho(1/T))$ dependencies disappear through metallization of the conductivity. Magnetic susceptibility measurements $\chi(x)$ of $\text{Er}_{1-x}\text{Zr}_x\text{NiSb}$ at 300 K confirmed the simultaneous generation of the structural defects of the acceptor and donor nature. $\text{Er}_{1-x}\text{Zr}_x\text{NiSb}$ samples are Pauli paramagnets, their magnetic susceptibility is determined by free electrons and proportional to the electron density at the Fermi level $g(\varepsilon_F)$. There is a complete correlation in the behavior of $\chi(x)$ and $g(\varepsilon_F)$ for $\text{Er}_{1-x}\text{Zr}_x\text{NiSb}$.

THE NdT_{1-x}Ge_xIn (T = Rh, Pd) SYSTEMS

N. Dominyuk^{1,2}, M. Horiacha^{1,2}, G. Nychporuk¹, R. Pöttgen², V. Zaremba¹

¹*Ivan Franko National University of Lviv,*

Kyryla and Mefodiya str., 6, 79005 Lviv, Ukraine

²*Institut für Anorganische Chemie, Universität Münster,*

Corrensstraße 30, D-48149 Münster, Germany

e-mail: halyna.nychporuk@lnu.edu.ua

The NdT_{1-x}Ge_xIn (T = Rh, Pd, x = 0÷1) systems were investigated by X-ray powder diffraction and energy dispersive X-ray analysis.

Samples were synthesized by arc-melting and subsequent annealing at 870 K for one month. Phase analysis was made by means of X-ray powder diffraction (Enraf-Nonius FR552, CuK α_1 -radiation) and energy dispersive X-ray analysis (REMMA-102-02 scanning electron microscope).

The existence of the solid solutions with the ZrNiAl-type structure (space group *P-62m*) [1] were observed. The limited solubility of Germanium in the NdRhIn and NdPdIn compounds was determined and unit cell parameters for solid solutions were calculated [2]:

NdRh_{1-0.5}Ge_{0-0.5}In: $a = 0.7534\text{--}0.73139(7)$, $c = 0.4028\text{--}0.42944(4)$ nm,

NdPd_{1-0.5}Ge_{0-0.5}In: $a = 0.76825\text{--}0.73367(6)$, $c = 0.40054\text{--}0.43309(4)$ nm.

The results of partial substitution of Rh atoms by Ge atoms were confirmed by single crystal X-ray analysis (STOE IPDS II diffractometer, MoK α -radiation). Single crystals were grown using special thermal mode. The structure was solved and refined using programs from the SHELX-97 package [3].

NdRh_{0.70}Ge_{0.30}In compound crystallizes with ZrNiAl-type structure (*P-62m*, $a = 0.74755(11)$, $c = 0.41886(8)$ nm, $R1 = 0.0183$ for 360 F^2 values, 16 variables), which agrees well with the results of phase analysis and EDX data (JEOL 5900LV scanning electron microscope system).

This work was supported by the DAAD foundation.

- [1] P. I. Krypyakevych, V. Ya. Markiv, E. V. Mel'nyk, *Dopov. ANURSR, Ser. A.* (1967) 750-753.
- [2] J. Rodríguez-Carvajal, *Commission on Powder Diffraction (IUCr). Newsletter*, 26 (2001) 12-19.
- [3] G.M. Sheldrick, *Acta Crystallogr. A.*, A64 (2008), 112-122.

NEW TERNARY EuPt_2Al_3 AND EuIr_2Al_4 ALUMINIDES*

Nazar Zaremba^{1,2}, Ihor Muts¹, Viktor Hlukhyi², Volodymyr Pavlyuk^{1,3}, Oliver Janka⁴, Rainer Pöttgen⁴

¹ Department of Inorganic Chemistry, Ivan Franko National University of Lviv, Kyryla and Mefodiya str., 6, 79005 Lviv, Ukraine

² Department of Chemistry, Technische Universität München, Lichtenbergstr. 4, D-85747 Garching, Germany

³ Częstochowa Jan Długosz University, Institute of Chemistry, Environmental Protection and Biotechnology, al. Armii Krajowej 13/15, 42200, Częstochowa, Poland

⁴ Institut für Anorganische und Analytische Chemie, Universität Münster, Corrensstrasse 30, Münster 48149, Germany
nazar.zaremba@gmail.com

During phase-analytical investigations of the Eu-Pt-Al and Eu-Ir-Al ternary systems at 873 K, the existence of two new ternary compounds has been established. The structures of both compounds were investigated by X-ray single crystal diffraction. Good quality EuPt_2Al_3 and EuIr_2Al_4 single crystals were isolated from samples of compositions $\text{Eu}_{0.25}\text{T}_{0.25}\text{Al}_{0.50}$ ($T = \text{Pt}, \text{Ir}$) which were obtained after special heat treatment in sealed Ta containers. Intensity data of EuPt_2Al_3 was collected at room temperature on a STOE StadiVari equipped with a Mo micro focus source and a Pilatus 100K detection system diffractometer and EuIr_2Al_4 was measured at room temperature on a STOE IPDS-II (MoK α radiation) diffractometer.

EuPt_2Al_3 crystallises in space group $Pm\bar{m}n$ ($oP36$, $a = 4.2032(2)$ Å, $b = 11.5261(8)$ Å, $c = 13.8792(9)$ Å; $R_1 = 0.0335$, $wR_2 = 0.0392$, 1491 F^2 values, 62 variables), whereas the crystal structure of EuIr_2Al_4 was refined in space group $P4/ncc$ ($tP28$, $a = 7.9181(2)$ Å, $c = 7.7335(4)$ Å, $R_1 = 0.0235$, $wR_2 = 0.0560$, 474 F^2 values, 19 variables). The Eu atoms in the EuPt_2Al_3 structure fill hexagonal prisms and the aluminum atoms form connected trigonal nets. The EuIr_2Al_4 structure can be described as 3D 48₂-framework where eight-membered rings are filled by Eu atoms and four-membered rings from Al and Ir atoms are empty (Fig. 1).

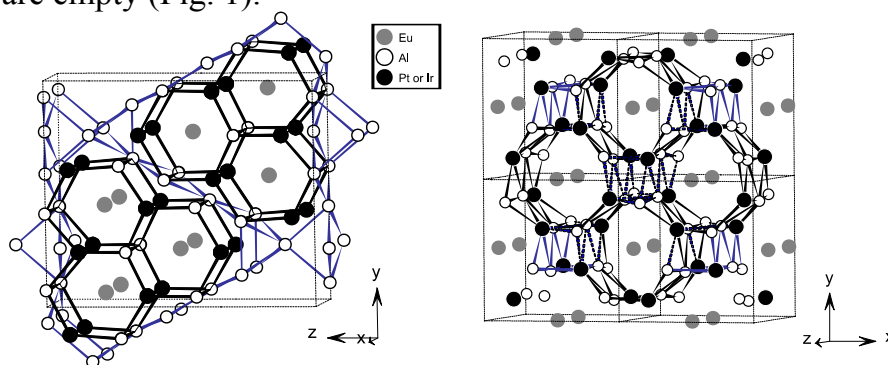


Figure 1. – Prisms and nets in EuPt_2Al_3 and EuIr_2Al_4 structures

The electronic structure calculations for both phases confirm that the atoms of aluminum and transition metal form atomic nets with much higher values of the electron localization function (ELF) than around the Eu atoms, where the electron localization function is minimal.

*This work was supported by DAAD, Germany (Nr 91619802 and Nr 91573440) and National Science Centre, Poland (Nr DEC-2017/25/B/ST8/02179)

EFFECT OF SUBSTITUTIONS ON MAGNETISM OF $\text{NdCo}_{4.5}(\text{Al}, \text{Li})_x$

I. Stetskiv^{1,2}, V. Kordan¹, I. Tarasiuk¹, H. Michor², V. Pavlyuk^{1,3}, E. Bauer²

¹ Department of Inorganic Chemistry, Ivan Franko National University of Lviv,
Kyryla i Mefodiya St., 6, 79005 Lviv, Ukraine

² Institute of Solid State Physics, Vienna University of Technology,
Wiedner Hauptstraße 8-10, A-1040 Vienna, Austria

³ Institute of Chemistry, Jan Dlugosz University in Czestochowa,
al. Armii Krajowej 13/15, 42-200 Czestochowa, Poland,

It was previously reported, that NdCo_5 compound is known for its ferromagnetic, strongly anisotropic behavior. Easy direction reorientation from c -axis to the basis plane is observed while cooling down. The spin reorientation (SR) occurs gradually between 230 and 290 K [1]. Al doping affects anisotropy constant values, they decrease with increasing Al composition. High value of Curie temperature of binary compound decreases several times after doping [2].

It is of interest to see what impact on magnetic properties the substitution of cobalt with aluminum and lithium has. NdCo_5 , $\text{NdCo}_{4.5}\text{Al}_{0.4}\text{Li}_{0.1}$ and $\text{NdCo}_{4.5}\text{Al}_{0.3}\text{Li}_{0.2}$ samples were prepared by arc melting. Phase composition and cell parameters were determined by X-ray powder diffraction and energy dispersive X-ray spectroscopy. The cell parameters increase with increase of Li amount in the alloy and are $a = 5.0089(5) \text{ \AA}$, $c = 3.9783(6) \text{ \AA}$, $V = 86.44(2) \text{ \AA}^3$ for NdCo_5 ; $a = 5.0160(8) \text{ \AA}$, $c = 4.0011(9) \text{ \AA}$, $V = 87.18(3) \text{ \AA}^3$ for $\text{NdCo}_{4.5}\text{Al}_{0.4}\text{Li}_{0.1}$; $a = 5.0246(5) \text{ \AA}$, $c = 4.0048(6) \text{ \AA}$, $V = 87.56(2) \text{ \AA}^3$ for $\text{NdCo}_{4.5}\text{Al}_{0.3}\text{Li}_{0.2}$.

The electrical resistivity down to 4 K was measured employing an A.C. measuring technique. The electrical resistivity of samples increases with increase of the alkali metal amount in the alloy.

Bulk polycrystalline samples were studied in a vibrating-sample magnetometer in magnetic fields up to 9 T at 5 K and in magnetic field range from 0.1 to 3 T in temperature range from 3 to 400 K. Al and Li substitution does not affect substantially the value of the saturation magnetization ($\sim 8\mu_B/\text{f.u.}$ at 9 T), but the increase of Li content leads to faster saturation. The SR transition cone has less pronounced maximum in magnetic field of 3 T compared with 0.1 and 1 T results. At smaller magnetic fields Al and Li doped samples have higher values of T_{SR1} , but T_{SR2} is approximately equal for doped and binary samples and smaller cone may suggest weaker anisotropy for substituted compounds.

[1] H. Bartholin, B. van Laar, R. Lemaire et al., J. Phys. Chem. Solids 27(8) (1966) 1287-1293.

[2] K. Konno, H. Ido, S. F. Cheng et al., J. Appl. Phys. 73 (1993) 5929-5931.

CRYSTAL, ELECTRONIC STRUCTURE AND HYDROGENATION PROPERTIES OF $Zr_{5-x}Mg_xNiSn_3$

Agnieszka Balińska¹, V.Pavlyuk^{1,2}

¹*Institute of Chemistry, Jan Dlugosz University in Czestochowa, al. Armii Krajowej 13/15, 42-200 Czestochowa, Poland, e-mail: a.balinska@ujd.edu.pl*

²*Department of Inorganic Chemistry, Ivan Franko National University of Lviv, Kyryla and Mefodiya str. 6, 79005 Lviv, Ukraine*

New ternary compound of $Zr_{5-x}Mg_xNiSn_3$ was prepared from elemental zirconium (foil, 0.25mm thick 99.8 at.%, Aldrich), magnesium (powder, 98 at.%, Aldrich), nickel (powder, 99.7 at.%, Aldrich) and tin (granules, 99.85 at.%, POCH). The pieces of the pure metals were pressed into pellet. The sample was melted in arc furnace under continuous argon flow. X-ray powder diffraction of the samples were carried out using STOE powder diffractometer (Mo – radiation). Rietveld refinements of X – ray powder diffraction data were performed by using the FULLPROF program [1]. The phase content of synthesized alloy was carried out using the TESCAN electron microscope equipped with EDS detectors. Hydrogen absorption-desorption properties of the alloy was studied using a Sieverts type apparatus.

The crystal structure of $Zr_{5-x}Mg_xNiSn_3$ and $Zr_{5-x}Mg_xNiSn_3H_6$ phases were investigated by powder methods. The $Zr_{5-x}Mg_xNiSn_3$ and $Zr_{5-x}Mg_xNiSn_3H_6$ crystallises in the Hf_5CuSn_3 -type with $P6_3/mcm$ space group, respectively $a = 8.5051 \text{ \AA}$, $c = 5.8135 \text{ \AA}$ and $a = 8.6904 \text{ \AA}$, $c = 5.9081 \text{ \AA}$. The electronic structures of the compounds were calculated using the tight-binding linear muffin-tin orbital (TB-LMTO) method in the atomic spheres approximation (TB-LMTO-ASA) [2–4], using the experimental crystallographic data. The maximum electron localization around the Sn atoms are obtained.

[1] J. Rodriguez-Carvajal, Recent advances in magnetic structure determination by neutron powder diffraction, *Physica B*, 1993, 192, 55–69

[2] O.K. Andersen, Linear methods in band theory, *Phys Rev B*, 1975, 12, 3060–3117

[3] O.K. Andersen, O. Jepsen, Explicit, First-Principles Tight-Binding Theory, *Phys Rev Lett*, 1984, 53, 2571–2574

[4] O.K. Andersen, Z. Pawłowska, O. Jepsen, Illustration of the linear-muffin-tin-orbital tight-binding representation: Compact orbitals and charge density in Si, *Phys Rev B*, 1986, 34, 5253–5269.

Financial support from the National Science Centre, Poland NCN (No 2017/25/B/ST8/02179)

NEW TERNARY COMPOUNDS IN THE Ta-Ni-P SYSTEM

V. Babizhetskyy¹, V. Smetana², M. Dzevenko¹, Ya. Lomnytska¹

¹ Ivan Franko National University of L'viv, Kyryla and Mefodia Str. 6, 79005 L'viv, Ukraine

² Stockholm University, Svante Arrhenius väg 16 C, 106 91 Stockholm, Sweden

The new compound TaNi_2P was found and the existence of $\text{Ta}_{0.92(1)}\text{Ni}_{0.08(1)}\text{P}_2$ and $\text{Ta}_5\text{Ni}_4\text{P}_4$ phosphides was confirmed during the study of the ternary system Ta-Ni-P [1, 2]. The crystal structure of $\text{Ta}_5\text{Ni}_4\text{P}_4$ was determined by single-crystal X-ray data (diffractometer Bruker D8 Venture, MoK_α -radiation): refined composition $\text{Ta}_{4.811(9)}\text{Ni}_{4.189(9)}\text{P}_4$, $\text{Nb}_5\text{Cu}_4\text{Si}_4$ -type, space group $I4/m$, $a = 9.8474(17)$, $c = 3.5182(7)$ Å, $R_1 = 0.028$, $wR_2 = 0.047$. The crystal structures of the last two phosphides were determined by powder X-ray data (diffractometer STOE STADI, $\text{CuK}\alpha_1$ - radiation). The $\text{Ta}_{0.92(1)}\text{Ni}_{0.08(1)}\text{P}_2$ is isotypic with OsGe_2 -type: space group $C2/m$, $a = 8.85716(6)$, $b = 3.6529(3)$, $c = 7.48572(4)$ Å, $\beta = 119.310(1)^\circ$, $R_1 = 0.031$, $R_p = 0.099$. The new ternary phosphide TaNi_2P crystallize in own structure type: refined composition $\text{Ta}_{0.95(2)}\text{Ni}_{2.05(2)}\text{P}$, space group $Pnma$, $a = 8.3588(3)$, $b = 3.5208(1)$, $c = 6.7051(3)$ Å, $R_1 = 0.044$, $R_p = 0.161$. The structure of all these compounds can be considered as a packing of trigonal prisms. However, the trigonal prisms in the structure of $\text{Ta}_5\text{Ni}_4\text{P}_4$ and TaNi_2P compounds are built from transition metal atoms and centered by P atoms, while in the structure of $\text{Ta}_{0.92(1)}\text{Ni}_{0.08(1)}\text{P}_2$ the situation is vice versa: the transition metal atoms are in the center of trigonal prisms from P atoms (Fig. 1).

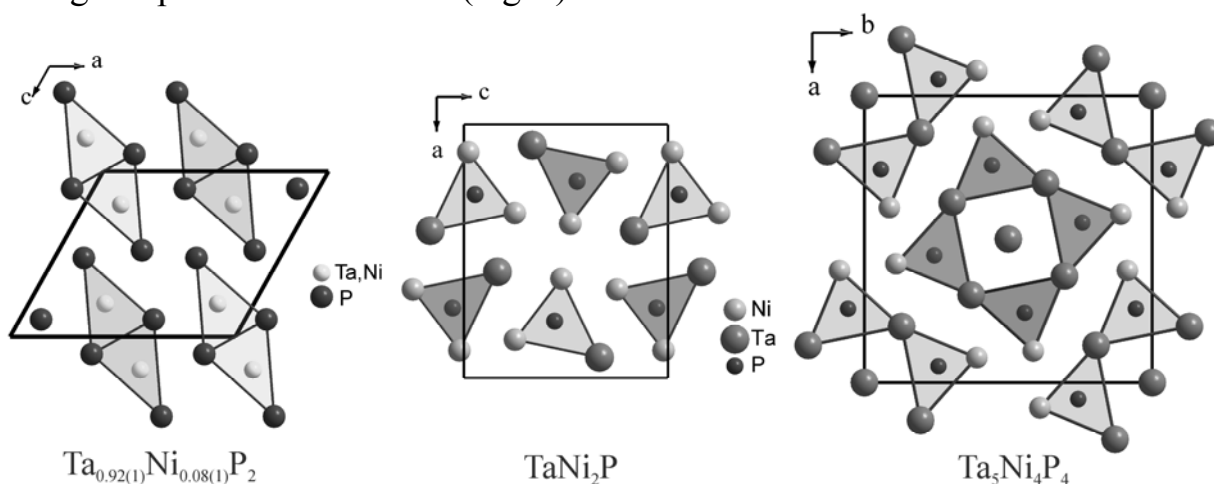


Figure 1: The arrangement of the metal atoms trigonal prisms in the structures of $\text{Ta}_{0.92(1)}\text{Ni}_{0.08(1)}\text{P}_2$, TaNi_2P and $\text{Ta}_5\text{Ni}_4\text{P}_4$.

- [1] Ya. Lomnytska, M. Dzevenko, V. Babizhetskyy, M. Schöneich, J. Köhler, *J. Solid State Chem.* 277 (2019) 77-82.
 [2] R. Berger, *Acta Chem. Scand. A* 34 (1980) 77.

NEW REPRESENTATIVES OF THE STRUCTURE TYPE $Y_3NiAl_3Ge_2$

Svitlana Pukas¹, Nataliya Semuso¹, Roman Gladyshevskii¹

¹*Department of Inorganic Chemistry, Ivan Franko National University of Lviv,
Kyryla i Mefodiya St. 6, 79005 Lviv, Ukraine*

The aim of the present work was to search for new representatives of the structure type $Y_3NiAl_3Ge_2$ (*hP9*, *P-62m*) [1] in *R-Ni-Al-Si* systems. The majority of the representatives of this structure type are rare-earth aluminogermanides $R_3TAl_3Ge_2$ ($R = Y, Sm, Gd-Lu$, $T = Mn, Fe, Co, Ni$). Considering that Ge and Si atoms are analogues with respect to their electronic and size factors, the probability of existence of isotypic compounds $R_3TAl_3Si_2$ is rather high.

Eight new rare-earth nickel aluminosilicides, $R_3NiAl_3Si_2$ ($R = Y, Gd-Tm, Lu$), were synthesized by arc melting under an Ar atmosphere, annealed at 873 K for one month and their crystal structures were refined from X-ray powder diffraction data (diffractometer STOE STADI P, Cu $K\alpha_1$ radiation; program DBWS-9708). The existence of compounds with Sm and Yb was not observed under the experimental conditions. The cell parameters of the isotypic compounds $R_3NiAl_3Si_2$ are listed in the table; they decrease with decreasing radius of the rare-earth metal from Gd to Lu.

Crystallographic parameters of the compounds $R_3NiAl_3Si_2$

Compound	$r_R, \text{\AA}$	$a, \text{\AA}$	$c, \text{\AA}$	$V, \text{\AA}^3$
$Y_3NiAl_3Si_2$	1.801	6.85746(9)	4.16590(6)	169.65(1)
$Gd_3NiAl_3Si_2$	1.802	6.90979(8)	4.20368(5)	173.81(1)
$Tb_3NiAl_3Si_2$	1.782	6.86802(8)	4.17427(6)	170.51(1)
$Dy_3NiAl_3Si_2$	1.773	6.83711(9)	4.15675(5)	168.27(1)
$Ho_3NiAl_3Si_2$	1.766	6.81341(9)	4.13947(6)	166.41(1)
$Er_3NiAl_3Si_2$	1.757	6.79541(8)	4.12357(5)	164.90(1)
$Tm_3NiAl_3Si_2$	1.746	6.76825(9)	4.11438(6)	163.22(1)
$Lu_3NiAl_3Si_2$	1.734	6.72303(7)	4.09142(5)	160.15(1)

[1] J.T. Zhao and E. Parthé, *Acta Crystallogr. C* 46 (1990) 2273-2276.

STRUCTURE FORMATION BY RAPID QUENCHING OF Al-BASED ALLOYS

Olena Shved, Stepan Mudry

Physics of Metals Department, I. Franko Lviv National University, Lviv 79005, Ukraine
E-mail: Olenkawved01@gmail.com

Although the first glass-forming synthesis by rapid quenching method took place a long time ago [1], research interest in the structure formation processes under non-equilibrium conditions is relevant today [2]. In particular, it's due to a wide range of possible structural states obtained in this way and variety of new properties that could be achieved on the path of evolution from the state of local equilibrium of as quenched alloy to the crystalline state equilibrium. There are some rules of phase formation of Al-based alloys with *d*- and *f*-metals [3], but general laws that would describe a metal's interaction and the effect of heat treatment conditions on structure formation have not been yet established and needs systematical studies.

We have studied four systems with transition metals: Al–V, Al–Fe–V, Al–Fe–Nb, Al–Fe–Cr–Ti. Al-enriched alloys in the form of ribbons of about 30µm thickness were prepared by melt-spinning method at cooling rate $\sim 10^6$ K/s. Structural changes were studied by X-ray diffraction, mossbauer spectroscopy and differential scanning calorimetry methods. Binary alloys with composition of $Al_{90-91}V_{10-9}$ demonstrate a totally crystalline structure. Instead of them, multicomponent alloys consisting of a fine-grained structure with quasicrystalline icosahedral-like Fe-atoms local order appears in a metastable $FeAl_6$ phase and in amorphous state. Such microstructure resulted in enhancement of microhardness. It is shown that as quenched Al–Fe–V ribbons consist of a ternary icosahedral phases in an amorphous matrix.

- [1] R.H. Willens, W. Klement, P. Duwez, J. Appl. Phys. 31 (1960) 1136-1137.
- [2] W. Strunk Jr., E.B. White, The Elements of Style, third ed., Macmillan, New York, 1979.
- [3] X. Yue, A. Inoue, C.-T. Liu, X. Shen, P. K. Liaw 22 (2019)

NON-DESTRUCTIVE TESTINGS OF ANELASTIC INTERNAL FRICTION IN NANO COMPOSITES OF MULTIWALLED CARBON NANOTUBES AND POLYVINYL CHLORIDE, POLYETHYLENE, FOAM POLYSTYRENE

A. Onanko, D. Charnyi, Y. Onanko, M. Kulish, O. Dmytrenko, T. Pinchuk-Rugal, M. Aliksandrov, O. Pavlenko, T. Busko, O. Polovina, P. Ilyin, L. Kurochka

onanko@i.ua

The ultrasonic (US) device KERN-SG in figure 1, computer device KERN-4, acoustic emission in figure 2 measuring of velocities V is consist in measuring block and computer with operation system "Windows XP" are represented. The program KERN-4 ensures the management of measured block basic subsystems, the reflection of receiving signal in digital oscilloscope regime, which remember, and the calculation of ultrasound velocity V and indication of its size on indicators. The measuring block is consist of generator, force magnifier, management-1 module, management-2 module, receiver, power module. The frequency range $f = 0,3 \div 2$ MGz [1].

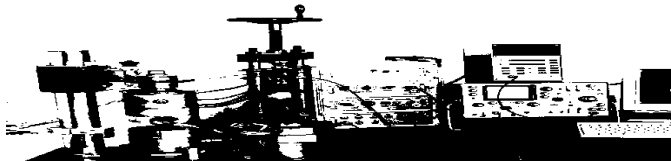


Figure 1: The ultrasound device KERN-SG of elastic waves velocities measuring. The appearance of acoustic emission (AE) device is presented in figure 2.

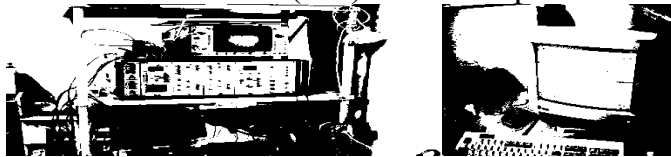


Fig. 2: The appearance of acoustic emission device on frequency $f_{\parallel} = 0,2 \div 0,5$ MGz $\alpha = 70$ dB for elastic waves velocities measuring.

The measuring of internal friction (IF) background Q^{-1}_0 after different heat treatments gives information about the changes of the fields of thermoelastic strains σ_i .

Conclusions

1. The broadening of internal friction maximums ΔQ_M^{-1} represents the relaxation process of structural defects new types in nano composites.
2. The growth of IF maximums Q_M^{-1} heights testifies the increasing of structural defects concentration.

[1] Y.A. Onanko, M.P. Kulish, A.P. Onanko et al. J. Metalphysics and new technology. 33(13) (2011) 529-533.

NEW TERNARY COMPOUNDS IN THE Hf-Ni-P AND Hf-Ni-As SYSTEMS

Zhak Olha

Ivan Franko National University of Lviv, Department of Analytical Chemistry,
Kyryla and Mefodiya Str. 6, UA-79005 Lviv, Ukraine, e-mail: olha.zhak@lnu.edu.ua

Interaction of the components in the ternary systems Hf-Ni-P and Hf-Ni-As was not systematically studied earlier, and their phase diagrams were not constructed, but a number of the ternary phases were discovered in these systems. In the ternary Hf-Ni-P system existence of the seven ternary phosphides was discovered: HfNiP, Hf₂Ni₃P₃, HfNi₄P₂, Hf₂NiP, Hf₂Ni_{10.85}P₂, Hf₅NiP₃, and Hf₄NiP. The last one is the limit composition of the solid solution of phosphorus on the base of the binary compound Hf₂Ni, and has an ordered structure of the Nb₄CoSi type. Four ternary arsenides were found in the Hf-Ni-As system: HfNiAs, HfNi_{0.75}As₂, HfNi₄As₂, and Hf₂Ni₃As₃. It should be mentioned that for all these compounds only lattice parameters obtained from powder X-ray diffraction data were reported, but no atomic coordinates in the crystal structure were refined. So, the main goals of our work were synthesis and crystal structure determination of the ternary phosphides and arsenides of hafnium and nickel.

By using of two different experimental methods: twice sintering or arc-melting of the preliminary sintered pellets from the mixtures of starting materials (powders of hafnium, nickel, red phosphorus or crystalline arsenic), a number of three-component samples of the Hf-Ni-P and Hf-Ni-As systems were synthesized and homogenized at 800 °C. Phase composition of the samples was established from X-ray powder diffraction data (diffractometers DRON-3M and STOE STADI P). Atomic coordinates and displacement parameters in the crystal structures of compounds were refined using the full-profile Rietveld method. For all calculations WinCSD software [1] was used.

Three new ternary phosphides of Hf and Ni were synthesized, and their crystal structures were solved from X-ray powder diffraction data:
Hf₂Ni₁₂P₇ (Zr₂Fe₁₂P₇-type, space group *P*-6, *a* = 0.90042(1), *c* = 0.35598(1) nm);
Hf₆Ni₂₀P₁₃ (Zr₆Ni₂₀P₁₃-type, space group *P*-6, *a* = 1.24684(2), *c* = 0.35935(1) nm);
Hf₃Ni_{3.6}P_{2.4} (Fe₂P-type structure, space group *P*-62*m*, *a* = 0.62592(2), *c* = 0.37147(1) nm).

New ternary arsenide Hf₂NiAs₂ with the hexagonal Ho₂NiAs₂ structure was found for the first time (space group *P*6₃/*mmc*, *a* = 0.3920(3), *c* = 1.276(5) nm). The earlier known ternary arsenide HfNiAs was confirmed at 800 °C, and its atomic positional parameters were refined: TiNiSi type, space group *Pnma*, lattice parameters are *a* = 0.64000(6), *b* = 0.38050(2), *c* = 0.73378(5) nm.

[1] L. Akselrud, Yu. Grin, J. Appl. Crystallogr. 47 (2014) 803–805.

CRYSTAL STRUCTURE OF THE NOVEL COMPOUND



Ya.M. Kalychak¹, L.D. Gulay², M. Daszkiewicz³

¹*Department of Analytical Chemistry, Ivan Franko National University of Lviv,
Kyryla i Mephodiya St. 6, 79005 Lviv, Ukraine*

²*Department of Ecology and Protection of Environment, Lesya Ukrainka Eastern European
National University, Voli Ave. 13, 43009 Lutsk, Ukraine*

³*Institute of Low Temperature and Structure Research, Polish Academy of Sciences,
P. O. Box 1410, 50-950 Wrocław, Poland*

In the course of our systematic investigation of the RE-T-In systems (RE = rare earths and T= d-metals), the formation of a novel ternary compound $\text{Ce}_{24.02}\text{Ag}_{64.64}\text{In}_{53.21}$ was discovered. The sample was prepared by arc-melting elemental constituents under an argon atmosphere and subsequent annealing at 870 K for 13 months. The product was examined by X-ray powder diffraction data on a Stoe STADI P diffractometer ($\text{CuK}_{\alpha 1}$ radiation, $\lambda = 1.5406 \text{ \AA}$). The X-ray single crystal experiment was performed using an Oxford Diffraction four-circle diffractometer equipped with a CCD Atlas detector (graphite-monochromatized MoK_{α} radiation, $\lambda = 0.71073 \text{ \AA}$). Absorption correction of the raw data was performed with the CrysAlis Data Reduction program. The measured intensities were corrected for Lorentz and polarization factors. The crystal structure was solved by Patterson methods and refined by the full-matrix least-squares method using SHELXL-2014.

The composition of the single crystal was analyzed in a scanning electron microscope-microanalyser TESCAN 5130 MM with an Oxford Si-detector (SEM and EDX modes). The experimentally determined composition of single crystal (18 ± 2 at % Ce, 45 ± 2 at % Ag, 37 ± 2 at % In) is rather close to the composition of the sample and agree well with the calculated composition from the crystal structure refinement.

The compound crystallizes with a hexagonal structure closely related to $\text{Gd}_{13}\text{Zn}_{58}$ (= $\text{Ce}_{13}\text{Cd}_{58}$) type (space group $P6_3/mmc$, No. 194, lattice parameters: $a = 15.4658(4)$, $c = 15.2888(5) \text{ \AA}$, $Z = 1$, $R_1 = 0.0509$, $wR_2 = 0.1314$). The cerium atoms in $2a$ site of $\text{Ce}_{13}\text{Cd}_{58}$ ($\text{Ce}_{26}\text{Cd}_{116}$) are replaced by atoms of silver in split position in $4e$ site of $\text{Ce}_{24.02}\text{Ag}_{64.64}\text{In}_{53.21}$. All five another positions of silver atoms are also splitted as well as of cerium atoms in $6h$ and $12k$ sites. The indium atoms occupy seven positions (six ordered and one partially occupied).

SINGLE-CRYSTAL INVESTIGATION OF Eu_5Si_3

B. Belan¹, M. Dzevenko¹, M. Daszkiewicz², and R. Gladyshevskii¹

¹*Ivan Franko National University of Lviv, Kyryla i Mefodiya St. 6, 79005 Lviv, Ukraine*

²*Institute of Low Temperature and Structure Research, Polish Academy of Sciences,
P. O. Box 1410, 50-950 Wrocław, Poland*

The crystal structure of the binary silicide Eu_5Si_3 was studied in detail by X-ray single-crystal diffraction. The crystal was selected from a sample that had been prepared by arc-melting compact metals under an argon atmosphere and annealed at 670 K for 360 h. X-ray diffraction was performed at $T = 295$ K on an Oxford Diffraction X'calibur Atlas four-circle diffractometer (MoK α radiation). The structure was solved by direct methods and refined using the SHELX-2018/3 program package [1]. The Eu_5Si_3 compound adopts the tetragonal Cr_5B_3 -type: space group $I4/mcm$ (#140), Pearson code $tI32$, $Z = 4$, $a = 7.9339(6)$, $c = 15.308(2)$ Å, $R1 = 0.0317$, $wR2 = 0.0482$, for 321 independent reflections with $I > 2\sigma(I)$ and 16 variables.

The crystal structure of Eu_5Si_3 has been studied earlier by Pöttgen and co-authors [2] on single crystals that had been grown *via* a special annealing procedure. Our results correlate well with theirs, except minor differences in the lattice parameters.

The most interesting feature of the structure of Eu_5Si_3 is the coordination sphere of the Si atoms. The Si1 (4a) atoms are isolated from the other silicon atoms and their coordination polyhedra are formed by 10 Eu atoms. On the other hand, the Si2 (8h) atoms form Si-Si pairs, which are surrounded by 12 Eu atoms (Fig. 1).

Binary silicides $R_5\text{Si}_3$ have been found with all the rare-earth metals, and their crystal structures adopt two structure types: tetragonal Cr_5B_3 ($R = \text{La, Ce, Pr, Nd, and Eu}$) and hexagonal Mn_5Si_3 ($R = \text{Nd, Sm, Gd-Lu, Y}$) [3]. Interestingly, the Nd_5Si_3 compound crystallizes in both structure types.

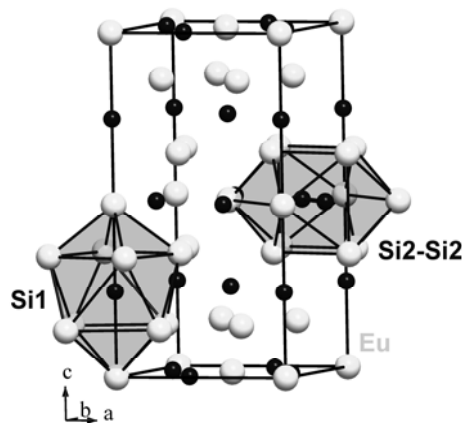


Fig. 1. Coordination polyhedra of the Si atoms in the structure of Eu_5Si_3 .

- [1] G. M. Sheldrick, *Acta Crystallogr. C* 71 (2015) 3–8.
- [2] R. Pöttgen, R.-D. Hoffmann, D. Kussmann, *Z. Anorg. Allg. Chem.* 624 (1998) 945-951.
- [3] P. Villars, K. Cenzual (Eds.), *Pearson's Crystal Data – Crystal Structure Database for Inorganic Compounds*, Release 2017/18, ASM International, Materials Park (OH), 2017.

CRYSTAL STRUCTURES OF EuSi AND LuSi

B. Belan¹, M. Manyako¹, M. Dzevenko¹, M. Daszkiewicz², and R. Gladyshevskii¹

¹Ivan Franko National University of Lviv, Kyryla i Mefodiya St. 6, 79005 Lviv, Ukraine

²Institute of Low Temperature and Structure Research, Polish Academy of Sciences,
P. O. Box 1410, 50-950 Wrocław, Poland

The crystal structures of the EuSi and LuSi compounds were investigated by X-ray single-crystal diffraction. The crystals were selected from arc-melted samples, which had been annealed at 400°C (Eu samples) or 500°C (Lu samples). X-ray diffraction was performed at room temperature on an Oxford Diffraction X'calibur four-circle diffractometer (MoK α radiation). The structures were solved by direct methods and refined by the SHELX-2018/3 program package [1] with anisotropic atomic displacement parameters. Both compounds crystallize in the structure type TII: space group *Cmcm* (# 63), Pearson code *oS8*, *Z* = 4, *a* = 4.6955(6), *b* = 11.1528(13), *c* = 3.9845(4) Å, *R*1 = 0.0224, *wR*2 = 0.0338, for 180 independent reflections with *I* > 2 σ (*I*) and 10 variables for EuSi; *a* = 4.1493(3), *b* = 10.2641(7), *c* = 3.7518(2) Å, *R*1 = 0.0186, *wR*2 = 0.0415, for 174 independent reflections with *I* > 2 σ (*I*) and 10 variables for LuSi. The final atomic positional and displacement parameters of the compounds are listed in the Table. All the crystallographic positions are fully occupied.

Table. Atomic coordinates and equivalent displacement parameters for EuSi and LuSi

Compound	Atom	Wyckoff	<i>x</i>	<i>y</i>	<i>z</i>	<i>U</i> _{eq} , Å ²
EuSi	Eu	4 <i>c</i>	0	0.3595(4)	1/4	0.01110(17)
	Si	4 <i>c</i>	0	0.0652(2)	1/4	0.0102(5)
LuSi	Lu	4 <i>c</i>	0	0.35892(4)	1/4	0.0061(2)
	Si	4 <i>c</i>	0	0.079(3)	1/4	0.0066(5)

Binary silicides of equiatomic composition exist in all the systems with rare-earth metals and silicon [1] and adopt two related structure types. The binary silicides with La, Ce, Pr, Nd, Sm, Gd, and Tb crystallize in the FeB-type. The silicides with Eu, Tm, Yb, and Lu adopt the TII-type and the compounds with Dy, Ho, and Er crystallize in both these structure types.

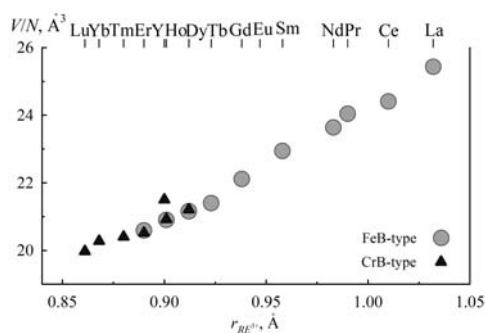


Fig. Dependence of the parameter *V*/*N* on the *RE*³⁺ radius in *RESi* compounds.

- [1] P. Villars, K. Cenzual (Eds.), *Pearson's Crystal Data – Crystal Structure Database for Inorganic Compounds*, Release 2017/18, ASM International, Materials Park (OH), 2017.
- [2] G. M. Sheldrick, *Acta Crystallogr. C* 71 (2015) 3-8.

INFLUENCE OF Ni NANOPARTICLES ON STRUCTURE-SENSITIVE PROPERTIES OF Sn–Ag–Cu ALLOYS

O. Tkach, Yu. Plevachuk, V. Sklyarchuk, R. Serkiz, Yu. Kulyk

Ivan Franko National University of Lviv, Department of Metal Physics,
Kyryla i Mefodiya St. 8, 79005 Lviv, Ukraine

The electrical conductivity of nanocomposite $\text{Sn}_{95.5}\text{Ag}_{3.8}\text{Cu}_{0.7}$ (SAC387) alloys with different weight percentages of Ni nanoparticles (from 1 to 3 wt.%) was measured over a wide temperature range. The samples were produced from pure Ag, Cu, Sn (99,999% purity, Alfa Aesar) by induction method in A_R atmosphere and mixed mechanically with Ni nanopowders. Ni nanoparticles were synthesized via a chemical reduction method and characterized by a core/shell structure. Temperature dependencies of the electrical conductivity revealed a hysteresis between the heating and cooling curves in a wide temperature range above the melting temperature. This fact is connected with structure transformations accompanied by dissolution of the Ni nanoparticles, which should be retarded due to an oxide/hydroxide shell on the surface of the nanoparticles. A microstructure analysis of the samples in the solid state showed a fine distribution of intermetallic compounds in the Sn-based matrix. The Ni atoms substituted for Cu atoms in the Cu_6Sn_5 compound forming a $(\text{Cu},\text{Ni})_6\text{Sn}_5$ phase. Unlike the finely dispersed small microregions of the $(\text{Cu},\text{Ni})_6\text{Sn}_5$ phase, $(\text{NiCu})_3\text{Sn}_4$ crystals are present in the form of relative large needles. Higher absolute electrical conductivity values of liquid SAC387 as compared to the conductivity of liquid SAC387+nanoNi is due to the fact that the Ni atoms form additional centers of electron scattering, and an increase of the Ni content leads to a decrease of the electrical conductivity.

STRUCTURAL AND MICROSTRUCTURE OF Al-BASED HIGH-ENTROPY ALLOYS WITH TRANSITION ELEMENTS

M. Dufanets, Yu. Plevachuk, V. Sklyarchuk

Ivan Franko National University of Lviv, Department of Metal Physics,
Kyryla i Mefodiya St. 8, 79005 Lviv, Ukraine

Recently the significant fundamental and applied interest began to be shown in multicomponent alloys, where content of each constituent element is equal. Entropy of such alloys increases with increasing of the elements number and is close to ideal entropy of multicomponent solution. Phase formation processes in equiatomic AlCoCuFeNiCr high entropy alloys have been studied by means of XRD method, microstructure analysis and microhardness measurements. Thermodynamic and structural criteria for predicting the phase composition of alloy are considered.

It is shown that in AlCoCuFe, AlCoCuFeNi and AlCoCuFeNiCr alloys the two-phase mixture of solid solutions on the base of BCC and FCC- lattices are formed. With a decrease in the fraction of Al atoms, the tendency to disordering of BCC- solid solution occurs. It is established also that alloys under investigation reveal a dendritic structure in which Cu-enriched FCC phase is deposited in the regions between the dendrites of the main BCC- phase. Correlation of microhardness of alloys with volume fractions of phase constituents and their thermodynamic characteristics are revealed.

INFLUENCE OF OXIDATION ON THE SURFACE TENSION OF Ga₇₀Bi₃₀

Roman Ovsianyk, Roman Bilyk, Stepan Mudry

Ivan Franko National University of Lviv, Lviv, 79005, Ukraine

Understanding of the various surface properties of metals and their alloys is an important thing for the development of the theory of interphase phenomena. Much attention is paid to the theoretical and experimental study of the surface properties of metals and alloys. One of the most important phenomena influencing the surface properties of the liquid alloys is the oxidation. In the present work, we studied an influence O₂ on the surface tension Ga₇₀Bi₃₀. Studying the structure of liquid Ga₇₀Bi₃₀ alloy showed that in the liquid state there is significant segregation of one-kind atoms. In addition, systems with segregation do not form a single-phase and in the solid state. The production of such materials is complicated due to the large difference in the melting points of the components and the strong tendency of some alloys to not mix in the liquid state in a certain temperature and concentration ranges. The exploitation of such alloys is the only possible basis on the accurate knowledge of their structure and properties.

The surface tension and the density Ga₇₀Bi₃₀ alloy were measured using the sessile drop method. The temperature was measured with an accuracy ± 1 K. A computer-controlled camera was used for the determination of the drop parameters. An image of the drop profile is captured by the camera. The surface tension was calculated using the method, which is based on the Laplace-Young equation.

It was found that the surface tension of Ga₇₀Bi₃₀ system in both cases (with&without oxidation) decreases linearly with increasing temperature. Analysis obtained data shown that oxygen is an effective surfactant for Ga₇₀Bi₃₀ and its presence in a surrounding atmosphere reduces the surface tension of the liquid Ga₇₀Bi₃₀ alloy near the critical point of segregation more than 1.2 times. This fact should be taken into account in production and exploitation alloys with significant segregation of one-kind atoms in a liquid and a solid state.

TRANSFORMATION OF THE STRUCTURE OF INTERMETALLIC ALLOYS AFTER MELTING

Z.M. Oliinyk, A.V. Korolyshyn, S.I. Mudry, U. I. Liudkevych.

andry.korolyshyn@lnu.edu.ua

The structure in the liquid state of intermetallic compounds, which are the basis of multicomponent alloys with different functional characteristics depending on the type of these phases and the nature of alloying elements, has been studied. For a wider and more efficient use of such systems, the question of the relationship between the specific structure of these alloys in the solid state, the short-range order in the liquid phase and the thermodynamic conditions of their crystallization.

In this work the results on influence of cooling at different rates on structure of intermetallics has been investigated by means of X-ray diffraction method. Diffraction patterns have been obtained at different temperature within wide temperature range, including both solid and liquid state. The results on structure data in liquid state were analyzed and used to determine the main short range order structure parameters anteratomic distances, number of neighbors and size of structural units (clusters). Parameter of chemical ordering has been also determinate for liquid phase.

Similar structure parameters have been obtained for cooling with different rates crystalline intermetallic and compared with data for liquid alloy.

**NEW INORGANIC AND ORGANIC MATERIALS
(SYNTHESIS, STRUCTURE AND PROPERTIES)**

STRUCTURE AND PROPERTIES OF THE PHASE $\text{Tb}_2\text{Ni}_{15}\text{LiMg}$

Kordan V.¹, Nytko V.¹, Stetskiv I.^{1,2}, Tarasiuk I.¹, Zelinska O.¹, Pavlyuk V.¹
Müller H.², Bauer E.²

¹*Department of Inorganic Chemistry, Ivan Franko National University of Lviv,
Kyryla i Mefodiya St., 6, 79005 Lviv, Ukraine*

²*Institute of Solid State Physics, Vienna University of Technology,
Wiedner Hauptstraße 8-10, A-1040 Vienna, Austria*

The phases with $\text{Th}_2\text{Ni}_{17}$ -type structure are potential hydrogen storage and electrode materials in Ni-MH batteries. These compounds have interesting physical properties too. During electrochemical hydrogenation of the $\text{Tb}_2\text{Ni}_{17-x}\text{M}_x$ solid solutions, where M is s - or p -element we noticed that these alloys demonstrate good efficiency and sufficient amount of absorbed/desorbed hydrogen. The $\text{Tb}_2\text{Mn}_{17}\text{C}_{2.5}$ -superstructure is formed as a result of the hydrogen insertion in a Wyckoff position $6h$ of the structure.

An alloy with nominal composition $\text{Tb}_{10.5}\text{Ni}_{79.5}\text{Li}_5\text{Mg}_5$ was synthesized by arc-melting (5 wt. % excess of Li and Mg) of pure components several times to insure homogeneity. The joint solubility of Li and Mg in the binary compound $\text{Tb}_2\text{Ni}_{17}$ does not exceed two atoms per formula unit. The results of X-ray phase

analysis (PANalytical X'Pert Pro MPD, CuK_α -radiation) showed that the alloy

consists of the expected phase with $\text{Th}_2\text{Ni}_{17}$ -type structure (space group $P6_3/mmc$, $a = 8.3329(6)$ Å, $c = 8.0497(7)$ Å, $V = 484.07(6)$ Å³) and trace amounts of Ni. The composition of the solid solution was confirmed by X-ray fluorescent spectroscopy (ElvaX Pro analyzer) and energy-dispersive X-ray spectroscopy (Tescan Vega3 LMU microscope, Oxford Instruments Aztec ONE system). The temperature dependence of electrical resistivity showed the form typical for metallic compound (Fig.). Linear plot of dependence is observed at 120-290 K, $\rho_0 = 35.7$ $\mu\Omega\cdot\text{cm}$. The value of specific resistivity is lower than for other phases with stoichiometry 2:17 and 1:5. Low value of this parameter is required for electrode materials in order to reduce electric energy loss.

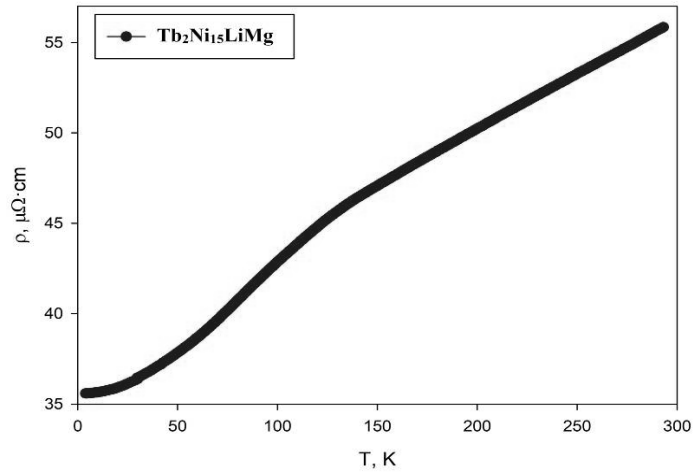


Figure. Electric resistance dependence $\rho = f(T)$

COMPOSITIONAL AND TEMPERATURE DEPENDENCE OF THE REFRACTIVE INDEX OF NEW ARGENTUM-BASED CHALCOGENIDE GLASSES

Shpak O.

Uzhgorod National University, Ukraine, Uzhgorod, Pidhirna Street, 46;
e-mail: shpak@uzhnu.edu.ua

According to [1], using a uniaxial model, the coefficient $\beta=dn/dT$ for solids in the region far from the phonon absorption bands ($\lambda > 10 \div 12 \mu\text{m}$) can be represented as a sum of two components:

$$\frac{dn}{dT} = -\frac{6\pi\chi_e}{n} \alpha - \frac{4\pi\chi_e}{n} \frac{1}{\omega_g} \frac{d\omega_g}{dT} \frac{1}{1 - \left(\frac{\omega}{\omega_g}\right)^2}$$

where α is the coefficient of linear expansion, χ_e is the electron polarization (susceptibility), ω_g is the frequency of the oscillator. The first component occurs due to the change in the density of matter, the second - due to the temperature change of its electronic structure, that is, the change in the magnitude ω_g .

Given that the parameter $d\omega_g/dT$ is generally negative, the components (1) respectively have opposite signs. In the visible spectral region for the ChSG system, the predominant contribution to dn/dT is made by the first component. As the proximal self absorption band ($\omega \rightarrow \omega_g$) approaches, the contribution of the second component increases, and for certain (characteristic) wavelengths λ_0 , these components are mutually balanced ($dn/dT = 0$), and for the wavelengths smaller than some limiting λ_0 the second component determines the sign of the temperature derivative n . In addition, the obtained results indicate that the value of λ_0 depends on the size of the band gap of the glasses under study, or in other words, the smaller ω_g , the greater λ_0 . For the studied glasses, the determined values of λ_0 are in the range of 1-3 microns. Among the studied alloys of the Ag-As-S system, only the stoichiometric composition of As_2S_3 takes the value $dn/dT = 0$ with a defined value of λ_0 equal to $\sim 0.96 \mu\text{m}$. For other compositions, the values $\lambda_0 \rightarrow dn/dT = 0$ are outside the studied region of the spectrum. The negative value of the coefficient dn/dT indicates the fact that in the investigated part of the spectrum, the temperature change of the density of glasses plays a dominant role.

[1] Y.F. Tsay, D. Bendov, S.S. Mitra, Phys. Rev. B. 8(6), 2688 (1973).

X-RAY SPECTRA, ELECTRON STRUCTURE AND PHYSICAL PROPERTIES OF THE CeScSi COMPOUND

I. D. Shcherba¹, V. N. Antonov², M.V. Kovalska¹, Z. M. Shpyrka¹,
H. Noga³, B. M. Yatcyk⁴, V. A. Denys¹

¹Ivan Franko National University, Kyryla & Mefodiya Str. 8,
79-005 Lviv, Ukraine

²Institute of Physics of Metals, NASU, Kyiv, Ukraine

³Institute of Technology, Pedagogical University,
Podchoranzych Str. 2, 30-084 Cracow, Poland

⁴Lviv National University of Veterinary Medicine and Biotechnologies, Ukraine

In rare earth compounds, where 4f levels are relatively close to the Fermi energy, various anomalous phenomena frequently appear. Most of them can be attributed to the hybridization between the 4f states and conduction bands. A mixed-valence (MV) state is one of these phenomena. The MV phenomenon has attracted a great deal of interest during the last several decades in connection with valence fluctuations. In the gas phase most rare earths are divalent, but in the solid state most are trivalent, due to the large cohesive energy gained by promoting a 4f electron into an extended bonding state. The rare earth compounds based on Ce, Sm, Eu, Tm and Yb ions frequently exhibit a mixed-valence state consisting of divalent and trivalent valences. In the mixed-valence compounds, therefore, one must also consider the charge degrees of freedom of the 4f ions in addition to the spin and orbital degrees of freedom.

The aim of this report is the experimental and the theoretical study from the "first principles" of the electronic structure and x-ray absorption and emission spectra of CeScSi compound. The energy band structure of the compounds was calculated within the ab initio approach considering strong electron correlations by applying a local spin-density approximation to the density functional theory supplemented by a Hubbard U term (LSDA+U). The Ce L_{III} absorption spectrum in the ternary CeScSi compound was obtained at 300 K using a tube spectrometer equipped with an RKD-01 coordinate detector. In the XPS spectrum of the valence band of the CeScSi compound, two groups of maxima with binding energies of ~2 eV and 6-12 eV, correspondingly, are observed. The maximum near the Fermi level is caused mainly by a contribution of the 4f-electrons of Ce and 3p-states of Si. Match of the singularity with energy 7 eV with the main maximum A of the SiL_{2,3}-band explains displaying the 3s-states of Si in the XPS spectrum.

It is found that structure of the valence band of the CeScSi compound being studied considerably differs from that in similar compounds, however with the 3d-transition elements, namely by the absence of high electron density at the Fermi level. The near Fermi region of the populated part of the valence band is formed by states of Ce and the 3d-states of Sc. The middle of the valence band is occupied by the p-states of Si. Contribution of the 3s-states of silicon in the bottom of the valence band is dominating.

HEAT CAPACITY AND THERMOELECTRIC PROPERTIES OF TbNiC₂

V. Levytskyi^{1,2}, P. Wyzga², O. Isnard³, V. Babizhetskyy¹, B. Kotur¹

¹ Department of Inorganic Chemistry, Ivan Franko National University of Lviv, Kyryla i Mefodiya Str. 6, UA-79005 Lviv, Ukraine

² Institute of Experimental Physics, TU Bergakademie Freiberg, Leipziger Str. 23, 09596 Freiberg, Germany

³ Institut Néel, University Grenoble Alpes and CNRS, BP 166, F-38042 Grenoble cedex 9, France

Crystal structure of TbNiC₂ refers to CeNiC₂ structure type – a two-layered (**AB**) noncentrosymmetric orthorhombic derivative of the hexagonal AlB₂ structure: the rare earth atoms corresponding to Al position (layer **A**) form distorted hexagonal plane net, whereas the boron site is split in such a manner that the nickel atom replace one boron atom of the hexagonal cell, and the C₂-dumbel – another one (layer **B**). The crystal structure of TbNiC₂ has been refined using powder X-ray diffraction: $a = 3.6000(2)$ Å, $b = 4.5129(2)$ Å, $c = 6.0563(3)$, $R_{B(t)} = 3.72$ %, $R_p = 5.46$ %.

Heat capacity (C_p) of TbNiC₂ has been measured in zero-field regime and temperature range 1.9–300 K. Below 25 K it showed λ -anomaly, which is characteristic to a respective long-range antiferromagnetic ordering [1]. Detailed analysis of the C_p curve revealed in Sommerfeld coefficient $\gamma = 8(1)$ mJ mol⁻¹ K⁻², phonon coefficient $\beta = 1.18(1) \cdot 10^{-4}$ J mol⁻¹ K⁻⁴ with the derived Debye temperature of $\Theta_D \approx 404$ K. Using LuNiC₂ [2] as a phonon reference Tb-4*f*-electron contribution to the magnetic entropy has been evaluated. A doublet ground state for a non-Kramer's Tb³⁺ ion together with high impact of crystalline and molecular electric field have been confirmed in agreement with earlier investigations by neutron diffraction [1].

Thermopower and electrical resistivity of TbNiC₂ have been measured in the range 310–855 K and reveal values characteristic for metallic systems. Seebeck coefficient decreases with increasing temperature nearly linear in the all studied interval, and at ~660 K changes its sign from positive to negative one, whereby the electrical resistivity increases from 310 K reaching maximum at ~640 K and afterwards decreases insignificantly. Maximum power factor value of 27 μ W m⁻¹ K⁻² has been observed at 310 K.

- [1] J. K. Yakinthos, P. A. Kotsanidis, W. Schäfer, G. Will, *J. Magn. Magn. Mater.* 81 (1989) 163-167.
- [2] S. Steiner, H. Michor, O. Sologub, B. Hinterleitner, F. Höfenstock, M. Waas, E. Bauer, B. Stöger, V. Babizhetskyy, V. Levytskyy, B. Kotur, *Phys. Rev. B* 97 (2018), 205115(1-11).

PHASE FORMATION IN THE $\text{Tl}_2\text{Se}-\text{CdSe}-\text{GeSe}_2$ SYSTEM

A.O. Selezen, I.D. Olekseyuk, L.V. Piskach

*Department of Chemistry and Technology, Lesya Ukrainka Eastern European National University, 13 Voli Ave., 43025 Lutsk, Ukraine
andrijandrij1993@gmail.com*

Quaternary phases of the $\text{A}^{\text{I}}_2\text{B}^{\text{II}}\text{D}^{\text{IV}}\text{X}_4$ type formed in chalcogenide systems $\text{A}^{\text{I}}-\text{B}^{\text{II}}-\text{D}^{\text{IV}}-\text{X}$ (A^{I} - alkali metals, Cu, Ag, Tl; B^{II} – Mn, Fe, Co, Ni, Cd, Hg, Pb; D^{IV} – Si, Ge, Sn; X – S, Se, Te) find much application in nonlinear optics and other areas of semiconductor technology.

The existence of two new quaternary compounds, $\text{Tl}_2\text{CdGeSe}_4$ and $\text{Tl}_2\text{CdGe}_3\text{Se}_8$, was established in the powder XRD investigation of the $\text{Tl}_2\text{Se}-\text{CdSe}-\text{GeSe}_2$ system. The former is formed at the 1: 1: 1 ratio of Tl_2Se , CdSe and GeSe_2 , respectively, the latter, at 1: 1: 3 ratio.

$\text{Tl}_2\text{CdGeSe}_4$ crystallizes in the non-centrosymmetric tetragonal space group $I-42m$, with the lattice parameters $a = 0.80145$ (9), $c = 0.67234$ (9) nm [1].

The composition of the second compound were further confirmed by SEM-EDS on a scanning electron microscope Tescan Vega 3 LMU with energy-dispersive X-ray microanalyzer Oxford Instruments Aztec ONE with detector X-Max^N20 (magnification x1000).

Fig. 1 shows a photomicrograph of the cleaved crystal used for quantitative elemental analysis (a) as well as EDS results (b). The averaged values from the results of the study of six samples indicate the single-phase sample over the entire surface and the composition close to $\text{Tl}_2\text{CdGe}_3\text{Se}_8$.

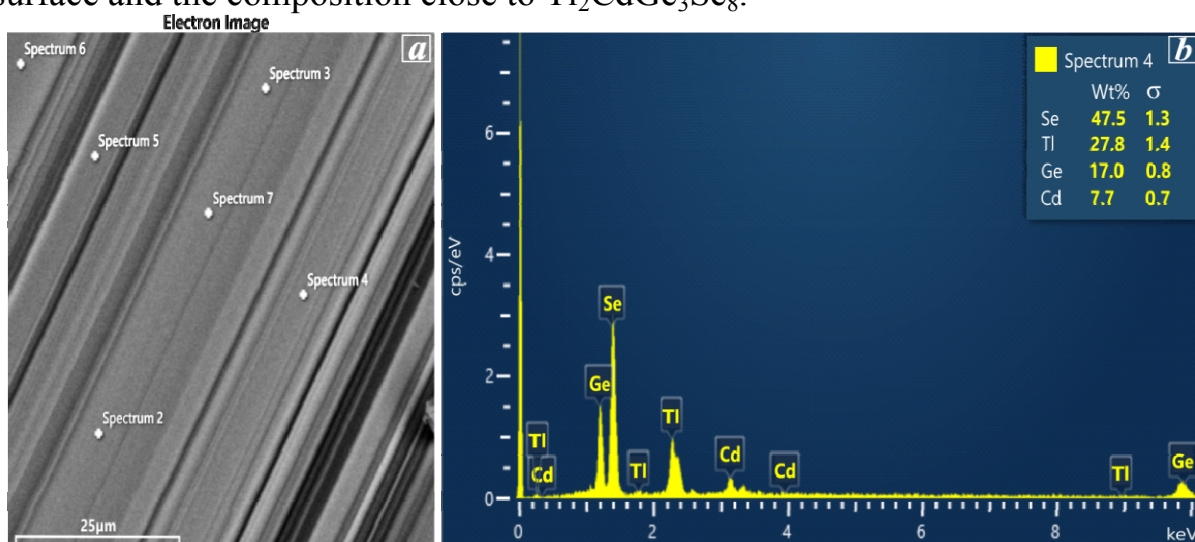


Fig. 1. SEM (a) and EDS (b) results for $\text{Tl}_2\text{CdGe}_3\text{Se}_8$

- [1] A.O.Selezen, I.D.Olekseyuk, G.L.Myronchuk, O.V.Smitiukh, L.V.Piskach, JSSC, (2020) (in press) <https://doi.org/10.1016/j.jssc.2020.121422>

STRUCTURAL AND MAGNETIC PECULIARITIES OF PHASES WITH Au₄Al-TYPE STRUCTURE IN THE Cr–{Mn,Fe,Cu,Ru,Pd}–Ni–Si SYSTEMS

Romana-Iryna Martyniak¹, Nataliya Muts¹, Matej Bobnar²,
Lev Akselrud¹, Roman Gladyshevskii¹

¹ Ivan Franko National University of Lviv, Kyryla i Mefodiya St. 6, 79005 Lviv, Ukraine

² Jožef Stefan Institute, Jamova Cesta 39, 1000 Ljubljana, Slovenia

Sustainability of data storage technologies is the cornerstone of development in the information age. Skyrmionic materials, magnets containing swirling defects of the magnetization texture called magnetic skyrmions, may successfully meet such a demand. In this work, we present the progress of our attempts to synthesize skyrmionic material (previous work in [1]), and discuss some structural and magnetic peculiarities observed along the course of the investigation.

The 13 alloys investigated within the frame of this study, $\text{Cr}_{28}\{\text{Mn,Fe,Cu,Ru,Pd}\}_5\text{Ni}_{49}\text{Si}_{18}$, $\text{Cr}_{27}\{\text{Mn,Fe,Cu,Pd}\}_5\text{Ni}_{48}\text{Si}_{20}$, and $\text{Cr}_{26}\{\text{Mn,Fe,Cu,Pd}\}_5\text{Ni}_{47}\text{Si}_{22}$, were synthesized by arc-melting of pure (≥ 99.9 wt.%) elements and subsequent 26-day annealing at 900°C. The crystal structures were refined from X-ray powder diffraction patterns recorded with a Huber Image Plate Camera – G670 diffractometer (Cu $K\alpha_1$ radiation), using the WinCSD – 2000 and FullProf software packages.

The results of the X-ray phase analysis indicated the presence of a phase with Au₄Al-type structure (Pearson symbol $cP20$, space group $P2_13$) in all of the investigated samples except $\text{Cr}_{26}\text{Mn}_5\text{Ni}_{47}\text{Si}_{22}$. Three alloys, $\text{Cr}_{28}\text{Fe}_5\text{Ni}_{49}\text{Si}_{18}$, $\text{Cr}_{28}\text{Cu}_5\text{Ni}_{49}\text{Si}_{18}$, and $\text{Cr}_{28}\text{Pd}_5\text{Ni}_{49}\text{Si}_{18}$, were single-phased.

The temperature-dependent susceptibilities of $\text{Cr}_{28}\text{Fe}_5\text{Ni}_{49}\text{Si}_{18}$, $\text{Cr}_{28}\text{Cu}_5\text{Ni}_{49}\text{Si}_{18}$, and $\text{Cr}_{28}\text{Pd}_5\text{Ni}_{49}\text{Si}_{18}$ showed paramagnetic behaviour and were fit to the modified Curie-Weiss law. In comparison to our previous studies [1], there is a significant increase of the Curie constant and the effective magnetic moment. Also notable is the increase of the Curie temperatures, which are approaching zero, especially for the Fe-containing alloy. Like in our previous investigation [1], the susceptibility of the conduction electrons is significantly enhanced due to electron correlations.

- [1] R.-I. Martyniak, N. Muts, O. Sichevych, H. Borrmann, M. Bobnar, L. Akselrud, R. Gladyshevskii, *Solid State Phenom.* 289 (2019) 108-113.

CRYSTAL STRUCTURES OF THE RNi_3Ga_9 COMPOUNDS

Nataliya Muts¹, Mariana Sadzhenytsia¹, Romana-Iryna Martyniak¹,
Yaroslav Tokaychuk¹, Pavlo Demchenko¹, Roman Gladyshevskii¹

¹ Department of Inorganic Chemistry, Ivan Franko National University of Lviv,
Kyryla i Mefodiya St. 6, 79005 Lviv, Ukraine

Our investigations in the Yb–Ni–Ga system showed the existence of a new ternary compound in the Ga-rich region – $Yb_{0.67}Ni_2Ga_6$ ($a = 0.41656(2)$, $c = 0.91557(6)$ nm [1]) with $Yb_{0.67}Ni_2Al_6$ -type structure (Pearson symbol $hP11-2.33$, space group $P-6m2$). Further studies indicated three compounds, $GdNi_3Ga_9$ ($a = 0.72624(2)$, $c = 2.74876(5)$ nm) [2], $DyNi_3Ga_9$ ($a = 0.72455(2)$, $c = 2.74346(7)$ nm) and $ErNi_3Ga_9$ ($a = 0.72351(2)$, $c = 2.74087(9)$ nm) [3], with the structure type $DyNi_3Al_9$ ($hR99$, $R32$), which is a partially ordered variant of the ordered structure type $ErNi_3Al_9$ ($hR78$, $R32$), and of the disordered type $Yb_{0.67}Ni_2Al_6$. The purpose of this work was to search for new isostructural compounds in R –Ni–Ga systems.

$R_{7.7}Ni_{23.1}Ga_{69.2}$ ($R = Y, La, Ce, Pr, Nd, Sm, Eu, Tb, Ho, Tm, Lu$) samples were synthesized by arc-melting of elements with the following purities: $R \geq 99.89$ wt.%, $Ni \geq 99.89$ wt.%, and $Ga \geq 99.89$ wt.%. The alloys have been annealed at 600°C for 3 months.

The existence of seven new ternary compounds RNi_3Ga_9 ($R = Pr, Nd, Sm, Tb, Ho, Tm, Lu$) was established based on X-ray powder diffraction (STOE Stadi P diffractometer, $CuK\alpha_1$ radiation), using the program package FullProf Suite and energy-dispersive X-ray spectroscopy (scanning electron microscope ZEISS EVO 40XVP). The investigated compounds belong to the structure type $DyNi_3Al_9$. It was found that the unit-cell parameters of the isostructural compounds gradually decrease from the $PrNi_3Ga_9$ compound ($a = 0.73068(1)$, $c = 2.76376(5)$ nm) to the $LuNi_3Ga_9$ compound ($a = 0.72193(1)$, $c = 2.73615(6)$ nm), due to the lanthanoid compression of the rare-earth atoms.

- [1] M. Boyko, N. Muts, V. Hlukhyy, T. Fässler, R. Gladyshevskii, XIII International Conference on Crystal Chemistry of Intermetallic Compounds, Lviv, Ukraine, September 25-29, 2016.
- [2] V. Topertser, R.-I. Martyniak, N. Muts, Ya. Tokaychuk, R. Gladyshevskii, Chem. Met. Alloys 12 (2020) 21-28.
- [3] V. Topertser, N. Muts, Ya. Tokaychuk, P. Demchenko, R. Gladyshevskii, XIV International Conference on Crystal Chemistry of Intermetallic Compounds, Lviv, Ukraine, September 22-26, 2019.

COMPOSITES BASED ON WATER-SOLUBLE POLYMERS AND POLYANILYLINE

V. Dutka¹, Ya. Kovalskyi², O. Aksimentyeva³, H. Halechko⁴

¹vdutka@ukr.net

²yaroslav.kovalskyi@lnu.edu.ua

³olena.aksimentyeva@lnu.edu.ua

⁴gzastavska@gmail.com

Polymer-polymer composites (PPCs) have unique properties that make them promising for use in many electronic devices. The conductive component is polyaniline (PANI) and water-soluble polymers, such as polyvinyl alcohol (PVA), polymethacrylic acid (PMAC), and styrene copolymer with maleic anhydride (SMA), which are part of such PPCs are of great interest since along with conductivity they have film-forming properties [1, 2]. The kinetic peculiarities of PPCs formation in the process of oxidative polymerization of aniline in the presence of PVA and SMA were studied. By varying the content of the PANI in the polymer matrices, it is possible to adjust the electrical conductivity (σ) of composites over a wide range. The study of σ dependence on the temperature for the interval of $T = 273\text{--}393$ K allowed us to calculate the activation energy of the charge transport (E_a). Numerical values of $E_a = 0.38\text{--}0.64$ eV indicate that the PPCs studied are typical organic semiconductors. Besides this, the presence of a polymer matrix doesn't change a character of the optical absorption of PANI films in the range of $\lambda = 380\text{--}1100$ nm [1].

One of the important properties of PPCs is their thermo-mechanical (TM) properties, which affect the performance and durability of devices formed with their participation. The TM curves of PVA and SMA have a classic character and the glass transition temperature determined for these polymers is consistent with the literature [2]. Studies of the thermo-mechanical properties of PPCs based on PVA and PANI and SMA and PANI indicate a strong interaction between the components. The interaction of PANI with polymer matrices was confirmed by the X-ray method and IR spectroscopic studies. The quantum-chemical calculation indicates the strong polarization of PANI molecules that can form hydrogen bonds with PVA, PMAC and SMA macromolecules. The morphological properties of the obtained polymer-polymer composites were studied.

[1] O. I. Aksimentyeva, B. R. Tsizh, Yu. Yu. Horbenko, et al. *Mol.Cryst.Liq.Cryst.*, **2018**, 670, 3–10.

[2] V. Dutka, O. Aksimentyeva, H. Halechko, Ya. Kovalskyi, *Proceedings of NTSH. Chem. Science.*, **2018**, LIII, 164–169 (in Ukr.).

A STUDY OF $\text{Ca}_{0.5}\text{R}_{0.5}\text{MnO}_3$ PEROVSKITE PHASES ($R = \text{RARE-EARTH METAL}$)

Oksana Zaremba¹, Olia Kotyk¹, Oksana Cherepaka¹, Andriy Horyn¹, and Roman Gladyshevskii¹

¹*Department of Inorganic Chemistry, Ivan Franko National University of Lviv,
Kyryla i Mefodiya St. 6, 79005 Lviv, Ukraine
oksanazaremba@gmail.com*

The compounds ABO_3 , so-called perovskite phases, crystallize with the cubic structure type CaTiO_3 (Pearson symbol $cP5$, space group $Pm-3m$). Many different cations can be included into the structure, allowing the development of diverse functional materials. The simple structure type has several deformation derivatives, one of the most widespread ones being the orthorhombic structure type GdFeO_3 ($oP20$, $Pnma$).

The aim of this work was the synthesis, structural characterization, and measurements of the magnetic properties of $\text{Ca}_{0.5}\text{R}_{0.5}\text{MnO}_3$ perovskite phases.

The samples were synthesized by solid-state reaction at 1200°C . X-ray phase and structural analysis, carried out on powder diffraction data, indicated that all the samples were single-phase (structure type GdFeO_3). The unit-cell volume regularly decreases with increasing atomic number of the rare-earth metal (Fig. 1). Magnetic susceptibility measurements vs. temperature were performed by the Faraday method. For instance, the temperature dependence of the magnetic susceptibility, χ vs. T , for $\text{Ca}_{0.5}\text{Nd}_{0.5}\text{MnO}_3$ and $\text{Ca}_{0.5}\text{Sm}_{0.5}\text{MnO}_3$ phases showed paramagnetic behavior.

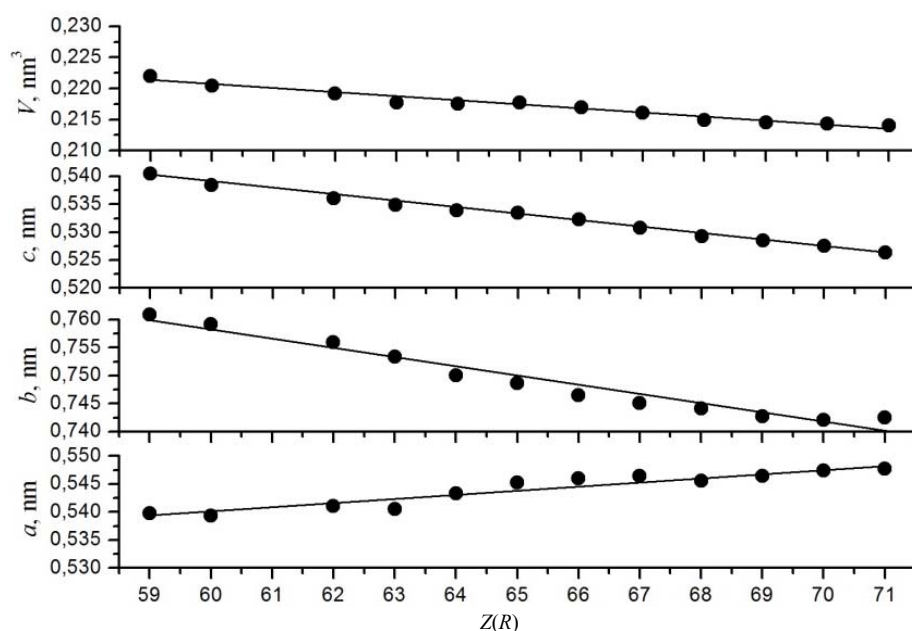


Figure 1: Cell parameters of $\text{Ca}_{0.5}\text{R}_{0.5}\text{MnO}_3$ phases as a function of the atomic number of the rare-earth metal.

ELECTRONIC STRUCTURE OF $\text{K}_2\text{SO}_4:\text{Cu}^{2+}$ (3%) CRYSTALS

M.Ya. Rudysh^{1,2,3}, R.B. Matviiv², V.Yo. Stadnyk², A.O. Fedorchuk⁴,
P.A. Shchepanskyi^{1,2}, R.S. Brezvin², O.Y. Khyzhun^{3,5}

¹Faculty of Science and Technology, J. Dlugosz University in Czestochowa, Armii Krajowej 13/15, 42-201 Czestochowa, Poland

²Faculty of Physics, Ivan Franko National University of Lviv, Dragomanova 19, Lviv 79000, Ukraine

³Faculty of Information Systems, Physics and Mathematics, Lesya Ukrainka Eastern European National University, Voli Ave. 13, Lutsk 43025, Ukraine

⁴Department of Inorganic and Organic Chemistry, Lviv National University of Veterinary Medicine and Biotechnologies, 50 Pekarska Str., UA-79010 Lviv, Ukraine

⁵Frantsevych Institute for Problems of Materials Science, National Academy of Sciences of Ukraine, 3 Krzhyzhanovsky Str., UA-03142 Kyiv, Ukraine

Electronic structure of $\text{K}_2\text{SO}_4:\text{Cu}^{2+}$ (3%) crystal are studied using complex experimental and theoretical methods. An X-ray photoelectron spectroscopy and X-ray emission spectroscopy are used to experimental study of structure of energy levels. These allowed to measure binding energy values of the core-level electrons of the constituting atoms, energy distribution of electronic states within the valence-band region and partial distribution of O 2*p* states.

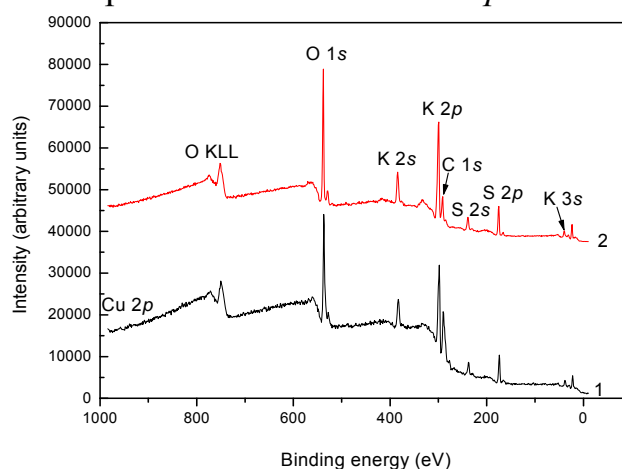


Fig. 1. Survey XPS spectra of pristine surfaces of (1) K_2SO_4 crystal doped with 3% of copper and, for comparison, (2) pure K_2SO_4 .

The additional theoretical study with using density functional theory is performed to confirm experimental data. Regarding the band-structure calculations of $\text{K}_2\text{SO}_4:\text{Cu}^{2+}$ (3%) suggesting that O 2*p* electronic states contribute mainly at the top of the valence band of this compound, they are supported experimentally when matching the XPS valence-band spectrum and X-ray emission O $K\alpha$ band of the Cu-doped K_2SO_4 crystal on a common energy scale with the curve of partial O 2*p* density of states of this compound. The experimental data is found to be in good agreement with theoretical band-structure calculations.

ELECTRONIC ENERGY STRUCTURE CALCULATION OF LaF₃:Pm AND LaF₃:Sm CRYSTALS

V. O. Karnaushenko¹, Y. M. Chornodolsky¹, V. V. Vistovsky¹,
S. V. Syrotyuk², A. S. Voloshinovskii¹

¹ Ivan Franko National University of Lviv, 8 Kyryla and Mefodiya str., 79005, Lviv, Ukraine

² National University "Lviv Polytechnic", 12 S. Bandera Str., 79013, Lviv, Ukraine
karnaushenkovo@gmail.com

Heavy inorganic scintillating crystals based on fluoride compounds with rare-earth elements become more popular among researchers due to high temperature stability and high luminescence intensity [1]. In particular, an important advantage of these compounds, compared to similar oxide compounds, is the low phonons energy, which makes the light yield efficiency much higher [2]. Big amount of experimental studies of LaF₃:Sm [3] and LaF₃:Pm [4] crystal's optical properties have been reported in recent years, but there is almost no theoretical information about their energy structure, what is very important for their effective use in lasers and scintillation detectors.

The calculation of the crystals electron-energy structure in this work is carried out using the projected augmented waves (PAW) method within density function theory framework. The Hubbard correction (DFT + U) is used to take into account the peculiarities of strongly localized states of lanthanides.

In the current work the results of the theoretical calculations of the partial and total density of states of LaF₃:Sm and LaF₃:Pm crystals are reported. The energy positions of 4f and 5d states of activator ions in the energy structure of the host material have been analyzed. Electronic band structures of the crystals have been calculated and the energies of the most probable optical transitions have been analyzed. Quantitative and qualitative comparison between the energy structure of LaF₃:Sm and LaF₃:Pm crystals is analyzed.

- [1] Sharma, Rahul Kumar, Anja-Verena Mudring, and Pushpal Ghosh, *Journal of Luminescence* 189 (2017): 44-63.
- [2] Ha, Hoang Manh, Tran Thi Quynh Hoa, and Nguyen Ngoc Long, *Journal of Materials Science: Materials in Electronics* 28.1 (2017): 884-891.
- [3] Macfarlane, R. M., and R. M. Shelby. *Physics Letters A* 116.6 (1986): 299-301.
- [4] Shinn, Michelle D., et al. *IEEE journal of quantum electronics* 24.6 (1988): 1100-1108.

STUDY OF THE PROCESSES OF FORMING OF SOLID SUBSTITUTION SOLUTIONS IN THIN FILMS OF THE (Ge₂)_x(GaSb)_{1-x} SYSTEM

N.Yu.Lutsyk

Ivan Franko National University of L'viv, Physical Faculty, Physics of Metals Department

E-mail: *nyuluts@i.ua*

Recently, there has been a significant increase in interest in the study and use of materials in the metastable crystalline state in microelectronic devices. Of particular interest is the study of semiconductor quasi-binary systems formed by elements of group (C⁴) and compounds A³B⁵. Structure, substructure, concentration areas of existence of metastable solid solutions and a kinetics of structural transformations depending on technological conditions of evaporation of thin films of system GaSb-Ge were studied by methods of electronography and transmission electron microscopy. Films of the thickness near 500Å were prepared using method of a flash vacuum evaporation. Glass, ceramic and spallings NaCl monocrystals were served as substrates. Equilibrium of system GaSb-Ge in a massive state is featured by the diagram of the eutectic type, and mutual solubility of components on the molar composition does not exceed 1 %. The composition of films is more convenient to represent using the formula (GaSb)_{1-x}(Ge₂)_x because in the investigated system solid thin-film solutions are formed by substitution.

Films of all explored compositions, precipitated on substrates at room temperature, were amorphous. The linear relation of the proximate interatomic distance (from 2.72Å for a-GaSb to 2.45 Å for a-Ge) in amorphous films from composition is observed. The linear relation of the proximate interatomic distance in coordinate Ge₂ specifies random distribution of atoms with forming "alloyed" structure such as a solid solution of substitution. In amorphous films GaSb threefold coordination in distribution of the proximate atoms is observed. The magnification of concentration Ge gives in conversion of allocation of the proximate atoms. At concentrations Ge₂ about 20 % transferring from threefold coordination to tetrahedral is observed.

With an increase of temperature of a substrate there is a forming the nonuniform amorphous films. Areas of initial ordering on a basis GaSb are observed. With the further increase of temperature of substrates on the isotropic substrates polycrystalline films of a metastable solid solution of substitution are formed, and on spallings NaCl monocrystals are formed textured and epitaxial films. In case of epitaxial films the feeble modulation of a composition detected by transmission electron microscopy is observed.

THEORY OF SOLID-STATE CONDENSED SYSTEMS

RESONANT TUNNELING IN A DOUBLE-BARRIER JOSEPHSON JUNCTION

P. Shygorin¹, B. Venhryn²

¹ Department of Theoretical and Mathematical Physics, Lesya Ukrainka Eastern European National University, Volya Avenue 13, 43025 Lutsk, Ukraine

² Department of Applied Physics and Nanomaterials Science, Lviv Polytechnic National University, Bandera street 12, 79013 Lviv, Ukraine

This work represents studies of the Josephson current in a tunnel junction that has multilayer “sandwich” structure SISIS (S – superconductor, I – isolator). Microscopic description of the current states in this junction can be developed by using the quasiclassical equations of the theory of superconductivity and partially has been provided in paper A. Svidzynskij (2017) [1].

The calculations show that value of supercurrent through SISIS junction has significant difference from the current in the case of single-barrier SIS-junction. The value of supercurrent has a non-monotonous dependence on distance between barriers with the presence of resonance peaks (Figure 1a). This is related to the resonant tunneling of Cooper pairs through the double-barrier structure. Another feature of the supercurrent in a double Josephson junction is that it exhibits a non-sinusoidal current-phase relation. Current-phase relation for SISIS-junction at different values of a transparency is shown in Figure 1b.

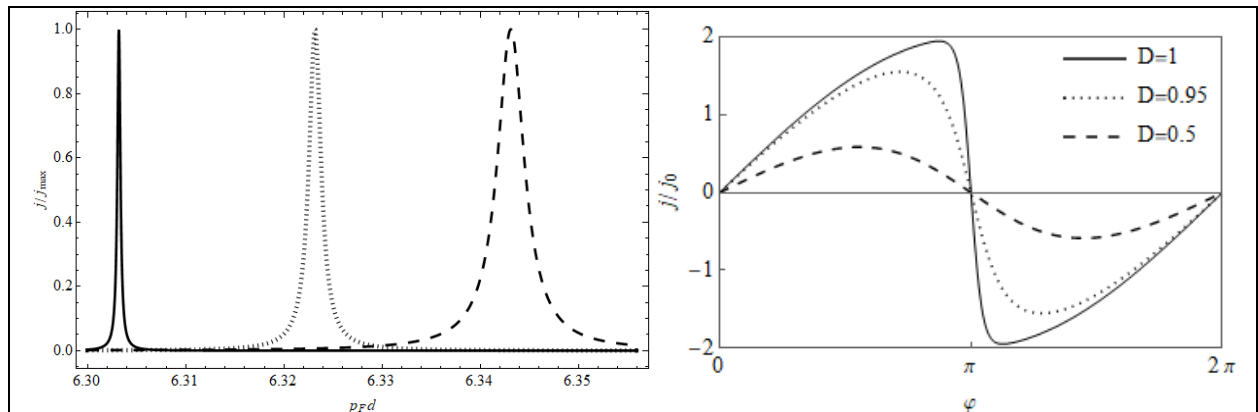


Figure 1a (left): Dependence of a current density on a distance between the barriers (a thickness of interior superconducting layer). Figure 1b (right): Current-phase relation curves for SISIS-junction at different values of a transparency.

In the present work we also derive equation for calculation of the thickness of interior superconducting layer that corresponds to the maximum value of a supercurrent. That gives futures for designing sensitive Josephson junctions for SQUIDs.

[1] P. Shygorin, A. Svidzynskyi and I. Material, Ukr. J. Phys. 62 (2017), 518-522.

NUMERICAL SIMULATION AND MODELING

ELECTRONIC PROPERTIES OF III-GROUP ELEMENTS DOPED ARMCHAIR ZNO NANORIBBONS

Bovgyra O., Kovalenko M., Dzikovskyi V., Ilchyshyn N.

Faculty of Physics, Ivan Franko National University of Lviv, 8a, Kyrylo and Mefodiy str.,
79005 Lviv, Ukraine.

Zinc oxide (ZnO) is the object of an increasing interest in the last decades due to its potential applications in transparent conducting oxide thin films for light-emitting diodes, optoelectronic devices, and spintronics. For the construction and implementation of ZnO based devices, doping is one of the most applicable issues. Nanoribbon (NR) is one type from big family one-dimensional nanostructures, length of which is greatly larger than their width. However, in the cross-section of NR, the quantum confinement effect is not uniform compared to its nanowire and nanotubes analogs. The effective realization of general applications based on ZnO nanoribbons (ZnONRs), as functional construction bricks in different nanodevices, depends on the possibility to tune their electrical transport properties. Besides, the armchair and zigzag shape edges of the ZnO nanoribbons produce original electronic, magnetic, and mechanical properties. An efficient way to controlling the electrical properties of semiconductor nanostructures is their doping and this method extensively used in the production of the semiconductor.

In this study, we represent based on the density functional theory the theoretical study of the structural, electronic, and optical properties of pure and doped (Ga, In, and Al) ZnONRs with the armchair-shaped edge. This study is the first step for a real understanding of the unique properties of doped ZnO nanoribbons, which is significant to employ them as building bricks for future applications.

The ultrasoft pseudopotentials were used to describe the electron-ionic core interaction. To describe the exchange-correlation interaction we used the generalized gradient approximation (GGA) in the parameterization of the Perdew-Burke-Ernzerhof (PBE). Also, to represent the electronic structures more accurately, we performed the GGA+ U method. The surface of ZnO nanoribbons was presented in periodic supercells and for eliminating the interaction between neighboring cells we made 10 Å of vacuum gap.

Calculation results show that all pristine and edge-passivated armchair ZnONRs are nonmagnetic semiconductors despite their widths. The value of the aZnONRs band gap monotonically decreases with increasing of their width. We observed configuration dependency of structural and electronic properties of doped ZnONRs. We find that electronic spectra aZnONRs doped by In, Al, Ga atoms, shows half-metallic properties and behave like an n-type semiconductor.

ELECTRONIC STRUCTURE AND ELASTIC PROPERTIES OF Sc_5CuIn_3 : FIRST PRINCIPLES STUDY

O.V. Bovgyra¹, I.V. Kutsa¹, P.M. Yakibchuk², N.L. Gulay², Ya.M. Kalychak²

¹ Faculty of Physics, Ivan Franko National University of Lviv,
Kyryla i Mefodiya Str. 8, 79005 Lviv, Ukraine

² Faculty of Chemistry, Ivan Franko National University of Lviv,
Kyryla i Mefodiya Str. 6, 79005 Lviv, Ukraine

Ternary systems of rare earth metals with transition elements, especially Ni, Co, Cu, and In have been investigated intensively because of existence of numerous compounds with different crystal structures and interesting physical properties. Sc–Cu–In system has not been investigated systematically as yet. So far four compounds $\text{Sc}_2\text{Cu}_2\text{In}$, ScCu_2In , ScCu_4In and Sc_5CuIn_5 have been reported. However, influence of Sc additions on the mechanical and related properties of multi-component alloys, has been widely discussed in the literature [1].

In this work, we report the lattice structure, electronic structure and mechanical properties of Sc_5CuIn_5 intermetallic compound obtained by first-principles calculations based on density functional theory (DFT). Calculations are performed using the PWscf (Quantum-Espresso) package. The electron-ionic core interaction is represented by the ultrasoft pseudopotentials with valence electron configuration of $3s^23p^63d^14s^2$ for Sc, $3d^{10}4s^1$ for Cu, $4d^{10}5s^25p^1$ for In. The PBE form of the generalized gradient approximation (GGA) is adopted to describe the exchange correlation interaction. To describe the electronic structures more accurately, we used GGA+U method. Geometrical optimizations were performed using Broyden–Fletcher–Goldfarb–Shanno (BFGS) method.

The calculated structural parameters agree with the corresponding experimental values [2]. The optimized structure was used for obtaining the five independent elastic constants C_{ij} . Also, the polycrystalline elastic moduli (such as, bulk modulus B, shear modulus G, Young's modulus E and Poisson's ratio ν) have been gained from single-crystal elastic constants using the Voigt–Reuss–Hill method. The ductility of Sc_5CuIn_5 have been analyzed using three criteria: Pugh's rule, Cauchy's pressure and Frantsevich's rule.

The spin-polarized electronic band structures has no band gap at the Fermi level, and, hence, Sc_5CuIn_5 is metallic. The bands at the Fermi level are mainly contributed by Sc d-orbitals and by In p-orbitals. The s-states of Cu lying below the Fermi level whereas the Sc d-states are situated above the Fermi level.

- [1] S. Riva, K. V. Yusenko, N.P. Lavery, D.J. Jarvis, S.G.R. Brown, *Int. Mater. Rev.* 61(3) (2016) 203-228.
- [2] N.L. Gulay, Yu.B. Tyvanchuk, M. Daszkiewicz, D. Kaczorowski, Ya.M. Kalychak, *J. Alloys Compd.* 815 (2020) 152660.

MODELING OF IDEALITY FACTOR VALUE IN SILICON SOLAR CELLS

Olikh O.Ya., Zavhorodnii O. V.

¹ Faculty of Physics, Taras Shevchenko National University of Kyiv, Kyiv 01601, Ukraine
olikh@univ.kiev.ua

Ideality factor (n) is one of a commonly used parameter of solar cell (SC). In the simplest case, $n = 2$ is used for Shockley-Read-Hall recombination current. But in fact, n depends on ambient conditions and recombination center parameters. The purpose of this work is to evident such dependencies for Si-SC.

The current-voltage characteristics of silicon n^+p-p^+ structure were calculated by using of one-dimensional code SCAPS in the temperature range 290-340 K. The both base depth d and acceptor (boron) concentration N_A were varied over 150-240 μm and $10^{15}\div 10^{17} \text{ cm}^{-3}$ respectively. The iron atoms are suggested to be present in p-layers with $N_{\text{Fe}} = 10^{10}\div 10^{13} \text{ cm}^{-3}$. The case of Fe_iB_s pairs as well as the case of interstitial Fe_i was under consideration. The ideality factor was determined according to the two-diode model. Some results are presented in Fig.1.

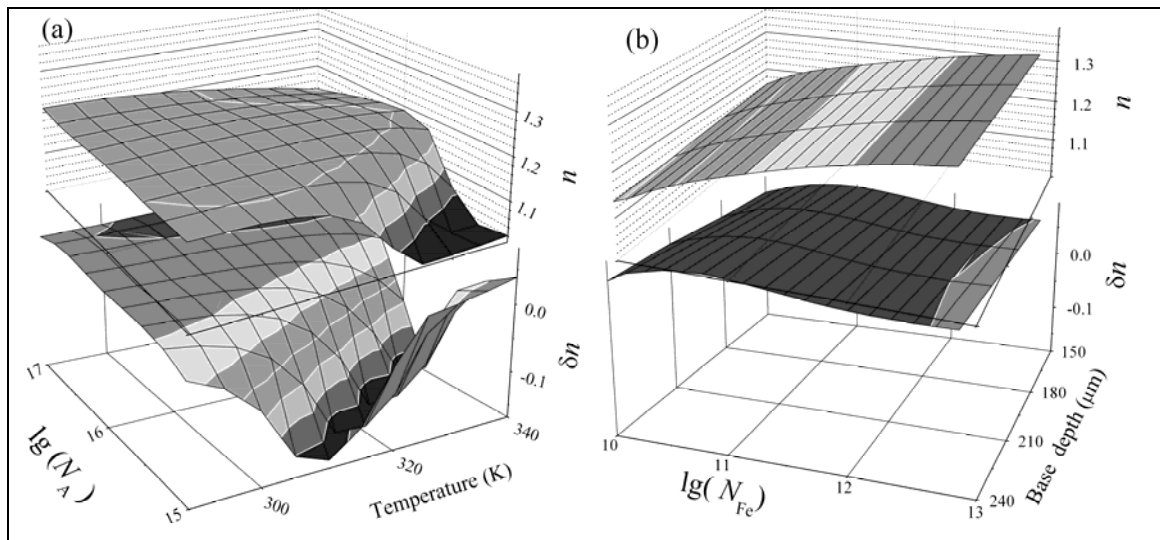


Figure 1: Dependencies of ideality factor in equilibrium state (n , upper surfaces) and alteration in ideality factor after Fe-B pair dissociation (δn , lower surfaces).

$N_{\text{Fe}} = 10^{10} \text{ cm}^{-3}$, $d = 240 \mu\text{m}$ (a), $N_A = 10^{17} \text{ cm}^{-3}$, $T = 340 \text{ K}$ (b).

It was established that i) the base depth affects the ideality factor value in the case of minority carrier diffusion length $L_n \gg d$; ii) the influence of temperature and doping level deals with change in a recombination level population mainly; iii) the dependence of n on the iron concentration is a monotonic function.

NONLINEAR OPTICAL EFFECTS IN CRYSTALS OF LANGASITE FAMILY

Nazar Ftomyn¹, Yaroslav Shopa²

¹Ivan Franko National University of Lviv, Faculty of Physics, Department of General Physics, 19 Drahomanov Street, 79005 Lviv, Ukraine, nazar.ftomyn@lnu.edu.ua

²Cardinal Stefan Wyszyński University in Warsaw ul. Dewajtis 5, 01-815 Warszawa, Poland, i.shopa@uksv.edu.pl

In recent years, researchers have become increasingly interested in investigating new nonlinear optical (NLO) materials such as crystals of langasite family ($\text{La}_3\text{Ga}_5\text{SiO}_{14}$, $\text{Ca}_3\text{Ga}_2\text{Ge}_4\text{O}_{14}$, $\text{Sr}_3\text{Ga}_2\text{Ge}_4\text{O}_{14}$, $\text{La}_3\text{Ga}_{5.5}\text{Ta}_{0.5}\text{O}_{14}$, $\text{La}_3\text{Ga}_{5.5}\text{Nb}_{0.5}\text{O}_{14}$, etc). These systems are promising in application in the midinfrared region (they are transparent up to $7\mu\text{m}$) [1]. Because of these materials are noncentrosymmetric (point group symmetry 32) only $d_{11} = -d_{12} = -d_{26}$ and $d_{14} = -d_{25}$ components of second-order NLO susceptibility tensor are non-zero in these crystals, respectively.

The major task of this study is to calculate the second-order NLO susceptibility d_{ijk} tensor components of langasite family crystals using dipole electron shifting (DES) model [2, 3]. In DES approach the d_{ijk} are calculated using equation [2]:

$$\varepsilon_{ij}(E_k^{Ext}) - \varepsilon_{ij}(0) = 2 \sum_k d_{ijk} E_k^{Ext}. \quad (1)$$

Here, \mathbf{E}^{Ext} denotes external electric field which shifts the atomic nuclei by the distance proportional to the electronic polarizability of ions, ε_{ij} the relative dielectric constants.

It is well known, that information about crystal structure, electronic polarizability of ions as well as data of optical activity of investigated materials ensure good results of calculations [4]. As a result, computation of the components of NLO susceptibility tensor in some crystals of langasite family will allow to compare the theoretical calculations with experimental ones expressed e.g., in [1].

- [1] Haichao Lan, Fei Liang, Zheshuai Lin, et al. International Journal of Optics. 2017 (2017) 1-13.
- [2] W. Kaminsky, Rep. Prog. Phys. 63 (2000) 1575–1640.
- [3] W. Kaminsky, D. Responde, D. Daranciang et al., Molecules. 15 (2010) 554-569.
- [4] N. Ftomyn, Ya. Shopa, I. Sudak, Acta Physica Polonica A 133 (2018) 933-935.

COMPARATIVE STUDY OF STRUCTURAL AND VIBRATIONAL STABILITY OF LAYERED TlInS_2 AND $\text{TlIn}(\text{S}_{0.75}\text{Se}_{0.25})_2$ FERROELECTRIC CRYSTALS

T. Babuka^{1,2}, M. Makowska-Janusik², K.E. Glukhov¹,
L.Yu. Kharkhalis¹, O.O. Gomonnai^{3,4}, A.V. Gomonnai^{3,5}, D.R.T. Zahn⁶

¹Institute for Physics and Chemistry of Solid State, Uzhhorod National University, 54 Voloshin St., 88000 Uzhhorod, Ukraine

²Institute of Physics, Faculty of Mathematics and Natural Science, Jan Dlugosz University in Czestochowa, Al. Armii Krajowej 13/15, 42-200 Czestochowa, Poland

³Uzhhorod National University, 46 Pidhirna Str., 88000 Uzhhorod, Ukraine

⁴Vlokh Institute of Physical Optics, 23 Dragomanov Str., 79005 Lviv, Ukraine

⁵Institute of Electron Physics, Ukr. Nat. Acad. Sci., 21 Universytetska Str., 88017 Uzhhorod, Ukraine

⁶Semiconductor Physics, Chemnitz University of Technology, D-09107 Chemnitz, Germany

Recently, layered crystals have attracted research interest due to promising structural and physical properties. A possibility to create new multifunctional artificial materials obtained through the arrangement of several layered crystals became a new subject of studies. One such class of materials representatives is a TlInS_2 crystal [1] which belongs to the $A^{\text{III}}B^{\text{III}}C^{\text{VI}}_2$ group of chalcogenide semiconductors and is regarded as a highly anisotropic structure [2].

These features motivate us to carry out quantum mechanical calculations of the structural stability of TlInS_2 crystal and their solid solutions in combination with the experimental measurements of its vibrational characteristics. TlInS_2 crystal has a prominent layered structure with two layers in the unit cell which is characterized by the so-called van der Waals (vdW) gap. In this case, first-principle calculations of electronic and optical properties of the TlInS_2 and $\text{TlIn}(\text{S}_{0.75}\text{Se}_{0.25})_2$ crystals have been carried out using a combination of the density functional theory (DFT) supplied with dispersion correction (D) and Hubbard correction (U) for improving the bandgap calculation. Also, for the explanation of their structural stability, the cohesive energy for both materials have been calculated. The vibrational properties of considered materials also were calculated utilizing DFT. The phonon frequencies of TlInS_2 and $\text{TlIn}(\text{S}_{0.75}\text{Se}_{0.25})_2$ crystals were studied experimentally by Raman spectroscopy. The measurements were performed in the frequency range of 16–340 cm^{-1} in the temperature range of $30 \text{ K} \leq T \leq 293 \text{ K}$. To determine the nature of lines in the experimental Raman scattering spectra they were compared with the phonon modes calculated within DFT-D+U methodology.

- [1] V. Grivickas, P. Scajev, V. Bikbajevas, O. V. Korolik, A. V. Mazanik, *Phys. Chem. Chem. Phys.* 21 (2018) 1-13.
[2] G. R. Offergeld, U.S. Patent, 3, 110 (1963) 685.

AB INITIO STUDY OF CRYSTAL STRUCTURE AND PHYSICAL PROPERTIES OF $\text{CuGa}(\text{S}_x\text{Se}_{1-x})_2$ SOLID SOLUTIONS

M.Ya. Rudysh^{1,2,3}, M.G. Brik^{1,4,5}, M. Piasecki^{1,3}, A.O. Fedorchuk⁶,
G.L. Myronchuk³

¹ Faculty of Science and Technology, J. Dlugosz University in Częstochowa, Armii Krajowej 13/15, 42-201 Czestochowa, Poland

² Faculty of Physics, Ivan Franko National University of Lviv, Dragomanova 19, Lviv 79000, Ukraine

³ Faculty of Information Systems, Physics and Mathematics, Lesya Ukrainka Eastern European National University, Voli Ave. 13, Lutsk 43025, Ukraine

⁴ A CQUPT-BUL Innovation Institute & College of Sciences, Chongqing University of Posts and Telecommunications, Chongqing 400065, P.R. China

⁵ Institute of Physics, University of Tartu, W. Ostwald Str. 1, Tartu 50411, Estonia

⁶ Department of Inorganic and Organic Chemistry, Lviv National University of Veterinary Medicine and Biotechnologies, Lviv, Ukraine

The ternary chalcogenide crystals of I-III-VI₂ group are a class of materials with chalcopyrite crystal structure [1]. This material is non-centrosymmetric and transparent in the mid-infrared region of spectra which makes them promising for a nonlinear optical application like second harmonic generation, optical parametric oscillation, etc. [2-4]. Also, these materials are suitable for solar cell applications because of the high absorption coefficient and bandgap near-optimal value.

This work is devoted to the theoretical study of $\text{CuGa}(\text{S}_x\text{Se}_{1-x})_2$ chalcopyrite solid solutions. For the investigation of titled crystals, the computational simulation within density functional theory (DFT) was used. The structural, electronic and optical properties are calculated and discussed.

Study was supported by PRELUDIUM 15 program of Polish National Science Center (Grant No. 2018/29/N/ST3/02901).

- [1] J. L. Shay, J. H. Wernick, Ternary Chalcopyrite Semiconductors: Growth, Electronic Properties, and Applications. Pergamon Press, Oxford, 1975.
- [2] J-J. Zondy, D. Touahri, and O. Acef, J. Opt. Soc. Am. B 14 (1997) 2481-2497.
- [3] H. Kildal, J.C. Mikkelsen, Optics Communications 9 (1973) 315-318.
- [4] P. Jackson, D. Hariskos, E. Lotter, S. Paetel, R. Wuerz, R. Menner, W. Wischmann, and M. Powalla, Progress in Photovoltaics: Research and Applications 19 (2011) 894-897.

FREE VOLUME DISTRIBUTION IN BI-ZN LIQUID ALLOYS

I. Shtablavyi¹, V. Plechystyy¹, B. Tsizh^{2,3}, S. Mudry¹

¹ Ivan Franko National University of Lviv, Kyrylo i Mephodiy 8, 79005 L'viv, Ukraine

² Stepan Gzytsky Lviv National University of Veterinary Medicine and Biotechnologies, 50, Pekarska Str., 79010, Lviv, Ukraine

³ Kazimierz Wielki University, J.K. Chodkiewicza 30, 85-064 Bydgoszcz, Poland

Investigations of the liquid state of matter are of interest not only from the fundamental point of view, but also from the practical point. Recently, metal melts are being studied not only to improve casting processes, but also in connection with the more exotic use of melts. In particular, low-melting alloys are used as a catalyst in the synthesis of carbon nanotubes, and they are also used in flexible electronics systems. Recently, liquid metals are proposed to be used as media for the synthesis of intermetallic compounds with unique properties. In order to successfully use liquid metals and alloys, further in-depth study is needed.

Until now, the structure of metal melts was mainly studied by interpreting changes in interatomic distances, coordination numbers and their partial values depending on external factors. However, the structure of disordered systems must be considered comprehensively, i.e. taking into account both the arrangement of atoms and the distribution of free volume. Such complex researches became possible due to intensive development of computer methods of modeling of structure and properties of disordered systems.

In this work, a comprehensive study of the structure and distribution of the free volume of Bi-Zn melts in the vicinity of the monotectic point was carried out. Alloys based on the bismuth-zinc system are promising for use as lead-free solders, directionally crystallized and dispersed materials. Due to the fact that Bi-Zn alloys belong to systems with an immiscibility gap in the liquid state, the decisive role in the process of homogenization of such alloys is played by the distribution of free volume. In order to further analyze the distribution of free volume in the melts at different temperatures, the results of experimental studies and computer simulations were used.

BINARY STRUCTURING AND OPTIMIZATION OF MICROELECTROMECHANICAL SYSTEMS WITH "GOLD" PROPORTION

P.Kosobutskyy¹, I.Onishechko²
¹ petkosob@gmail.com
² onishechko.lviv@gmail.com

Correct formulation of the basic principles of the dynamics of oscillations of elastic elements of microelectromechanical systems (MEMS), made it possible to expand the functionality of the Pareto optimization algorithm of the basic elements of MEMS using the Cauchy criterion [1]. Subsequent studies [2] have shown that an effective method for such problems is the binary structuring of physical systems by the "golden" proportion as the ratio of parameters between the divided unequal parts at the phase point $p=1, q=1$ in the plane of Cartesian coordinates $p0q$. It is established [3-4] that the so-called "golden" properties have

the roots $\Phi = \frac{1}{2}p + \sqrt{\left(\frac{p}{2}\right)^2 + q}$, $\varphi = \frac{1}{2}p - \sqrt{\left(\frac{p}{2}\right)^2 + q}$ of the equation $\varphi^2 + p\varphi - q = 0$ in other phase points $p = q = k$, which significantly expands the functionality of the method of "golden" proportion in one-dimensional optimization.

References

- [1] P.Kosobutskyy, et.al. Physical principles of optimization of the static regime of a cantilever-type power-effect sensor with a constant rectangular cross-section. Journal of Electronic Research and Application (Australia). **2**(5). – P.11–15, 2018.
- [2] P.Kosobutskyy P. Modelling of electrodynamic Systems by the Method of Binary Separation of Additive Parameter in Golden Proportion. Jour. of Electronic Research and Application (Australia). **3**(3), 8-12, 2019.
- [3] Kosobutskyy P. S. Phidias numbers as a basis for Fibonacci analogues. Notes on Number Theory and Discrete Mathematics (Bulgaria). **26**(1), 172—178, 2020.
- [4] P.Kosobutskyy , et.al.. Mathematical methods for cad: the method of proportional division of the whole into two unequal parts . Bulletin of the LPNU. Lviv. Collection of scientific works. Scientific publication. Series: Computer Design Systems. Theory and practice. №908, 75-90, 2019

THE CRYSTAL SIZE INFLUENCE ON THE FOURIER SPECTRUM OF THE AMPLITUDE FUNCTION OF THE INCOMMENSURATE SUPERSTRUCTURE

S. Sveleba, I. Katerynychuk, I. Kuno, I. Karpa, O. Semotyuk

Ivan Franko National University of Lviv,
107 Tarnavsky St., UA-79017 Lviv, Ukraine
incomlviv@gmail.com

The linear size reducing of the samples of crystals $(\text{N}(\text{CH}_3)_4)_2\text{MeCl}_4$ causes the effect of the phase slip, the temperatures of phase transitions lowering and the temperature range narrowing of the incommensurate (IC) phase. This behavior of the properties of the IC of the superstructure is due to the influence of surface energy increasing on the energy of the incommensurate superstructure. Numerical calculations show that the surface effect cannot be replaced by the effect of electric field strength on the incommensurate superstructure. Therefore, the influence of the size limitation on evolution of the existence of a wave of the incommensurate modulation in the work considered.

Calculations of spatial changes in the amplitude of the order parameter were performed for systems described by two second-order differential equations with the symmetry of the thermodynamic potential $n = 3$ and the value of the longinfluence interaction $T = 1$. This system was solved by the numerical BDF method. The calculation of the spatial changes in the amplitude and phase of the order parameter was performed in the Python environment using the Skipy and JiTCODE libraries.

According to the obtained dependences, incommensurate superstructure is characterized by an increase in the period of spatial oscillations with the number of existing spatial modulation waves decrease. The transition to soliton mode is accompanied by the appearance of new oscillations ($K = 0.6$). The modulation harmonics behavior from the parameter K indicates complex transformations that occur during the transition from one mode to another, regardless of the sample size.

So, based on the studies of the Fourier spectra of oscillations of the amplitude function of the incommensurate modulation, it can be argued that the linear size of the crystal decrease cause a change in the spectrum of frequencies of the incommensurate modulation.

FOURIER SPECTRUM OF OSCILLATIONS OF THE AMPLITUDE FUNCTION OF THE INCOMMENSURATE PHASE FROM THE MAGNITUDE OF THE ANISOTROPIC INTERACTION, DESCRIBED BY DZIALOSZYNSKI INVARIANT

S. Sveleba, I. Katerynychuk, I. Kuno, I. Karpa, O. Semotyuk

Ivan Franko National University of Lviv,
107 Tarnavsky St., UA-79017 Lviv, Ukraine
incomlviv@gmail.com

The evolution of a incommensurate phase (IP) in the first approximation is determined by two competing influences: long-range and anisotropic interaction. The influence of each role (which is determined by the parameters T and K , respectively) at different stages of the dynamics of the superstructure, when the influence of the order parameter is both spontaneous deformation ($n = 3$) and spontaneous polarization ($n = 4$). To this end, the Fourier study of the spectrum of the amplitude modulation function from the magnitude of the anisotropic interaction was performed.

The calculation of the spatial changes in the amplitude of the order parameter was performed for systems described by two second-order differential equations. This system was solved by the numerical BDF method. The calculation of the spatial changes of the amplitude and phase of the order parameter was performed in the Python environment using the Skipy and JiTCODE libraries according to the method described.

According to the obtained dependences, incommensurate superstructure is characterized by a chaotic state in the process of its origin ($K = 0 \div 0.3$ for $n = 4$ and $K = 0 \div 0.1$ for $n = 3$). The transition to the soliton regime is accompanied by the appearance of new oscillations ($K = 2.1$ for $n = 4$ and $K = 0.6$ for $n = 3$). Subsequent changes in the parameter K cause the appearance of chaotic behavior q , which indicates the transition of the system to the stochastic mode of the superstructure with the emergence of a chaotic phase ($K > 4.2$ for $n = 4$ and $K \Rightarrow 1.5$ for $n = 3$). The behavior of the harmonics of the IP modulation from the parameter K indicates the complex transformations that occur during the transition from one mode to another.

Therefore, based on studies of the harmonics of the IP modulation, it can be confirm that the transition to the soliton mode of the IP superstructure is accompanied by change frequency spectrum of incommensurate modulation.

**PHYSICS AND CHEMISTRY OF LOW DIMENSIONAL
MATERIALS AND THEIR PROPERTIES**

MORPHOLOGY OF THIN FILMS $Y_2O_3:Eu$ OBTAINED BY DIFFERENT METHODS

Bordun O.M., Bordun I.O., Kofliuk I.M., Kukharskiy I.Yo.

Ivan Franko National University of Lviv; Faculty of Electronics and Computer Technology; Lviv, Drahomanova st., 50;

Considerable interest in the study of nanostructures of various chemical composition, structure, and morphology is caused by interesting physicochemical, electrical, optical, and other properties of nanomaterials, which open up broad prospects for their practical application [1-3]. Among them, a special place is occupied by materials doped with rare-earth ions (REI), which are key elements of modern devices for generating, transmitting, and controlling optical signals. One of the most used REIs is europium Eu^{3+} , which is widely used in nuclear power, to generate laser radiation in the visible spectral region with a wavelength of 0.61 μm , and $Y_2O_3:Eu^{3+}$ is the most efficient phosphor emitting in the red region of the spectrum.

Thin $Y_2O_3:Eu$ films 0.2 - 1.0 μm thick obtained by RF ion-plasma sputtering and discrete evaporation in vacuum on fused $v-SiO_2$ quartz substrates. RF sputtering was carried out in an argon atmosphere in a system using the magnetic field of external solenoids for compression and additional ionization of the plasma column. The feedstock was Y_2O_3 of the ИТO-И brand and Eu_2O_3 of the “oc. ч.” brand. The activator concentration was 1 mol. % After applying the films, they were heat treated at a temperature of 950-1050 $^{\circ}C$ in air.

Using the X-ray diffraction analysis (Shimadzu XDR - 600), the structure and phase composition of the films were studied. X-ray diffraction studies showed the presence of a polycrystalline structure with a predominant orientation in the (222) plane. The form of the obtained diffractograms is almost analogous to the diffractograms of pure Y_2O_3 films that we presented in [4]. All diffraction maxima are identified according to the selection rules and belong to the space group $T_d^2 = Ia\bar{3}$, which indicates the cubic structure of the obtained films.

The surface morphology of the films was investigated using an atomic force microscope (AFM) «Solver P47 PRO». Processing of experimental data and calculation of surface morphology parameters was carried out using the «Image Analysis 2» software package.

Based on the measurements, it was found that during RF ion-plasma sputtering and discrete evaporation, polycrystalline $Y_2O_3:Eu$ films consisting of nanometer grains are formed. The topography of the samples was quantitatively characterized by standard parameters: root mean square roughness, maximum grain height with diameter and grain height, which were calculated according to AFM data for sections of the same size (1000?1000 nm). The characteristic parameters of thin $Y_2O_3:Eu$ films obtained by various methods are listed in Table 1.

Table 1 - Parameters of crystalline grains of thin Y₂O₃:Eu films

Parameter	RF -sputtering	Discrete spraying
Diameter of the grains, nm	15,7	15,7
Root mean square roughness, nm	0,7	1,2
Maximum grain height, nm	6,0	10,3
Grain volume, nm ³	1123,5	1469,5

A slight decrease in the grain concentration and a simultaneous increase in grain sizes in thin Y₂O₃:Eu films upon transition from RF -sputtering into discrete evaporation (Table 1) indicate the possibility of the transition of the surface of the Y₂O₃:Eu film during discrete evaporation to a more nanostructured state due to crystallization of the surface layer .

According to AFM data, it is shown that upon transition from RF -sputtering to discrete evaporation, the mean square surface roughness increases, although the average grain diameter on the film surface in both cases is 15.7 nm. Moreover, the diameter distribution of grains during RF -sputtering corresponds to the normal logarithmic distribution with one distribution center, and for discrete evaporation with two distribution centers, which approximately correlate as 1:2, which indicates grain growth among themselves.

1. K.M. Nissamudeen and K.G. Gopchandran, J. Alloys and Compounds, **490**: 399 (2010).
2. P. Packiyaraj and P. Thangadurai, J. Luminescence., **145**: 997 (2014).
3. H. Huang, G.A. Xu, W.S. Chin and L.M. Gan, Nanotechnology, 13, **№3**: 318(2002).
4. O.M. Bordun, I. O. Bordun and I. Yo. Kukharskyy, J. Appl. Spectrosc., **82**, **№3**: 390 (2015).

CHARACTERIZATION OF GIANT PIEZODIELECTRIC EFFECT IN DISPERSIVE GaSe LAYERED CRYSTALS

Orest Fliunt

Faculty of Electronics and Computer Technologies,
Ivan Franko National University of Lviv, 50, Dragomanov str., 79005, Ukraine
email: Orest.Fliunt@lnu.edu.ua

Many solids showing giant piezoresistance effect are characterized by dispersive behavior of some physical parameters in the low-frequency range. Some works even consider giant piezoresistance effect as transition process leading with time to usual bulk strain properties of materials. These facts make interesting to consider giant strain effects in low-frequency range dispersive systems as ac response. Layered crystals can be considered as suitable materials because they often show frequency dispersion of dielectric constant and electrical impedance probably caused by structure disordering of different type, like layer' stacking faults, non-controlled intercalation, vibrational movement of single layers et al.

Hopping charge carrier systems show power fractional spectra in frequency domain obeying $B(j\omega)^{-(1-n)}$ law, where j is imaginary unit and exponent n is close to 0.8. This type of dielectric dispersion is often observed in high-resistivity GaSe layered crystals. In this work effect of stress on dispersive system of charge carrier type has been analyzed using distribution of parameters of effective dipoles according to power fractional law, which are formed in the consequence of sequel interaction of elementary hopping charge carries. In the results even previously equivalent elementary localized carriers may occupy positions with different parameters, which change with time. It has been proposed, that equivalent dipoles behave with stress like elementary ones, but with drastically lower dispersive equivalent of Young module.

It has been shown that stress properties can be characterized by stress dependence of B and exponent n . Predicted value of the ratio of this two parameters is close to experimentally observed in GaSe layered crystals [1, 2]. Frequency dependence of relative change of dispersive dielectric constant has been explained. The proposed model gives some possibility to control parameters of giant piezodielectric effect in dispersive solids. According to the model, dielectric dispersive systems may be considered as promising materials for revealing of giant piezoresistance or piezodielectric effect.

- [1] O. Fl'unt, Ya. Fiyala, X International Seminar on Physics and Chemistry of Solids (ISPCS'04), Lviv, Ukraine, June 6-9, 2004.
- [2] O. Fliunt, Appl. Nanosci. (2020) 1-7.

FORM OF POSITRON-ELECTRON ANNIHILATION KINETICS IN MgO-Al₂O₃ CERAMICS IN THE FREQUENCY DOMAIN

Orest Fliunt¹, Halyna Klym², Adam Ingram³

¹ Ivan Franko National University of Lviv, 50, Dragomanov Str, Lviv 79005, Ukraine

² Lviv Polytechnic National University, 12, Bandera Str, Lviv 79013, Ukraine

³ Opole University of Technology, 75, Ozimska Str, Opole 45370, Poland

Kinetic of positron-electron annihilation (PEA) in solids may be presented in the time or frequency domain [1, 2]. Experimentally observed time-domain PEA kinetics $h(t)$ gives time dependence of intensity of annihilation in time after abrupt termination of steady state positron flux irradiation of sample under study. Frequency-domain response represents in-phase (real) and quadrature (imaginary) components of intensity of PEA annihilation in sample under study illuminated by intensity modulated according to sinusoidal law positron flux at different frequencies within some range. Frequency spectra have some advantages in comparison with time-domain impulse characteristics that concern the possibilities of determining form of terms of relaxation. Frequency analysis also shows higher noise protection, satisfying higher accuracy of measurements and wider frequency or time range.

Spectra of modulated PEA annihilation of MgO-Al₂O₃ ceramics have been calculated from time domain PEA kinetics $h(t)$ using integral Fourier transform. Cubic spline interpolation of temporal impulse characteristics have been used for numerical calculation of Fourier integrals.

PEA spectra of sintered MgO-Al₂O₃ ceramics show large maximum at frequency of about 0.5-0.65 GHz that corresponds to characteristic relaxation time of about 0.26-0.35 ns. There is no any evidence to consider the large maximum as consisting of a few Debye type components [2]. At frequency of this maximum the most intensive interaction of modulated positron flux with ceramics takes place. After water treatment, some deviation of low-frequency side of large dispersion have been observed, allowing to consider large maximum as two components with much weaker lower frequency Debye type term. Water adsorption leads also to increasing weak low-frequency component at frequencies of about 59-80 MHz showing significant spreading of maximum and deviation from Debye law form [2,3]. Form of PEA spectra has been analyzed taking into account compatibility of spectra of real and imaginary components to integral Kramers-Kronig relations.

[1] O. Fliunt, H. Klym, A. Ingram, Appl. Nanosci. (2020) 1-7.

[2] O. Fliunt, H. Klym, A. Ingram, R. Szatanik, Appl. Nanosci. (2019) 1-6.

[3] O. Fliunt, H. Klym, A. Ingram, Appl. Nanosci. 9 (2019) 1005-1010.

**TECHNOLOGY AND ENGINEERING OF
NANOSTRUCTURED AND ADVANCED
MATERIALS**

FORMATION OF PERIODIC MICRO- AND NANOSTRUCTURES ON THE SURFACE OF MONOCRYSTALLINE SILICON USING LASER

I.A. Mohylyak

mohylyak@gmail.com

Experimental studies of the features of the formation of laser-induced periodic nanostructures on the surface of silicon wafers in the zones of action of second, millisecond and nanosecond laser pulses are conducted in the work. The results of microscopic investigations by optical and electron microscopes of periodic structures formed on surfaces with crystallographic orientation (111), (100) are presented.

Different types of periodic structures were obtained, such as periodic surface structures (LIPSS), concentric circles, micropyramids with square and triangular bases. Straight parallel lines are formed by irradiation of the specimen at an angle of 10° from the perpendicular. Such a structure in the form of straight parallel lines is a consequence of the interference between the incident and the electromagnetic wave reflected from the lower boundary of the sample surface melt. The period of the pair lines of these microstructures is $2\ \mu\text{m}$, which correlates with the laser wavelength of $1.06\ \mu\text{m}$ Nd:YAG laser.

Concentric circles, which in some cases are observed on the surface of irradiated silicon, differ in diameter from one to tens of microns. They can be explained by the formation of so-called plasmonic lenses on the surface of a semiconductor at a certain density of laser radiation energy.

The formation of micropyramids is due to the fact that, with the uniform excitation of semiconductors, laser radiation with a threshold power locally molten zones are formed on irradiated surfaces. Those zones reproduce the distribution of the concentration of nonequilibrium charge carriers, modulated by the intracrystalline field according to the symmetry of the crystal. It is established that the shape of local float holes is uniquely related to the crystallographic orientation of the semiconductor surface [1]. In this case, triangular square holes of floodplains are formed on the plane (111) and square ones on the plane (100). Both the individual micropyramids and the accumulation of micropyramids in the form of surface periodic structures were observed on the surface of the test samples throughout the sample surface.

The obtained results can be used to optimize the laser pulse mode for controlled micro- nanostructuring of the semiconductor surface.

- [1] O.Yu. Bonchyk, S.G. Kiyak, I.A. Mohylyak, D.I. Popovych, *Phys. Chem. Solid St.* 18(3) (2017) 309-312.

IMPACT OF SIZE EFFECTS ON THE THERMOCHROMIC PROPERTIES OF NANO- AND MICROCOMPOSITES BASED ON $(\text{NH}_2(\text{C}_2\text{H}_5)_2)_2\text{CuCl}_4$ CRYSTALS

V. Kapustianyk¹, Yu. Chornii¹, S. Semak²

¹ Department of Physics, Ivan Franko National University of Lviv, Dragomanova str. 50, 79005 Lviv, Ukraine

² Scientific-Technical and Educational Center of Low-Temperature Studies, Ivan Franko National University of Lviv, Dragomanova str. 50, 79005 Lviv, Ukraine

The absorption spectra of $[\text{NH}_2(\text{C}_2\text{H}_5)_2]_2\text{CuCl}_4$ (DEACC) nanocrystals and microcrystals incorporated into the polymer matrices were investigated. It has been found that contrary to the case of the initial bulk crystals undergoing the first order thermochromic phase transition the composites with the nanocrystals of an average size 160 nm are characterized only by continuous change of color [1]. The microcomposites with an average size of the microcrystal equal to 200 μm were found to possess the thermochromic properties were similar to those in a bulk crystal although their discontinuous thermochromic phase transition was shifted to higher temperatures (338 K at heating) in respect to the case of the bulk crystal (311 K). The microcomposites with a polystyrene (PS) matrix are characterized by a clear hysteresis loop, which is observed on the temperature dependence of the absorption coefficient at a constant wavelength, which reflects the temperature hysteresis of the phase transition. Such a pronounced thermochromic phase transition in combination with manufacturability of the polymer microcomposite look very attractive for the practical applications in the sensor technique and thermography.

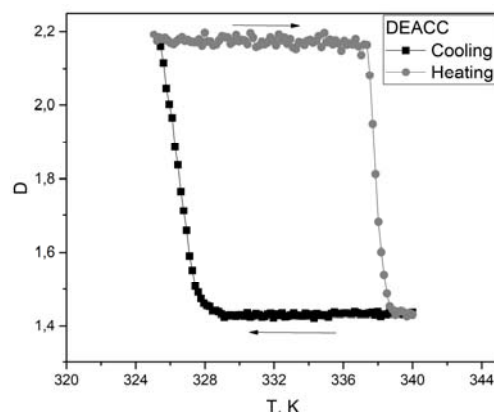


Fig. 1. Temperature evolution of absorbance of DEACC microcrystals incorporated into PS matrix at 590 nm

- [1] V. Kapustianyk, M. Partyka, V. Rudyk, M. Piasecki, M. G. Brik, S Traczyk, K. Ozga, K. Plucinski, S. Romanyshyn, I. V. Kityk, Spectroscopic Studies of the Size Effects in the Absorption Spectra of $(\text{NH}_2(\text{C}_2\text{H}_5)_2)_2\text{CuCl}_4$ Nanocrystals Incorporated into the PMMA Photopolymer Matrix, *Journal of Alloys and Compounds*. 493 (2010) 26-30.

<https://doi.org/10.1016/j.jallcom.2009.12.054>

MOCVD OF III-NITRIDE NANOSTRUCTURES FOR ELEMENTS OF RADIATION, CONVERSION AND ENERGY STORAGE

Vladimir Osinsky¹, Igor Masol², Alexander Radkevich³, Nina Sukhoviya⁴,
Natalia Lyahova⁵

¹ osinsky77@gmail.com

² masol@rostok.ua

³ radkevich@imd.org.ua

⁴ ninasukhoviya@gmail.com

⁵ lyahovann@gmail.com

MOCVD can allow a greater flexibility in dopant selection and great control over the compound stoichiometry. But it has not been systematically studied as for III-nitride nanowire physical properties. So, integration of nanowire components into current thin-film technologies is an important consideration.

Using site-controlled III-nitride quantum dots (QDs) has many advantages for the converting and emitting elements, including its quantum variant [1, 2] with possibility to realize single photon sources (SPS) for quantum processing in contrast to the self-assembled Stranski–Krastanov QDs [3]. We outline some general aspects of the optical properties of III-nitride QDs formed on non-polar surfaces of hexagonal nanowires discussing its high temperature properties for quantum processing.

We also discuss integration possibility of energy storage elements in a single process of MOCVD reactor as for sapphire nano-templates. It has been observed, that, on the nano-templated sapphire surface, a dense transparent film of anomalous surface resistance an order of magnitude lower compared to the original one may be formed through clustering of consolidated phases of BCN in the stream of triethylboron. It has been considered fittingness of such sapphire nano-templates for super capacitor through formation of h-BN in which graphene can be encapsulated

- [1] Zhang L. et al. Charge-tunable indium gallium nitride quantum dots //Physical Review B. – 2016. – T. 93. – №. 8. – C. 085301.
- [2] Osinsky, V., Sukhoviya, N., Masol, I., & Lyahova, N. (2019, April). MOCVD Integration Technology of Enestor through Grafene-Like III-Nitride, Nanocarbides and InGaN/GaN QDs. In 2019 IEEE 39th International Conference on Electronics and Nanotechnology (ELNANO) (pp. 335-339). IEEE.
- [3] Tu, R. C., Tun, C. J., Chuo, C. C., Lee, B. C., Tsai, C. E., Wang, T. C., ... & Chi, G. C. (2004). Ultra-high-density InGaN quantum dots grown by metalorganic chemical vapor deposition. Japanese journal of applied physics, 43(2B), L264.

INFLUENCE OF ELECTRODE STRUCTURE ON THE MORPHOLOGY OF POLYANILINE FILMS

Yatsyshyn M. M., Kostiv V. T., Vlad K. I., Serkiz R. Ya., Reshetnyak O. V.

Ivan Franko National University of L'viv, Kyryla & Mefodiya Str., 6, 79005 L'viv, Ukraine,
e-mail: mykhaylo.yatsyshyn@lnu.edu.ua

Polyaniline (PAN) is an electrically conductive polymer with a wide range of physicochemical properties. As electrodes during the electrochemical synthesis of polyaniline, including also in the form of nanostructured films, the metals of various nature are used [1]. Such films possess anticorrosion protection properties regard to the active metals and alloys on them base, and also are used widely for various applications [1]. Therefore, the studies of nanostructured PAN films deposited on various substrates is an urgent scientific problem.

The formation of PAN was carried out on polycrystalline aluminium and amorphous $\text{Al}_{87}\text{Ni}_8\text{Y}_4\text{Dy}_1$ electrodes in the potentiodynamic mode (in the (-200)–(+1200) mV potential range during 75 cycles of potential scanning with a rate of 25 mV/s) in the 0.25 M aniline aqueous solution in 1.0 M H_2SO_4 . The structure and morphology of PAN deposited on the surface of the working electrodes were studied using IR spectroscopy (NICOLET IS 10 ATR spectrometer), electrochemical impedance spectroscopy (Bode plot) and scanning electron microscopy (microscope-microanalyzer REMMA-102-02) methods.

The study of received SEM images (Fig. 1) shown that porous PAN films formed by rod-like aggregates (Fig. 1, *a*) deposited on the aluminium electrode, while films with closed fibrillar structures has been detected on the amorphous alloys electrode (Fig. 1, *b*).

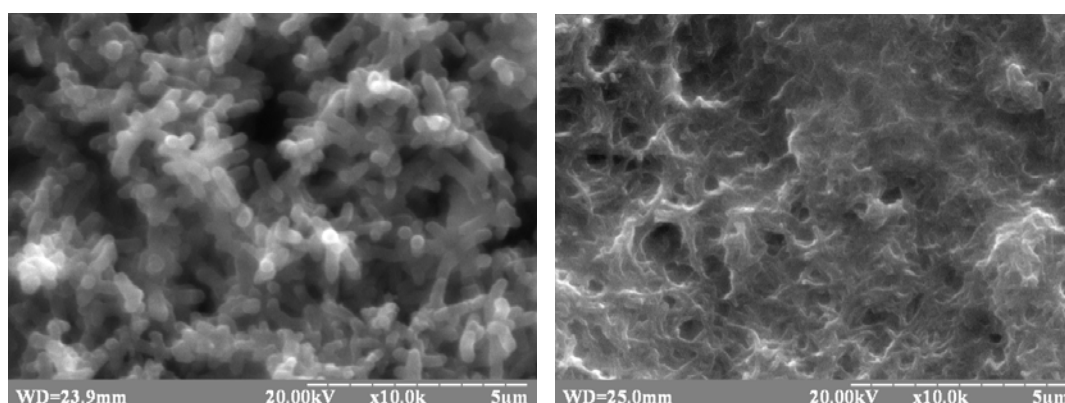


Figure 1: SEM images of the surfaces of PAN films deposited on crystalline aluminium (*a*) and amorphous $\text{Al}_{87}\text{Ni}_8\text{Y}_4\text{Dy}_1$ (*b*) electrodes. Magnification $\times 10000$.

[1] Kuntiyi O., Yatsyshyn M., Zozulya G., Dobrovets'ka O., Reshetnyak O. Electrochemical synthesis of metallic nanoparticles and nanocomposite / O. Kuntiyi, O. Reshetnyak (Eds.). – Lviv: Publishing House of Lviv Polytechnic National University, 2019. – 288 p. (in Ukrainian).

IONIZATION OF AMORPHOUS ALLOY $\text{Al}_{87}\text{Ni}_8\text{Y}_5$ AT DIFFERENT POTENTIAL SCANNING RATE IN A NEUTRAL ENVIRONMENT

Boichyshyn L.¹, Kotur. B.², Khrushchyk Kh.³, Ivashko S.⁴, Hula T.⁵

¹ lboichyshyn@yahoo.com

² bohdan.kotur@lnu.edu.ua

³ khrushchyk.chem@gmail.com

⁴ sofochkaivashko@gmail.com

⁵ djunjer1@gmail.com

Aluminum alloys are quickly covered with oxide passivation films. But spontaneously formed oxide films are often having a poor quality because of a porous structure.

The amorphization process is accompanied by the localization of valence electron pairs, what leads to increased electrochemical activity of the alloy's surface and rapid formation of oxide films with high protective properties. But the penetration of moisture and ions from aggressive environment under passivation films provokes pitting corrosion [1].

The aim of the research work is to investigate the influence of the potential scanning rate on the ionization processes of electrodes from aluminum amorphous alloys and to control the formation of protective oxide films. To investigate the ionization of the $\text{Al}_{87}\text{Ni}_8\text{Y}_5$ electrode in 0.5 M NaCl aqueous solution we used the cyclic voltammetry method in the range of (-1000 ÷ +300) mV with potential scanning rates of 10, 20, 50, 100 mV/sec.

It was determined that the increase of the polarization time of amorphous electrodes at a scanning rate of 10 mV/sec leads to a shift of the corrosion potential in the cathodic direction on $0.72 \pm 0.05\text{V}$. The corrosion currents don't change with increasing number of cycles, which indicates inhibition of $\text{Al}_{87}\text{Ni}_8\text{Y}_5$ dissolving. As the potential scanning rate increases from 10 to 100 mV/sec, the corrosion potential shifts to the anodic side approximately on 200 mV, and the corrosion current decreases in 30 times. According to the Purbe diagrams, sequential ionization of Ni (second peak) and Al (third peak) from the alloy's matrix was identified.

An ion diffusion coefficient in 0.5 M NaCl aqueous solution at the boundary amorphous electrode/electrolyte solution was calculated. For example, the effective values of the calculated from the third cycle (electrochemical reaction time 780 sec) ionization diffusion coefficients of Ni and Al are $3.77 \cdot 10^{-4}$ and $3.18 \cdot 10^{-7} \text{ m}^2/\text{sec}$, respectively. To sum up, the ionization of the main component of aluminum is inhibited.

[1] C.H. Hamann, W. Vielstich. *Electrochemie*. - Wiley, Weinheim. (1998) - 367s.

[2] J.E. Sweitzer, G.J. Shiflet, J.R. Scully. *Electrochimica Acta*. 48 (2003) 1223-1234.

**NON-DESTRUCTIVE TESTING AND
CHARACTERIZATION TECHNIQUES APPLIED IN
THE MODERN MATERIALS SCIENCE**

OPTICAL SPATIAL DISPERSION IN TERMS OF JONES MATRIX CALCULUS

Nastyshyn S.¹, Bolesta I.¹, Lychkovskyy E.², Khaustov D., Nastishin Yu.³

¹Ivan Franko National University of Lviv, 50 Dragomanov St., Lviv 79005, Ukraine

²Lviv Danylo Halytsky National Medical University, 69 Pekarska St., Lviv 79010, Ukraine

³Hetman Petro Sahaidachny National Army Academy, 32, Heroes of Maidan St., Lviv 79012, Ukraine

Traditionally optical spatial dispersion (OSD) is defined as the dependence $\hat{\varepsilon}(\vec{k})$ of the dielectric permittivity tensor $\hat{\varepsilon}$ on the light wave vector \vec{k} , similarly as it is for the frequency (ω) dispersion of the dielectric tensor $\varepsilon(\omega)$. We have developed an approach for the description of the OSD phenomena in the framework of Jones matrix calculus

The Jones matrixes approach is a powerful tool for the description of light propagation through a medium. The entering \vec{E}_0 and exiting \vec{E} electrical field vectors of the light wave are linearly related through the 2×2 integral Jones matrix J : $\vec{E} = J\vec{E}_0$. In the case of a non-uniform medium, the integral Jones matrix J is defined through the differential Jones matrix $N(z)$ as: $J = e^{\int N(z)dz} J_0$, where J_0 is an integral Jones matrix of the entrance boundary of the medium. The differential Jones matrix N is the generalization for the light wave-vector \vec{k} in the same way as \vec{k} is the generalization for the light wavenumber k . The latter inspires to expect that there must exist a way to describe the OSD phenomena in terms of the Jones matrix approach.

In this work, we established the contribution of OSD to the Jones matrixes of the medium and shown how to take into account the correcting parameters describing OSD in terms of Jones matrix formalism.

The proposed Jones calculus approach is a general tool for the account of OSD in optically inhomogeneous media, in which several OSD correction parameters or all of them are simultaneously non-zero, for example, in liquid crystal cells with spatially non-uniform director field, including those containing defects.

ASSESSMENT OF PRE-DEFECT STATE OF INHOMOGENEOUS SURFACE LAYER OF STRUCTURAL MATERIALS ON THE BASIS OF DISPERSION ACOUSTIC EFFECTS OF RAYLEIGH SURFACE WAVES

Mokryy O.¹, Semak P.¹, Romanyshyn I.¹, Semak S.²,

¹ Karpenko Physico-Mechanical Institute of the NAS of Ukraine, Naukova str. 5, 79060, Lviv, Ukraine

² Scientific-Technical and Educational Center of Low-Temperature Studies, Ivan Franko National University of Lviv, Dragomanova str. 50, 79005 Lviv, Ukraine

An urgent task of fundamental materials science and technical diagnostics is to evaluate the parameters of the pre-defect state (damage, plastic deformation, etc.) of the inhomogeneous surface layer of structural materials by non-destructive methods.

To solve this problem, it is reasonable to use Rayleigh surface waves, not only in the traditional sense (based on the use of propagation velocity and attenuation as informative parameters), but also in a broader sense, which is based on the use of modulation, nonlinear, dispersion, dissipative acoustic effects that occur during material degradation much earlier than traditional (change of propagation velocity and attenuation). Since the velocity, attenuation and "structure" of the Rayleigh wave are related to the mechanical, thermal and other characteristics of the sample's surface layer in which it propagates, these parameters can be used to obtain information about the state of the sample's surface layer.

This paper considers the physical model of a sample with an inhomogeneous surface layer, the interaction of the parameters of this layer with the Rayleigh surface wave and the penetration depth, which depends on the frequency of the probing wave. The information technologies of estimation of material condition parameters by means of probing its surface acoustic waves of different frequency, registration of transmission waves on the basis of rigidly connected piezoelectric transducer of tandem type (emitter and two receivers are rigidly connected and located on one line) and processing of registered signals taking into account the dispersion effects (dependence of the wave propagation depth on the frequency) are resulted.

The results of experimental approbation of the developed method on the steam power plant and on the coated sample, as well as comparison of the results with metallographic studies are given. The obtained estimates of the inhomogeneous distribution of parameters by the non-destructive method showed good correspondence with the estimates by the destructive metallographic method.

MAGNETIC MATERIALS

PECULIARITY OF MAGNETIC AMORPHOUS ALLOYS MODIFICATIONS

Hertsyk O.M.¹, Kovbuz M.O.¹, Hula T.G.¹, Kulyk Yu.O.¹, Pandiak N.L.²

¹Ivan Franko National University of Lviv,
Kyryla and Mefodiya Str., 6/8, 79005 Lviv, Ukraine

²Ukrainian State University of Forestry and Wood Technology,
General Chuprynka Str., 103, 79057 Lviv, Ukraine

$\text{Fe}_{78.5}\text{Ni}_{1.0}\text{Mo}_{0.5}\text{Si}_{6.0}\text{B}_{14.0}$ and $\text{Fe}_{73.1}\text{Cu}_{1.0}\text{Nb}_{3.0}\text{Si}_{15.5}\text{B}_{7.4}$ alloys, which, along with Fe, contain Ni, Mo or Cu, Nb and are characterized by high values of specific magnetization $\sigma \approx 138 \text{ A m}^2/\text{kg}$, were studied, considering the high magnetic susceptibility of amorphous metallic alloys (AMA) based on iron and their extensive use in various fields of electric engineering [1,2]. The density of the alloy is decreased by the components with serial numbers higher than that of iron due to a change in the packing of solid spheres of different diameters and the transfer of external electrons from amorphizing boron additives to iron. However, these elements substantially improve the magnetic properties of AMA and control thermal structurization, which is the first stage of modification of the surface and its preparation to the second stage, namely, the application of the polymeric coating.

The results of the electrochemical research show the difference in reactivity in 0.5 and 0.05 M aqueous solutions of NaCl, not only of both alloys of different composition, but also of the contact and outer sides of each AMA ribbon. To optimize the modification of the surfaces of ribbon amorphous metallic materials, not only the differences in the elemental compositions of the alloys have to be taken into account, but also the contact and outer sides of the AMA ribbons, which significantly affect the formation of protective polymer layers.

The preliminary heat treatment of the AMA before the application of an oligomeric film and also the 1 h annealing (at 373–473 K) of samples coated by a film cause the fixation and consolidation of the protective cover. Regardless of the duration of application and sequence of heat treatment of samples, the contact side of the $\text{Fe}_{78.5}\text{Ni}_{1.0}\text{Mo}_{0.5}\text{Si}_{6.0}\text{B}_{14.0}$ AMA oxidizes easier than the external side. The opposite regularity is shown for the $\text{Fe}_{73.1}\text{Cu}_{1.0}\text{Nb}_{3.0}\text{Si}_{15.5}\text{B}_{7.4}$ AMA.

- [1] O. M. Hertsyk, T. G. Pereverzeva, M. O. Kovbuz, et al., *Metallofiz. Noveishie Tekhnol.* 39 (2017) 1023-1033.
- [2] O. M. Hertsyk, A. K. Borysyuk, M. O. Kovbuz et al., *Mater. Sci.* 48 (2010) 270–275.

THE Gd-Fe CONDENSED FILMS (STRUCTURE & PROPERTIES)

V. Prysyzhnyuk, O. Mykolaychuk, K. Trach

Ivan Franko National University of Lviv
Kyryla and Mephodiya Str. 8, 79005 Lviv, Ukraine
Web: <http://physics.lnu.edu.ua/en/employee/viktor-prysyazhyuk>
e-mail: viktor.prysyzhnyuk@lnu.edu.ua

By method of thermal evaporation on fluoroplastic substrates carriers at room temperature it is gained amorphous films $GdFe_2$, $GdFe_5$, Gd_2Fe_{17} . At magnification of temperature of an substrate carrier or at annealing of films the content of a polycrystal phase was incremented. The thickness of films was spotted by means of optical interferometer MIO-1 and made about 200 nanometers.

For investigation of magnetic properties of films and massive compounds the vibrating magnetometer was used. Films were precipitated on fluoroplastic substrates carriers. For martempering of accuracy of measurements from continuous films rings in diameter of 8 mm were cut out and stacked one on another in number of 100 pieces. This construction was then explored in a magnetometer. A measurement accuracy of a vibrating magnetometer depends on accuracy its calibration. For calibration the comparison method has been used. In an etalon role pure not porous nickel with density $\rho = 8,9 \text{ g/cm}^3$ was used. For calculation of specific magnetisation of the sample its moment of magnet was used.

Magnetic properties of films and volume samples of binary compounds of Gd-Fe system ($GdFe_2$, $GdFe_5$, Gd_2Fe_{17}) and also agency of formation of structure on magnetic properties were explored. The hysteresis curves for volume and thin-film samples specify in that fact that these materials belong to the class of magneto-soft compounds. It is necessary to score also the significant differences in character of hysteresis loops for volume and thin-film samples of all compounds of this system. Absolute values of a coercive force for amorphous and polycrystalline films, and volume compounds was determinate. Value of a coercive force decreases at formation of amorphous films in comparison with volume samples in 2 times. Formation of a polycrystalline phase in films give rise to increasing coercive force in 1.5 times in comparison with volume samples (polycrystalline films become more magneto-hard) [1].

Specific magnetisation and magnetic saturation of films decreases in comparison with volume samples. It is the fact speaks not disordered structure of films [2].

For conducting of the phase magnetic assaying it has been used properties of ferromagnetics which they gain in the strong magnetic fields (in a state of technical saturation). The weak dependence of a saturation magnetisation and a Curie point from a stressed state and a ferromagnetic degree of dispersion allows

to choose some parameters in the capacity of phase performances. Quantity of an exertion of a magnetic field at conducting of the magnetic phase assaying made 800 kA/m

It is carried out the magnitno-phase assaying of $GdFe_2$, $GdFe_5$, Gd_2Fe_{17} compounds and comparison of its results with the structures explored earlier. Results of the magnitno-phase assaying of compounds of GdFe system coincide with results of an X-ray diffraction analysis, except for $GdFe_3$ compound [2].

- [1] V.Prysyazhnyuk. Structural transformations and magnetic properties of amorphous films of Gd-Fe system / V.Prysyazhnyuk, O.Mykolaychuk // Edition, University Visnyk. Series: Physics. –2016. – Vol.51. –P.44-51.
- [2] V.Prysyazhnyuk. The processes of magnetization in films and binary compounds of the Gd-Fe intermetallic system / V.Prysyazhnyuk, O.Mykolaychuk, K.Trach // Edition, University Visnyk. Series: Physics – 2017. –Vol.54. –P.88-99.

**STRUCTURAL DEFECTS AND DEFECT-RELATED
PHENOMENA IN SOLIDS**

TEMPERATURE STUDIES OF OPTICAL ABSORPTION EDGE IN $(\text{Ag}_2\text{S})_x(\text{As}_2\text{S}_3)_{1-x}$ ($x \leq 0.2$) SUPERIONIC GLASSES

Shpak O., Studenyak I.

Uzhgorod National University, Ukraine, Uzhgorod, Pidhirna Street, 46;
e-mail: shpak@uzhnu.edu.ua

Optical absorption edge studies of glassy $(\text{Ag}_2\text{S})_{0.05}(\text{As}_2\text{S}_3)_{0.95}$ have revealed two temperature ranges: a range of parallel red shift of the optical absorption edge within the temperature interval $77 \text{ K} \leq T < 300 \text{ K}$ and a range of the Urbach behaviour of the absorption edge at $T \geq 300 \text{ K}$, in which the dependence of absorption coefficient on the photon energy and temperature is given by the Urbach rule. The parallel red shift of the optical absorption edge in $(\text{Ag}_2\text{S})_{0.05}(\text{As}_2\text{S}_3)_{0.95}$ and, consequently, the temperature invariance of the Urbach energy E_U are explained by the lack of medium-range order in the atomic distribution within a certain temperature range [1].

Temperature studies of the optical absorption edge in $(\text{Ag}_2\text{S})_{0.1}(\text{As}_2\text{S}_3)_{0.9}$ and $(\text{Ag}_2\text{S})_{0.15}(\text{As}_2\text{S}_3)_{0.85}$ glasses showed that in the temperature interval $77 \text{ K} \leq T \leq 390 \text{ K}$ a red shift of the absorption edge is observed with the temperature increase. The Urbach energy for $(\text{Ag}_2\text{S})_{0.1}(\text{As}_2\text{S}_3)_{0.9}$ glass in the temperature interval $77 \text{ K} \leq T < 300 \text{ K}$ decreases, while at $T \geq 300 \text{ K}$ remaining unchanged; the Urbach energy for $(\text{Ag}_2\text{S})_{0.15}(\text{As}_2\text{S}_3)_{0.85}$ glass in the temperature interval under investigation is a constant value. The non-Urbach behaviour of the optical absorption edge in $(\text{Ag}_2\text{S})_{0.1}(\text{As}_2\text{S}_3)_{0.9}$ and $(\text{Ag}_2\text{S})_{0.15}(\text{As}_2\text{S}_3)_{0.85}$ glasses can be explained using the formalism of separation of the contributions from static and dynamical structural disordering types. It is shown that in the temperature interval under investigation only the short-range order in the atomic arrangement $(\text{Ag}_2\text{S})_{0.1}(\text{As}_2\text{S}_3)_{0.9}$ and $(\text{Ag}_2\text{S})_{0.15}(\text{As}_2\text{S}_3)_{0.85}$ glasses is present. With the temperature increase, the medium-range order is gradually established, resulting in a decrease of dynamic structural disordering contribution $(E_U)_{X,dyn}$. The decrease of $(E_U)_{X,dyn}$ along with the increasing contribution of the temperature-related disordering $(E_U)_T$ at the constant contribution of static structural disordering contribution $(E_U)_{X,stat}$ results in a temperature independence of the Urbach energy E_U in the $(\text{Ag}_2\text{S})_{0.1}(\text{As}_2\text{S}_3)_{0.9}$ and $(\text{Ag}_2\text{S})_{0.15}(\text{As}_2\text{S}_3)_{0.85}$ glasses.

- [1] M. Kranjčec, I.P. Studenyak, M.V. Kurik, "On the Urbach rule in non-crystalline solids", J. Non-Cryst. Solids, vol. 355, pp. 54-57, 2009.

STRUCTURAL TRANSFORMATIONS AND OPTICAL PROPERTIES OF ELECTRON-IRRADIATED GLASSES AND THIN-FILMS OF THE As-S-Se SYSTEM

I. Shpak

Uzhhorod National University, 46 Pidhirna str., 88000, Uzhgorod, Ukraine
e-mail: shpak.univ@gmail.com

Glassy chalcogenides of arsenium are characterized by high transparency in a near and middle infrared and belong to a class of materials which are used as active or passive elements in optical engineering. Gody et al. [1] were the first to determine experimentally the proportionality $E_g^*(T, X)$ and (T, X) for a-Si:H. By using the Tauc's concept of "frozen" phonons he spread the idea of the equivalency of the effect of a structural W_s and thermal W_t of disorder onto the band width E_g^* and got a linear relation between E_g^* and W :

$$E_g^*(T, X) = E_g^*(0,0) + D \cdot \langle W^2 \rangle_0 - \frac{D}{K} W(T, X),$$

where D is a deformation potential, $\langle W^2 \rangle_0$ – mean-square shift due to zero oscillations. According to this model the optical pseudogap $E_g^*(T, X)$ is determined by the degree of disordering of a glass lattice which is described by $\langle W^2 \rangle_s$ parameter, ie. By changing it by sources of different nature it is possible to influence the E_g^* value indirectly.

Let us analyse our experimental results in the frameworks of this model. In the correlation between E_g^* and W for glassy $As_2S_3(Se_3)$ in dependence of the nature of disorder due to various external factors. This correlation shows that the optical pseudogap E_g^* and – this being more important – the slope of an exponential portion of the edge are changing in dependence of the disorder degree. A linear relation between E_g^* and W for chalcogenide glasses $As_2S_3(Se_3)$ is fulfilled practically in the whole range of the values of W energies which was studied up to this time. Thus it can be stated that in this case for these materials the contribution of the structural ("intrinsic" and induced) and the thermal contributions into a change of disorder potential is adequate, and the change of the slope probably reflects the change of the distribution of the states in the tails of zones.

[1] Gody G.D., Tiedje T., Abeles B., Brooks B., Goldstain Y. Phys. Rev. Letters 47 (1981) 1480.

THE VIBRATIONAL SPECTRA OF LANTHANUM LUTETIUM GALLIUM GARNET CRYSTALS DOPED WITH NEODYMIUM

Taras Grechukh, Oleksandr Bilyy
Ivan Franko National University of Lviv,
Dragomanova Str. 50, 79005 Lviv, Ukraine
E-mail: grech64@gmail.com

The crystals of $\text{Ln}_3\text{Lu}_2\text{Ga}_3\text{O}_{12}:\text{Nd}^{3+}$ have a structure of the garnet type with symmetry space group $\text{Ia}3\text{d-O}_h^{10}$. In structure of garnet the Ln cations occupy 24(c) positions with local symmetry $\text{D}_2(222)$, Lu cations occupy 16(a) positions with local symmetry $\text{C}_{3i}(3^-)$ and Ga cations occupy 24(d) positions with local symmetry $\text{S}_4(4^-)$. The oxygen ions are in 96(h) general positions with coordinates (x, y, z). The primitive unit cell will contain four formula units, that correspond to 80 atoms. However, as the crystals are cubic, the selection rules allow the Raman spectra to contain only vibrations of A_{1g} , E_g , T_{2g} types, whose total number is $25: 3\text{A}_{1g}+8\text{E}_g+14\text{T}_{2g}$. The number of IR-active lattice modes in crystals of garnet structure are 17T_{1u} type [1].

System researches of structure and spectroscopic properties of single crystals of $\text{Ln}_3\text{Lu}_2\text{Ga}_3\text{O}_{12}:\text{Nd}^{3+}$ is carried out in [2]. It is shown that Nd ions occupy dodecahedral positions of crystal, and ions of Lu are both in dodecahedral and octahedral positions in the crystal structure. It results that the structural disordering of the crystals is observed, and a structural formula of the crystal will be written down as $[\text{La}_{1-x-y},\text{Nd}_x\text{Lu}_y]_3[\text{Lu}_{1-z},\text{Ga}_z]_2\text{Ga}_3\text{O}_{12}$. These structural changes we observed in the Raman spectra of $\text{Ln}_3\text{Lu}_2\text{Ga}_3\text{O}_{12}:\text{Nd}^{3+}$ single crystal.

The Raman spectra and infrared absorption spectra of $\text{Ln}_3\text{Lu}_2\text{Ga}_3\text{O}_{12}$ single crystals at activated Nd^{3+} ions are described. The IR absorption spectra were examined with Specord M80 spectrometer. The Raman spectra were examined with DFS-24 spectrometer at excitation the radiation of laser lines 514.5 nm in geometry of experiment on a reflection and by laser lines 441,6 nm and 632,8 nm (transmission experiment). The phonons modes and vibrations are predefined by the defects of the structural disordered that are observed. At the frequency interval of $90 - 125 \text{ cm}^{-1}$ of the Raman spectra the wide structureless band are observed, and at the frequency interval of $400 - 600 \text{ cm}^{-1}$ of the Raman spectra the row of low-intensity vibrations are observed. The interpretation of the obtained results is carried out in this work.

[1] A.E. Nosenko, A.I. Bilyi, V.V. Artamonov, J. Appl. Spectrosc. 40 (1984) 298-301.

[2] T.H. Allik, S. A. Stewart, D.K. Sardar et al, Phys. Rev. B 37, (1988) 9129.

AUTHORS INDEX

Akselrud L. – 61
Aksimentyeva O. – 63
Alieksandrov M. – 43
Antonov V. – 58
Antonyak O. – 6, 12
Artemenko A. – 11
Aubrechtová Dragounová K. – 11
Awskiuk K. – 20
Babčenko O. – 11
Babizhetskyy V. – 40, 59
Babuka T. – 79
Balińska A. – 39
Bauer E. – 38, 55
Belan B. – 46, 47
Bilyk R. – 50
Bilyy O. – 113
Bobnar M. – 61
Markovych B. – 23
Boichyshyn L. – 15, 97
Bolesta I. – 101
Bordun I. – 87
Bordun O. – 87
Botsula A. – 19
Bovgyra O. – 75, 76
Brezvin R. – 16, 65
Brik M. – 80
Budkowski A. – 20
Bulyk L.-I. – 12
Busko T. – 43
Charnyi D. – 43
Cherepaka O. – 64
Chorna N. – 34
Chornii Yu. – 94
Chornodolskyy Ya. – 6, 66
Ciesielski W. – 21
Daszkiewicz M. – 45, 46, 47
Demchenko P. – 62
Demkiv L. – 7
Demkiv T. – 6, 7, 12
Dendebera M. – 6, 7
Denys V. – 58
Dmytrenko O. – 43
Dmytriv G. – 21, 34
Domantsevich N. – 31
Dominyuk N. – 36
Dufanets M. – 49
Dutka V. – 63
Dzevenko M. – 40, 46, 47
Dzhala R. – 43
Dzhala V. – 43
Dzikovskyi V. – 75
Ehrenberg H. – 21
Farenjuk O. – 19
Fedorchuk A. – 65, 80
Fliunt O. – 89, 90
Ftomyn N. – 78
Gamernyk R. – 12
Gladyshevskii R. – 41, 46, 47, 61, 62, 64
Glukhov K. – 79
Gomonnai A. – 79
Gomonnai O. – 79
Grechukh T. – 113
Gulay L. – 45
Gulay N. – 76
Halechko H. – 63
Hertsyk O. – 15, 105
Hlukhyy V. – 37
Horiacha M. – 36
Horon B. – 13
Horyn A. – 35, 64
Hula T. – 97, 105
Ilchyshyn N. – 75
Ilnytskiy Y. – 19
Ilyin P. – 43
Ingram A. – 90
Isnard O. – 59
Ivashko S. – 97
Janka O. – 37
Jia X. – 11
Kalychak Ya. – 45, 76
Kapustianyk V. – 94
Karnaushenko V. – 66
Karpa I. – 83, 84
Katerynychuk I. – 83, 84
Kharkhalis L. – 79

- Khaustov D. – 101
Khomenkova L. – 18
Khrushchuk Kh. – 97
Khyzhun O. – 65
Kluziak K. – 5
Klym H. – 90
Klyzub P. – 35
Kofliuk I. – 87
Konyk M. – 32, 33
Kordan V. – 34, 38, 55
Korolyshyn A. – 51
Korotchenkov O. – 24
Korsunska N. – 18
Kosobutsky P. – 82
Kostiv V. – 96
Kostrobij P. – 23
Kotur B. – 59, 97
Kotyk O. – 64
Kovalenko M. – 75
Kovalska M. – 58
Kovalskyi Ya. – 63
Kovbuz M. – 15, 105
Krayovskii V. – 35
Kromka A. – 11
Kukharskiy I. – 87
Kulish M. – 43
Kulyk Yu. – 27, 48, 105
Kuno I. – 83, 84
Kurochka L. – 43
Kutsa I. – 76
Kuzhel B. – 32, 33
Leno S. – 14
Levytskyi V. – 59
Lishchynskiy O. – 20
Liudkevych U. – 51
Lomnytska Ya. – 40
Lopachak M. – 15
Lozovan V. – 13
Lundberg P. – 11
Lutsyk N. – 67
Lyahova N. – 95
Lychkovskyy E. – 101
Mahi R. Singh – 26
Makowska-Janusik M. – 79
Malyi T. – 12
Manyako M. – 47
Mar A. – 34
Martyniak R.-I. – 61, 62
Masol I. – 95
Matviiv R. – 16, 17, 65
Melnichuk L. – 18
Melnichuk O. – 18
Michor H. – 38
Mikhailik V. – 6
Mohylyak I. – 93
Mokryy O. – 102
Morhunenko M. – 19
Mudry S. – 26, 27, 42, 50, 51, 81
Müller H. – 55
Muts I. – 37
Muts N. – 61, 62
Mykolaychuk O. – 106
Myronchuk G. – 80
Nadtochiy A. – 24
Nastishin Yu. – 101
Nastyshyn S. – 20, 101
Noga H. – 58
Nosenko V. – 15
Nychyporuk G. – 36
Nykyruy Yu. – 27
Nytka V. – 55
Olekseyuk I. – 60
Oliinyk Z. – 51
Olikh O. – 77
Onanko A. – 43
Onanko Y. – 43
Onishechko I. – 82
Osinsky V. – 95
Ovsianyk R. – 50
Pandiak N. – 105
Pasichnyk Y. – 19
Pavlenko O. – 43
Pavlyuk N. – 21
Pavlyuk V. – 5, 21, 34, 37, 38, 39, 55
Piasecki M. – 80
Pinchuk-Rugal T. – 43

- Piskach L. – 60
Plechystyy V. – 25, 81
Plevachuk Yu. – 48, 49
Podolian A. – 24
Polovina O. – 43
Polovyi V. – 23
Pöttgen R. – 36, 37
Prunitsa V. – 27
Prysyazhnyuk V. – 106
Pukas S. – 41
Raczkowska J. – 20
Radkevich A. – 95
Remeš Z. – 11
Reshetnyak O. – 96
Rokomanyuk M. – 35
Romaka L. – 32, 33, 35
Romaka V. – 32, 33, 35
Romanyshyn I. – 102
Rudchenko M. – 32
Rudysh M. – 17, 65, 80
Sadzhenytsia M. – 62
Selezen A. – 60
Semak P. – 102
Semak S. – 94, 102
Semotyuk O. – 83, 84
Semuso N. – 41
Serkiz R. – 48, 96
Shchepanskyi P. – 16, 17, 65
Shcherba I. – 58
Shmid V. – 24
Shopa Ya. – 78
Shpak I. – 112
Shpak O. – 57, 111
Shpyrka Z. – 58
Shtablavyi I. – 25, 27, 81
Shved O. – 42
Shygorin P. – 71
Shymborska Y. – 20
Sklyarchuk V. – 48, 49
Smetana V. – 40
Stadnyk V. – 16, 17, 65
Stadnyk Yu. – 32, 33, 35
Stetskiv I. – 38, 55
Stetsyshyn Yu. – 20
Studenyak I. – 111
Suchocki A. – 12
Sukhoviyy N. – 95
Sveleba S. – 83, 84
Syrotyuk S. – 66
Tarasiuk I. – 38, 55
Tkach O. – 48
Tokaychuk Ya. – 62
Trach K. – 106
Tsizh B. – 81
Venger I. – 18
Venger Ye. – 18
Venhryn B. – 71
Verbenets B. – 13
Vistovskyy V. – 6, 7, 12, 66
Vlad K. – 96
Voloshinovskii A. – 6, 7, 12, 66
Wågberg T. – 11
Wyżga P. – 59
Yakibchuk P. – 76
Yatcyk B. – 58
Yatsyshyn B. – 31
Yatsyshyn M. – 96
Zahn D. – 79
Zaremba N. – 37
Zaremba O. – 64
Zaremba V. – 36
Zavhorodnii O.
Zelinska O. – 34, 55
Zelinskiy A. – 34
Zhak O. – 44
Zhyshkovych A. – 6, 7